Master Thesis, Department of Geosciences

Localization and analysis of calving-related seismicity at Kronebreen, Svalbard

Hana Koubova

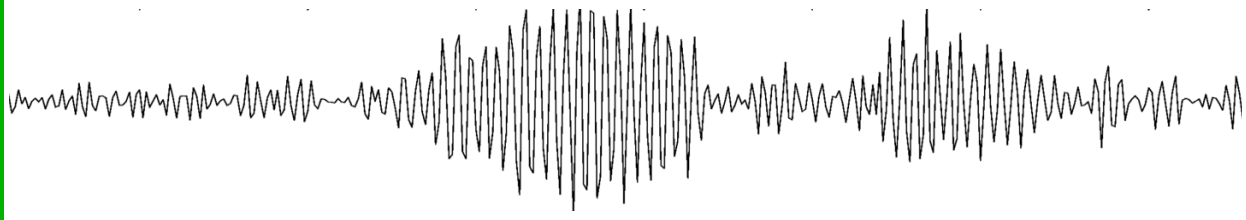

UNIVERSITY OF OSLO
FACULTY OF MATHEMATICS AND NATURAL SCIENCES

Localization and analysis of calving-related seismicity at Kronebreen, Svalbard

Hana Koubova

Master Thesis in Geosciences
Discipline: Geophysics
Department of Geosciences
Faculty of Mathematics and Natural Sciences

University of Oslo
June 2015

Acknowledgement

I want to use this opportunity and thank to everyone who supported my study during the past two years. The greatest gratitude belongs to my supervisor, Dr. Andreas Köhler, who was always positive and patient during my hectic student programe. I want to thank to my co-supervisor, Prof. Valerie Maupin, for her advices and optimism.

I thank to my friends who cheered up my days during dark winter periods and made me always laugh.

I want to express appreciation to my family, especially to my parents and grandparents, for the enormous love and encouragement they provided for my whole life. I thank to my older brother for his sarcasm, support and 'title sandstones' he made for me.

Hana Koubova
June, 2015

Abstract

The glacier calving process is poorly documented but closely related to glacier dynamics. Glaciers respond to many factors, such as air temperature or precipitation and can affect calving activity. Accessing calving rate data and mechanism can enhance understanding of the glacier behavior and may enable estimating future response of the polar areas to the changing environment. This thesis is testing a possible tool for continuous calving monitoring. A non-permanent seismometer deployment was used to record seismic activity at Kronebreen, glacier in western Spitsbergen (Svalbard). Calving-related seismic events were separated from other activity based on the signal characteristics predefined from previous studies and localization of the signal. Three methods were used to obtain the location: frequency-wavenumber analysis (FK), spatial mapping by multi-array beamforming (SMAB) and phase picking. These methods were compared in order to choose the most appropriate one for future studies. More than 1300 calving-related icequakes were recorded and successfully localized. Temporal distribution of calving activity was affected by several factors: precipitation, temperature, tides and season variations. Terminus of the glacier retreated between May and September which was possible to observe through calving-related events locations as those retreated with time. SMAB was found to be the most accurate method and most appropriate for similar studies in the future. Array aperture, location and configuration can be improved to decrease uncertainty of the localization. The seismic processing can be automatized in order to apply this method for larger dataset and enable long-term calving monitoring.

Contents

List of Figures

List of Tables

1 Introduction

Polar areas represent sensitive environments responding prominently to global climate change, especially to rising temperatures. Glacier calving contributes to ice loss with unknown rate and understanding of this process is poor compared to its important role. Calving and other ice dynamic processes such as sliding or crevassing emit seismic energy which can be recorded and analyzed. These seismic events caused by glacier activity are called icequakes. Continuous seismic records are expected to improve knowledge about glacier dynamics in a warming climate which is crucial for estimating future behavior. Seismic analysis can hence serve as a convenient tool for continuous glacier monitoring. This work compares different methods for analyzing calving-related seismic signals using a dataset obtained from Kronebreen, a glacier on Svalbard.

1.1 Cryo-seismology

Passive seismic recording of glaciers is becoming an important method since temporal resolution of glacier dynamics observations by other methods is strongly limited. These are usually obtained by visual or remote sensing observation of changes of the glacier size, geometry, terminus position and GPS velocity measurements. Calving observations are specifically limited due to often complicated access to the terminus and limited visibility (such as weather conditions or darkness in polar areas). If the access is however possible combined with good weather, direct observation can be performed only for short period and hence a long-term calving monitoring tool can enhance understanding of glacier dynamics.

Seismic signals released by calving events are of special interest even if the mechanism is not yet fully understood. Narrow frequency band and short duration is typical for calving often followed by high frequency acoustic wave (Richardson et al., 2010). Frequency band and length however vary depending on specific glacier. O'Neel (2007) for example analyzed calving event signal from Columbia Glacier in Alaska with dominant low frequency band between 1 - 3 Hz and long duration (up to 1000 s). Walter et al. (2012) detected calving with signal between 0.05 and 0.1 Hz with duration about 150 s from Jakobshavn glacier in Greenland. Bartholomaus et al. (2012) related calving seismic signal to direct observations at Yahtse Glacier on the Gulf of Alaska to explain principal mechanism that produces calving icequakes. In addition he observed that higher amplitudes of the icequakes are associated with topple events (which create bigger splashes) rather than with larger sizes of the icebergs which were only weakly correlated to the amplitudes. Icequake generation depends on style of calving, height of the cliff and also on the depth of the fjord. Bartholomaus suggests that icequakes are mainly generated from interaction between the iceberg and sea surface. Walter et al. (2012) conversely explains icequake generation as a result of interaction between iceberg and the glacier's cliff wall.

O'Neel et al. (2007) used icequake recordings for glacier retreat rate estimation at Columbia Glacier which shows how the glacier seismicity can be used for different purposes.

Studies focusing solely on calving-related seismic signals are still very few but this method is becoming popular in recent years especially if regional seismic record is available in polar areas. After distinguishing calving-related events in the seismic data, glacier dynamics can be traced back in the past (e.g. Köhler et al. 2015a,b).

1.2 Glacier-seismology on Svalbard

Svalbard is a Norwegian archipelago in the Arctic Ocean with it's largest island Spitsbergen. It is located roughly in the middle between the continental Norway and the North Pole. Approximately 60% of the archipelago is covered with glaciers (figure 1).
The regional seismicity of Svalbard is monitored by the Spitsbergen seismic array (SPITS) which includes six three-component seismometers. Another three stations are installed on Svalbard, each consisting of one three-component broadband seismometer: The Kings Bay seismic station (KBS), broadband seismic station in Barentsburg (BRBA) and Polish research station in Hornsund (HSPB). Data analysis has been focused mainly on tectonic-induced earthquakes, since strong seismic events occur at close Mid-Atlantic, Mohns and Knipovich ridge, on on-shore Svalbard and at active mines. Seismic events collected by NORSAR showed pattern correlated with seasonal variation which was not typical for tectonic or human activity and indicated glacier related activity (Köhler et al. 2015a).
Kronebreen glacier is part of Kongsfjord in western Svalbard. Chapuis et al. (2010) investigated Kronebreen calving combining direct observation and ground-based radar. Few different types of calving were classified based on direct observation from which two types were particularly distinguished by radar and these were column-drops and column-rotation events. These events are expected to be recorded with higher seismic amplitude, similar as in Bartholomaus et al., (2012).
Single-channel (vertical component) geophone was placed in the vicinity of Kronebreen (Köhler et al., 2012) which confirmed seismic monitoring as convenient for studying the calving process. Seismic data collected from SPITS and KBS were recently used to analyze signal originating from Kronebreen (Köhler et al., 2015a). That study was part of the Seismoglac research project focusing on regional and local glacier seismicity on Svalbard.

1.3 Objectives and structure of the thesis

Passive seismic investigation was done between May and September 2013 in order to examine seismic activity at Kronebreen with particular focus on calving-related seismic events. This glacier is located on north-west Svalbard and it is known for it's fast flow velocity of 2 meters per day (Hagen et al., 2003) and hence high rate of calving events per day is expected (Chapuis et al., 2010). The dataset will help understanding the relations between seismic signal characteristics and certain glacier activity which can be distinguished by localization of the event origins. Obtained locations will be further classified depending on the origin and signal features. Events classified as calving activity will be compared to weather conditions and their spatial and temporal distribution will be discussed. Different localization methods used in this analysis will be compared in order to choose the most convenient one for future studies.
Firstly, the raw dataset is introduced followed by method description. Processing is described together with scripts functions. Finally the results are presented and discussed.

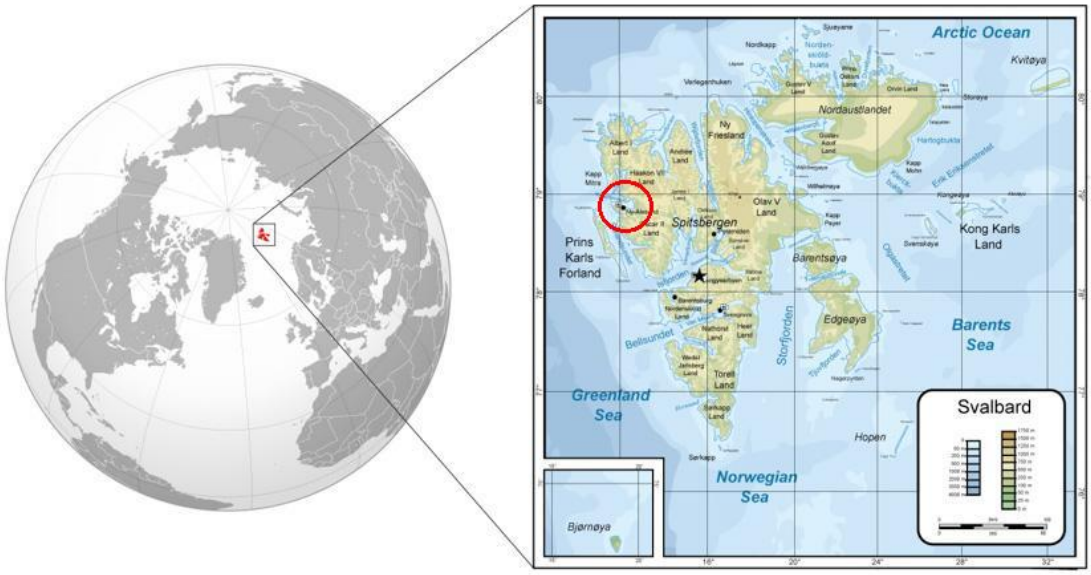

Figure 1: Map of Svalbard, Kronebreen location marked by red circle (https://luminous-landscape.com).

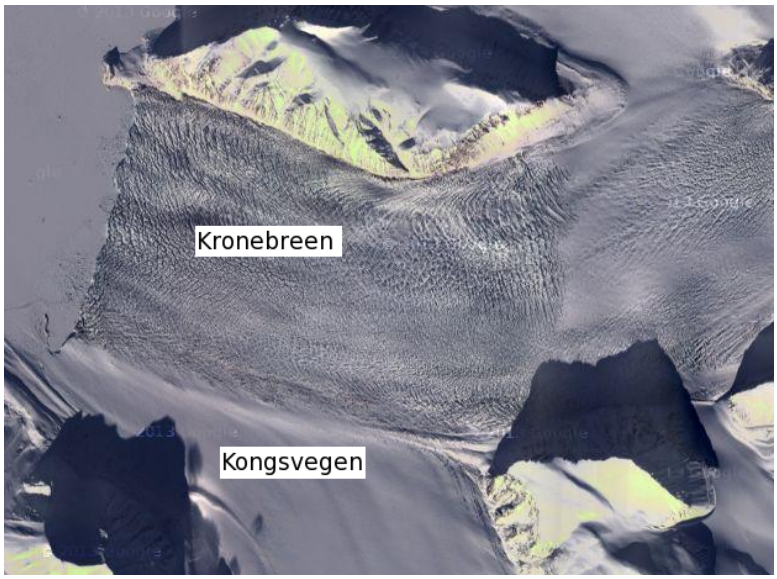

Figure 2: Map of the glacier complex Kongvegen/Kronebreen with combined terminus (google maps).

2 Data

2.1 Study site

Kronebreen is a glacier located in western Spitsbergen approximately 14 km south-east of Ny-Ålesund (78° 58'N, 12° 30'E). It is one of many subpolar, polythermal tidewater and surge-type glaciers with numerous calving events in Svalbard (Hagen et al. 2003). The whole Kronebreen glacier system is separated into three parts as follows: glacier tongue, Kronebreen; the larger upper catchment, Holtedahlfonna; and the cirque glacier, Infatfonna (Nuth et al. 2012). The total area of the glacier is 445 km^2 and it joins with Kongsvegen glacier 5 km away from their combined terminus (Trusel et al. 2010, figure 2). The glacier flow speed has average of 2 m d^{-1} (Hagen et al. 2003) with measured maximal speeds close to the calving front of 3.2 m d^{-1} (Schellenberger et al. 2014) and it contrasts to neighboring Kongsvegen which has velocity flow only 2-4 m a^{-1} (Nuth et al. 2012). The ice cliff at the terminus is approximately 3 km wide (measured from toposvalbard.npolar.no) and the elevation varies between 5 to 60 meters above the fjord surface (measured end of August 2008, Chapuis et al. 2010).
Even Kronebreen was never observed to surge, it was suggested that front position in the late 1800s resulted from a surge (Liestøl, 1988) and since then terminus has been retreating. This was however interrupted by Kongsvegen surge in 1948 which advanced the combined terminus about 1.5km (Kääb et al., 2005). The retreat is characteristic for post-surge quiescent phase and research indicates that retreat rate has slowed down since the 1948 surge and became almost stable since 1990 with only slight advance in period between 1999 and 2001 (Trusel et al., 2010). Terminus position however started retreating again which was revealed by observation between 2007 and 2012 when terminus moved back by $\sim$ 1.1km during this period. Terminus positioning has seasonal pattern with advance in the spring and summer and retread in autumn and winter. The terminus was advancing until May in 2013 and since than retreating until December 2013 (Schellenberger et al., 2014). Fast velocity of Kronebreen tongue indicates basal melting and sliding. Stable or retreating terminus position speaks for major mass loss from the glacier front by calving.
In figure 2 one can see different surface structures of the glacier complex. While Kongsvegen with slow surface velocity has a smooth surface not disturbed by any sudden movement, Kronebreen has a heavily crevassed surface which becomes more obvious in the vicinity of the terminus.

2.2 Record

Part of the Seismoglac project is a non-permanent seismometer deployment to investigate local glacier activity at Kronebreen and to relate it to regional data. A number of 8 broadband seismometers were placed near NyÅlesund. Furthermore, multiple geophone receivers grouped into three seismic arrays were placed around Kronebreen at three different sites. These were labeled as array A, B and C and each includes four receivers (table 1). All broadband seismometers and arrays geophones have sampling rates of 100 Hz and their distribution in the area is displayed in figure 3. Arrays A and B were placed on both sides of the glaciers front to record maximum number of calving. The third array C was placed to complete an imaginary triangle and to allow localization through triangulation. Because of complicated topography, array C was placed on top of a hill which made elevation difference between C and other two arrays around 500 meters. Detailed array components geometry is displayed in figure 4.

The distance between single geophones within an array varies. Array A has distance between geophones from 240 to 500 meters, array B from 190 and 350 and array C from 130 to 290 meters. The geometry and size of the aperture affects further processing which is discussed later.
Seismic arrays were composed of 3-D Geophones PE-6/B. This model is a three component geophone land case with steel spikes for connection with ground and operates between -40 to +100°C which is appropriate for Svalbard conditions.

Table 1: List of arrays and corresponding geophone labels.

Array A	SGLA1	SGLA2	SGLA3	SGLA4
Array B	SGLB1	SGLB2	SGLB3	SGLB4
Array C	SGLC1	SGLC2	SGLC3	SGLC4

2.3 Data selection

This thesis is focused on seismic activity of Kronebreen only and hence data collected from seismic arrays are the most important. Other seismometers were not used for data analysis in this study. Data collected from all three seismic arrays, comprises overall four and a half months starting 1st May and ending 15th September 2013. Two geophones were damaged during this period which can make the corresponding seismic array useless. SGLA2 was lost 14th August and the array A was no longer possible to use. SGLB1 stopped recording on 26th July but rest of the stations within array B were still connected and further processing was possible. However, the accuracy of the aperture can be decreased. Two geophones of array C lost ground coupling in the beginning of August due to rain eroding sand and gravel. Installation of the geophones was difficult because of rocky and icy ground and for that reason sand and gravel was used to couple and fix the instruments.
Time periods that contained data usable for further analysis ensuring maximum location accuracy (having three fully working arrays) was between 4th May (when the last geophone started recording) and 26th July. During the analysis only the vertical component from seismic arrays was used. Seismic background noise increases during the summer months due to the melting season (rain, flowing water) which also influences glacier dynamics. Temperature affects directly basal melting and sliding and both noise and calving rate is expected to rise. Seismic noise is randomly distributed in the seismic record with increased occurrence in late June and July. Array C became most noisy and was difficult to process. It was located on the top of a hill so the area was exposed to wind and precipitation more than array A and B. Array C also records weaker signal due to the location further away from the glacier's terminus.

3 Methods

Seismic events were extracted from the dataset and the origins were localized by different methods to separate calving events from other activity. Hence all events not originating from the glacier front of Kronebreen were not used in further analysis and discussion. Three methods were used for localization: Frequency-wavenumber analysis (FK), spatial mapping by multi-array beamforming (SMAB) and phase picking (grid search minimizing travel-time error). The last one is widely used

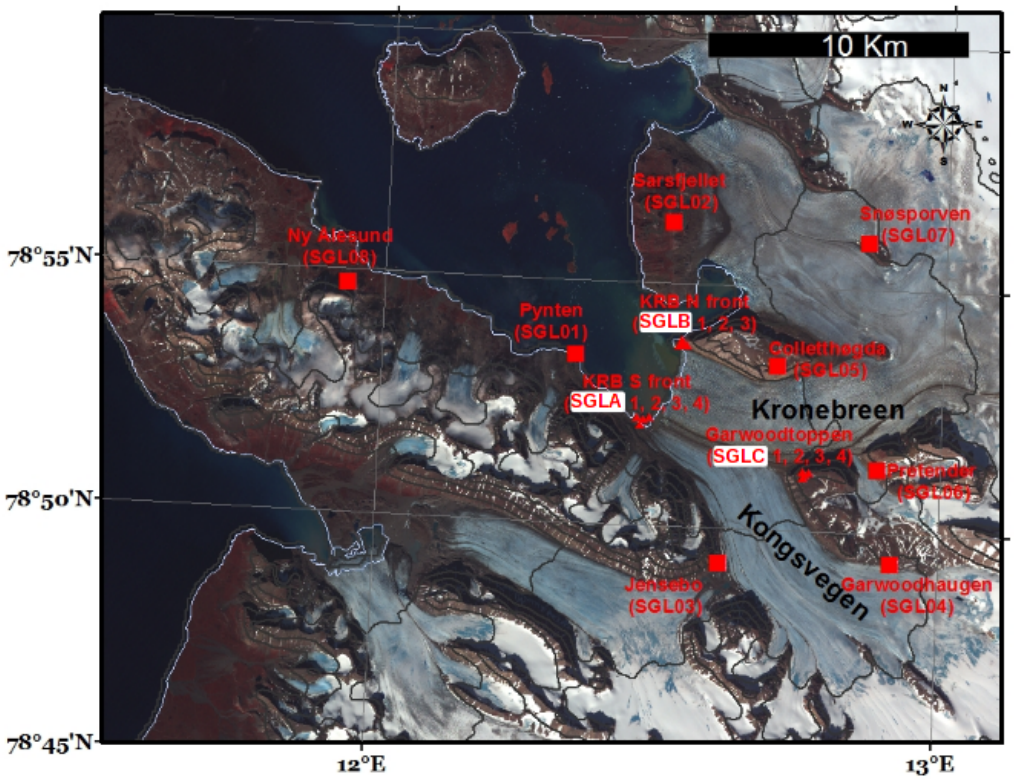

Figure 3: Distribution of seismometers and seismic arrays (SGLA, SGLB and SGLC) at Kongsfjord, Svalbard.

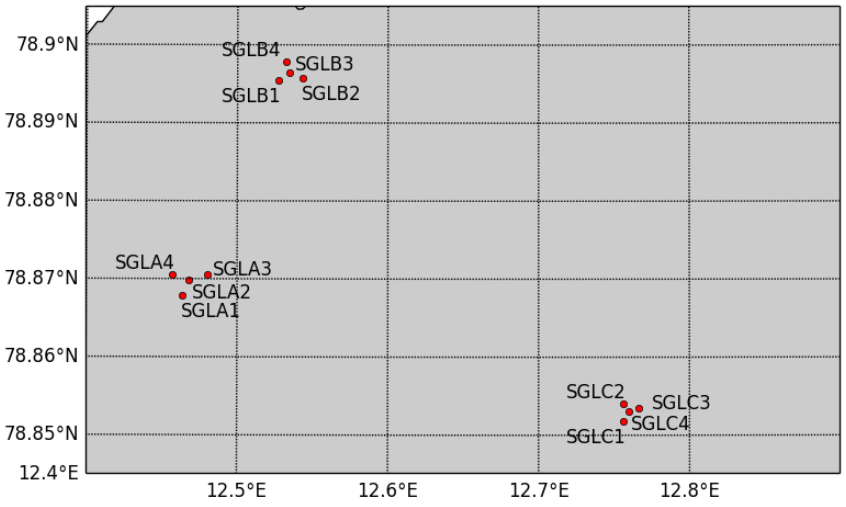

Figure 4: Arrays distribution with corresponding labels.

for earthquake origin localization. Calving-related events have however complicated phases arrivals and some of them are too weak and hence the phase picking can be used only for strong calving signals with clear phases. This method is expected to allow only for a small number of events to be localized and results obtained from phase picking will be used only as a supporting information. The main interest is the calving front activity and to investigate the differences between FK and SMAB methods. This should demonstrate which method is the most accurate.
A challenge is the constant increase of background noise during melting season. FK analysis and SMAB methods are however expected to overcome this problem as these are designed for weak signals.

3.1 Seismic arrays

A set of geophones related to a reference point (or reference station) with specific geometry is called a seismic array. The distance between single receivers varies depending on the purpose of the experiment and analysis technique. Precondition for the aperture is common and precise time basis on all stations (e.g. GPS). The main advantage of such a set of geophones is to enhance relative amplitudes of the seismic signals compared to the background noise by stacking traces. Hence this method can be suitable for weak earthquakes. An elastic wave arriving at the seismic array can be described with:
a) horizontal slowness u_{hor} which is inverse value of apparent velocity $1/v_{app}$ and is related to angle of incidence i and velocity v_0 (figure 5 *a)*),

$$u_{hor} = \frac{1}{v_{app}} = \frac{\sin i}{v_0} \tag{1}$$

b) and direction (backazimuth θ) of the energy which is measured as an angle between north and direction to the epicenter in degrees (figure 5 *b)*). These parameters are combined in space as a slowness vector $\mathbf{U_0}$:

$$\begin{aligned} \mathbf{U_0} &= (u_x, u_y, u_z) \\ &= (\frac{\sin\theta}{v_{app}}, \frac{\cos\theta}{v_{app}}, \frac{1}{v_{app}\tan i}) \\ &= u_{hor}(\sin\theta, \cos\theta, \frac{1}{\tan i}) \\ &= \frac{1}{v_0}(\sin i \sin\theta, \sin i \cos\theta, \cos i) \end{aligned} \tag{2}$$

The apparent velocity or horizontal slowness u_{hor} is the parameter which is measured on seismic arrays (Rost and Thomas, 2002).
To avoid errors in the analysis, the array needs to be placed far enough from potential source to avoid curvature of the wavefront and to ensure a planewave. Array aperture thus needs to be chosen with respect to the distance of the investigation site and wavenumber of the signal. Another assumption is a simple velocity model since the inhomogeneities of the medium affect the planewave propagation and cause backazimuth and slowness deviations. This is not possible to achieve in real world and certain level of inaccuracy is expected. In figures 5 *a)* and *b)* the process of plane wave

crossing a seismic array is displayed. The vertical plane illustrates signal arriving at the array with velocity which can be measures in the horizontal plane as horizontal slowness. The horizontal plane shows that backazimuth represents the angle between the signal direction of propagation and the north. 'Back' azimuth is used because the direction is traced back to the source.

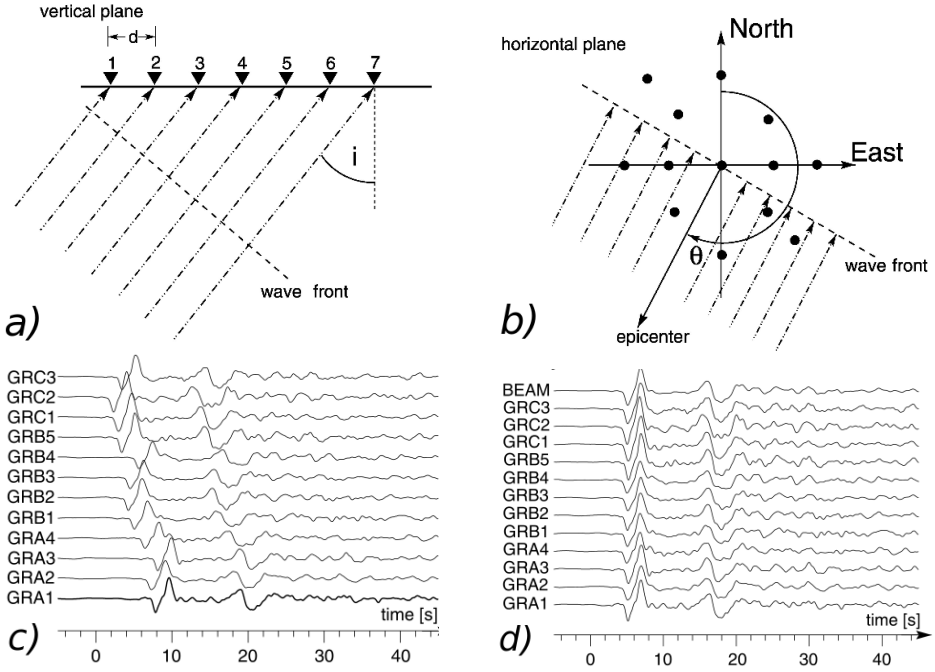

Figure 5: *a)* arriving wavefront at seismic array with angle of incidence i displayed in a vertical plane, *b)* planar wavefront crossing seismic array with backazimuth θ measured from North displayed in horizontal plane, *c)* example of seismic array with clear signature before time-delay, data from Tanzania, October 2000, *d)* coherent signal lined up after time-delay application (figures from Rost and Thomas, 2002).

3.2 Beamforming

Seismic arrays are suitable for recording weak earthquakes with low signal-to-noise ratio (SNR) where coherent signal can be separated from surrounding uncorrelated noise. Arriving seismic signals have different onset times at each array station. Beamforming uses this time difference and corrects this time-delay for each trace which depends on backazimuth and slowness of the planewave. If time-delay is chosen correctly, seismic signals are aligned and coherent signal will sum constructively while background noise will cancel out (figures 5 *c)* and *d)*). A set of computations is therefore done to find the correct combination of backazimuth and slowness to calculate the time-shift with respect to a reference point. This process is called 'beamforming' and the 'best beam' is chosen depending on the largest energy sum after stacking the coherent signal.
Another advantage is amplifying phases with certain slowness while suppressing phases with different slowness and noise. Hence beamforming can be used to enhance and investigate different phases that would otherwise stay hidden (Rost and Thomas, 2002). SNR can be improved with more number of array stations. Signals at each station of the array need to be similar otherwise

the signature will not stack successfully.

3.3 Conventional FK Analysis

This method is beamforming in the frequency domain to estimate frequency and wavenumber of a seismic signal. It uses time difference of arriving planewave to calculate best fitting backazimuth and slowness. Processing in the frequency domain uses phase-shift instead of time-shift. In this chapter the derivation of FK is introduced.
Wavenumber is an important parameter. It describes how the oscillation of a wave repeats in space. The wavenumber vector $\mathbf{k_0}$ relates to the wave slowness vector $\mathbf{u_0}$, which is horizontal component of $\mathbf{U_0}$. The relation is as follows:

$$\mathbf{k_0} = \omega \bullet \mathbf{u_0} \tag{3}$$

where

$$\omega = 2\pi f = \frac{2\pi}{T} \tag{4}$$

where ω is the angular frequency measured in *1/s*, T is the period and f is the frequency of the seismic signal. FK analysis computes the power distributed among different slownesses and backazimuths (Bormann 2012).
The derivation which follows is according to Kelly (1967), and Harjes and Henger (1973). Signal with horizontal velocity v_{app} and backazimuth θ arriving at the array's reference station is described as $s(t)$. N station positions are characterized with vector $\mathbf{r_n}$ with respect to the reference point and signal arriving at nth station is described as $x_n(t)$:

$$x_n(t) = s(t - \mathbf{u_0} \bullet \mathbf{r_n}), \tag{5}$$

with $\mathbf{u_0}$ as the slowness vector:

$$\mathbf{u_0} = \frac{1}{v_0}(\cos\theta, \sin\theta), \tag{6}$$

with v_0 as the medium velocity (as in equation 1). If the time shifts $\mathbf{u_0} \bullet \mathbf{r_n}$ disappear, signal is put in phase and sum of all stations amplitudes reaches maximum. Assuming the same slowness vector, the arrays output is computed by:

$$y(t) = \frac{1}{N}\sum_{n=1}^{N} x_n(t + \mathbf{u_0} \bullet \mathbf{r_n}) \tag{7}$$

Energy of the whole array can be obtained by squared summed amplitudes integration over time for different test wavenumbers. Using Parseval's theorem, this can be done in the frequency domain:

$$\begin{aligned} E(k - k_0) &= \int_{-\infty}^{\infty} y^2(t)dt \\ &= \frac{1}{2\pi}\int_{-\infty}^{\infty} \mid S(\omega) \mid^2 \left| \frac{1}{N}\sum_{n=1}^{N} e^{2\pi i \bullet (\mathbf{k}-\mathbf{k_0})\bullet \mathbf{r_n}} \right|^2 d\omega \end{aligned} \tag{8}$$

where $S(\omega)$ is Fourier transform of $s(t)$ and $\mathbf{k_0}$ is the wave number vector ($\mathbf{k_0}$ is real wavenumer corresponding with $\mathbf{u_0}$ while $\mathbf{k}$ represents the tested wavenumber):

$$\mathbf{k_0} = (k_x, k_y) = \omega \bullet \mathbf{u_0} = \frac{\omega}{v_0}(\cos\theta, \sin\theta) \tag{9}$$

The previous equation can be written as:

$$E(\mathbf{k} - \mathbf{k_0}) = \frac{1}{2\pi} \int_{-\infty}^{\infty} \mid S(\omega) \mid^2 |A(\mathbf{k} - \mathbf{k_0})|^2 \, d\omega \tag{10}$$

where

$$|A(\mathbf{k} - \mathbf{k_0})|^2 = \left| \frac{1}{N} \sum_{n=1}^{N} e^{2\pi i \bullet (\mathbf{k}-\mathbf{k_0}) \bullet \mathbf{r_n}} \right|^2 \tag{11}$$

which is array response function (ARF). When the slowness difference is zero, the factor $|A(\mathbf{k}-\mathbf{k_0})|^2$ becomes 1.0. This means that the correct slowness was used and it leads to partly suppressing all other energy traveling with different slowness. ARF is dependent on the frequency and is controlled by the array configuration, spacing and aperture. ARF and power spectral density $|S(\omega)|^2$ define the total energy recorded at the array, which is a function of slowness and backazimuth. The slowness and backazimuth can be computed from the wavenumber vector $\mathbf{k} = (k_x, k_y)$

$$|\mathbf{k}| = (k_x^2 + k_y^2)^{1/2} = \omega u_{hor} = \frac{\omega}{v_{app}} \tag{12}$$

$$\theta = \tan^{-1} \frac{k_x}{k_y} \tag{13}$$

The power spectral density can be displayed in a polar coordinate plot named fk diagram where backazimuth is plotted on the azimuthal axis and the slowness on the radial axis.
FK can be applied to a short time window to avoid more phases with different slowness in a time window of a few seconds length. In case of small-aperture arrays, the time differences between stations are small and sliding window can be short.
Sliding windows are applied for FK analysis. Chosen time window with specific length moves along the seismogram with certain shift size and investigates slowness and backazimuth for each segment. Outcome can be shown as a plot of power maximum over time during the event. Values are stored as time series of power, slowness and backazimuth (Rost and Thomas, 2002).
There are some general rules for array configuration. The larger the aperture, the smaller are the wavenumbers that can be measured with the array. If the aperture has a size a, the upper limit of measurable wavelength is $\lambda = a$. The array behaves as a single station for signals with $\lambda >> a$. Another rule states that distance between stations of an array defines the position of side lobes of the ARF and also the largest wavenumber that can be resolved. With smaller mean distance it is possible to resolve signal with smaller wavelength (for a given velocity, Bormann, 2012).
Example of ARF is displayed in figure 6 where ARF is first computed for monochromatic 1 Hz wave with slowness $u = 0\ s/^\circ$(left figure) and than FK analysis is performed for signal arriving with backazimuth of 225° and slowness of $u = 7.75 s/^\circ$ (right figure). In the figure slowness has two dimensions (s_x and s_y) and color represents the third dimension: power spectral density where the maximum is normalized to 0 dB (represented with red colour, Thomas and Rost, 2002).

To sum up FK, this method uses a seismic array to estimate slowness and backazimuth of the signal propagation. With several seismic arrays recording the coherent signal, triangulation of the backazimuths can reveal the origin of the seismic event. Hence at least two seismic arrays need to be used, but three seismic arrays improve the accuracy of the event localization.

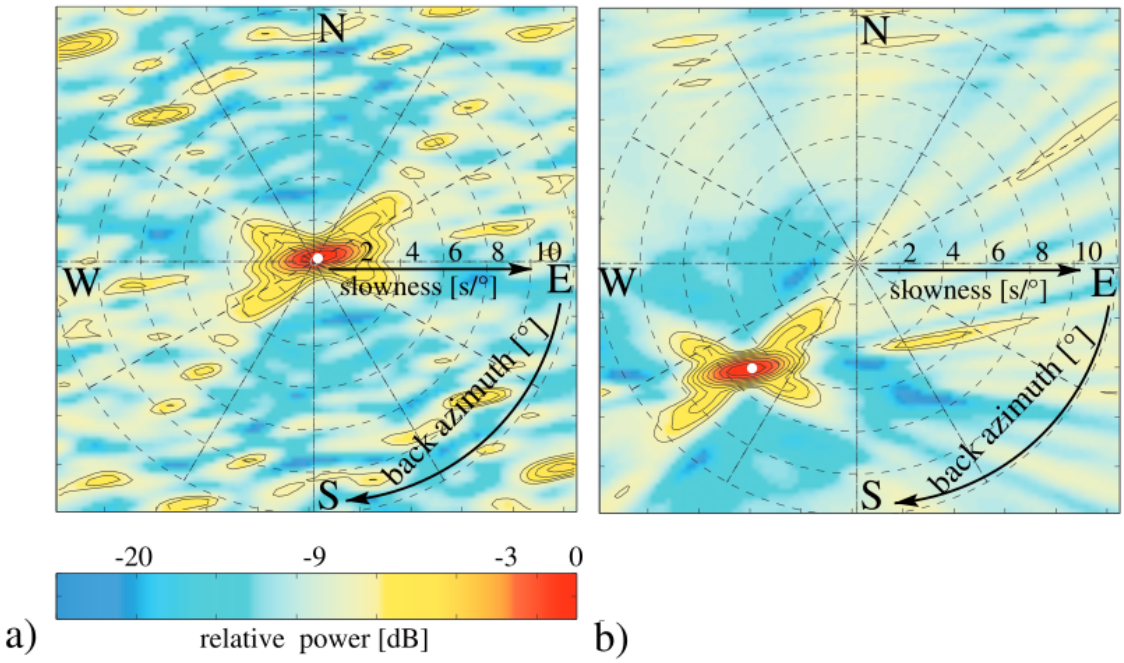

Figure 6: Example of ARF function first for 1 Hz signal with $u = 0$ $s/^\circ$ (left) and FK analysis for real signal (right), with scale where maximum power is normalized to 0 dB (red color). Example from GRF array (large size), figure used from Rost and Thomas, 2002.

3.4 Conventional FK Analysis based on cross-spectral matrix (CVFK2)

In this study a conventional FK analysis was used as a first method to localize icequakes. The implementation used is based on the evaluation of the cross-spectral matrix $R(\omega)$ (CVFK2, Ohrnberger et al., 2004):

$$R(\omega) = E < X(\omega)X^H(\omega) > \tag{14}$$

where $E <>$ indicates the expectation value. $X(\omega) = [X_1(\omega), ..., X_N(\omega)]$ are the complex spectral coefficients of the signal at all N receivers for certain frequency ω. The frequency wavenumber estimator is written as:

$$P(\omega_b, \mathbf{k}) = \sum_{\omega_b} (A(\omega, \mathbf{k})R(\omega)A(\omega, \mathbf{k})^H) \tag{15}$$

with ω_b as discrete angular frequency in the chosen band of interest. $\mathbf{A}$ represents the steering

vectors for wavenumber vector $\mathbf{k}$ at certain frequency ω:

$$\mathbf{A}(\omega, \mathbf{k}) = \left[e^{j\mathbf{kr_1}} ... e^{j\mathbf{kr_N}} \right]^T \tag{16}$$

and $\mathbf{r_1}...\mathbf{r_N}$ are vectors between array stations and origin of coordinate system or reference point. In practice the steering vectors are the time shifts applied for each station of the array related to the reference point. There is assumption of planar wavefront as mentioned before and hence constant wavenumber vector $\mathbf{k}$ is used for all the stations. After the time shift the traces can be stacked.
The normalization factor is calculated as:

$$norm = \sum_{i==j} \left(\left| \sum_{\omega_b} (R_{ij}(\omega_b)) \right| \right) \times N \tag{17}$$

and it is used for computing the relative beampower RP. Equation 15 is than normalized as:

$$RP(\omega_b, \mathbf{k}) = \sum_{\omega_b} \left(\frac{P(\omega, \mathbf{k})}{norm} \right) \tag{18}$$

This is done for each time window (the same sliding window technique as in previous chapter). The time window is used if the relative power RP of the coherent signal reaches certain threshold (details in chapter 4.4) and the corresponding backazimuth determines the direction of the signal. Using three seismic arrays, the triangulation can be done.

3.5 Spatial mapping by multi-array beamforming (SMAB)

The second method used in this study is very similar to FK analysis but without assumption of planar wave. This is very convenient since FK locations can contain errors due to small distance of expected calving events from seismic arrays.
Area of interest is discretized and each point is considered as possible source location. Time delay is calculated at each station for corresponding location and seismic traces of the whole network are stacked after time shifting. Stacking traces for different source locations creates beams with low or strong amplitudes sums. To use this method, one needs a velocity as an input for the calculation in contrast to FK.
This method is based on CVFK2 with improvement of non-planar wavefronts. The steering vectors have specific wavenumber $\mathbf{k_1}...\mathbf{k_N}$ for each station of an array (compared to the previous method where all the steering vectors had the same wavenumber, equation 16). These are pointing from the tested source location to the array station ($\mathbf{x}$) with assumption of equal seismic velocity for each array (which is later adapted for different velocities):

$$\mathbf{A}(\omega, \mathbf{k}) = \left[e^{j\mathbf{k_1(x)(r_1 - x)}} ... e^{j\mathbf{k(x)(r_N - x)}} \right]^T \tag{19}$$

where $\mathbf{r_1}...\mathbf{r_N}$ represent again the vectors between the array stations and the origin location of the coordinate system. Relative power is than computed the same as in FK method with new steering vectors (equations 15 and 18).

This method was applied for all arrays available. For each array there is a grid search of all possible locations and relative and absolute power is computed. The method results into a map for each array that are stacked together to obtain the maximum power overlap pointing at the best source location (figure 7). Here two arrays are used (A, B) and stacking is performed as follows:

$$\mathbf{x} = argmax \frac{RP_A(\omega_b, \mathbf{x}) + RP_B(\omega_b, \mathbf{x})}{2} \tag{20}$$

To get the source location, the data from time windows corresponding to high values of relative power above a certain threshold are selected. The final location is calculated as a mean value from time windows above the threshold (figure 8, left). This is later referred to as *mean location* approach.
Another way to find the source location can be used when the best time window maps (with the highest amplitude sum) of each array are selected separately and those maps are stacked (figure 8, right). The source location is obtained:

$$\mathbf{x_{best}} = argmax \frac{(RP_{Abest}(\omega_b, \mathbf{x}) + RP_{Bbest}(\omega_b, \mathbf{x})}{2} \tag{21}$$

where RP_{Abest} does not need to be in the same time window as RP_{Bbest} (as in the *mean location* approach). This is later referred to as *the best time window location* approach.
To sum up the SMAB method, the wave arriving at the seismic array does not need to be planar. The method searches for beams with strong amplitude sums. With several seismic arrays, the sum of beams can be done. SMAB can be used in two ways, the first one is to use a threshold of relative beampower to separate locations of coherent signals from noise using maps stacked over both arrays (*mean location*). The second one is to obtain the best time window for each array and then stack the maps and get the location (*the best time window location*). Both methods were tested for three days (210 events) and compared to get the optimal setting which was further used to analyze the whole dataset, see SMAB configuration in Processing chapter.

3.6 Phase picking and time-velocity triangulation

The third method used for obtaining the source locations is through phase picking. High SNR is crucial for this method and hence only strong and clear events with coherent phases at different stations can be tested. The phase pick of the signal at one station of each array is used to compute the observed travel time difference between the stations. Constant seismic velocity is used to calculate theoretical time difference for each point of discretized area of interest. Grid search is done to find the best fit between observed and theoretical time difference.
To find the origin, one needs to have a velocity estimation. Here, velocity obtained from FK analysis were used for the calculation. With existing velocity (derived from slowness) v_a, v_b and v_c, location of the stations and time differences, a set of computation can be performed with assumption of constant elevation across the area and straight ray paths.

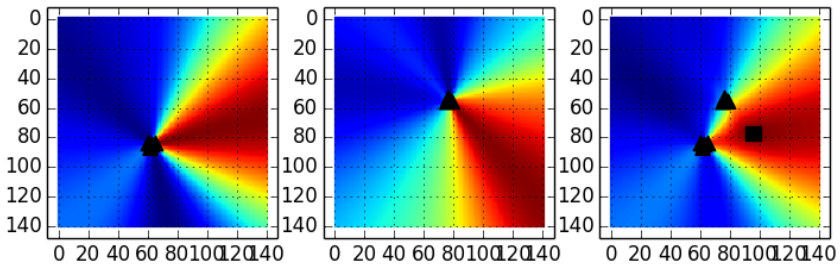

Figure 7: SMAB relative power maps, left: relative beampower for array A, middle: relative power for array B, right: stacked and normalized map. Triangles represents array stations, square is the best event location, example from day 180.

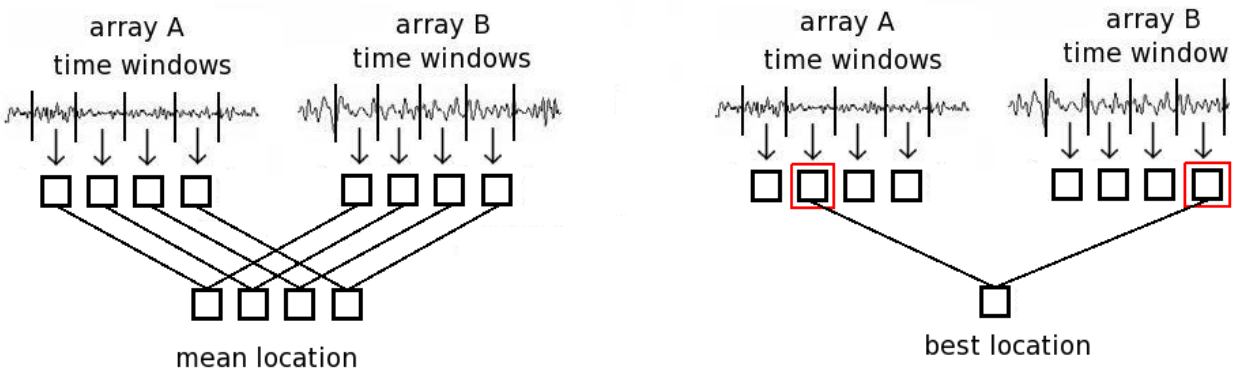

Figure 8: Simple sketch of how the map is created in SMAB for each time window of array A and B.

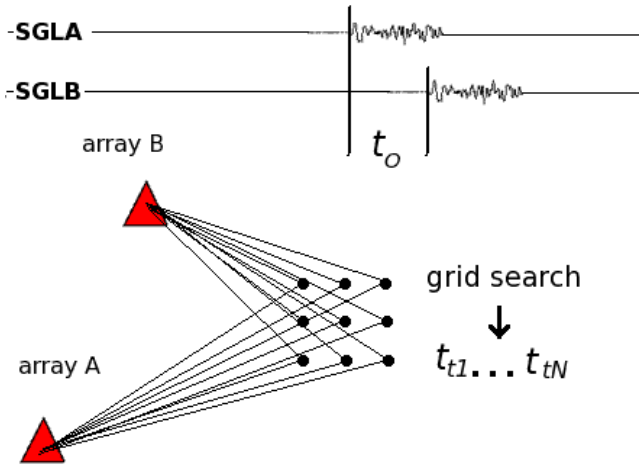

Figure 9: Simple sketch of a grid search for phase picking in the area for arrays A and B. The same phase is picked on one station from each array (SGLA and SGLB) to obtain t_o and a grid search is made to calculate t_t for each point of the grid.

Grid search is done to calculate theoretical time difference for each point of the area. In case of two geophones, the theoretical time difference t_t was compared to the observed (picked) t_o to find the lowest time difference t_{diff} with use of least squares method. Example of grid search is illustrated in figure 9. For array $A(x_a, y_a)$ and $B(x_b, y_b)$ and grid point $G(x_g, y_g)$ the calculation of the time difference is as follows:

$$\begin{aligned} \mid AG \mid &= \sqrt{(x_a - x_g)^2 + (y_a - y_g)^2} \\ \mid BG \mid &= \sqrt{(x_b - x_g)^2 + (y_b - y_g)^2} \\ t_a &= \frac{\mid AG \mid}{v_a} \\ t_b &= \frac{\mid BG \mid}{v_b} \\ t_{t_{ab}} &= t_a - t_b \\ t_{diff_{ab}} &= \sqrt{(t_{o_{ab}} - t_{t_{ab}})^2} \end{aligned} \tag{22}$$

This computation needs to be done for each grid point of the area. Points exhibiting the lowest t_{diff} values show origin of the event. The outcome is a curve of all possible origins of the seismic event.
In case of three geophones there are three time differences between A and B, A and C and B and C. These were summed:

$$t_t = t_{t_{ab}} + t_{t_{bc}} + t_{t_{ac}} \tag{23}$$

and compared to the observed time difference

$$\begin{aligned} t_o &= t_{o_{ab}} + t_{o_{bc}} + t_{o_{ac}} \\ t_{diff} &= \sqrt{(t_o - t_t)^2} \end{aligned} \tag{24}$$

There is only a single point (or small area) exhibiting the lowest difference t_{diff} in case of picking the phase on three stations.
The velocity obtained from FK analysis represents locally measured velocity below the array which may differ from the average along the ray path. This is drawback for this method.

4 Processing

4.1 Software

Several programs were used for reading and analyzing the data. As a starting program for finding and picking events Snuffler was used. It is a simple program which allows to display seismic data, apply basic filtering and pick several types of events with different phases if needed (Heimann 2012). For later analysis of the picked events Obspy package was used which is a Python framework for processing seismological data (Beyreuther et al., 2010). Package includes different ways of plotting, filtering seismograms and also Beamforming. This package was combined with self-made Python programs.

4.2 Coordinate system

For calculation purposes the latitude and longitude were converted to Cartesian coordinate system with center of the system at 78° 52' 22.9188"N, 12° 35' 13.4088"E. Later this was converted back to world-coordinates for map plotting purposes. Therefore figures displayed are both in world and Cartesian coordinates.
The area of interest was limited between the three seismic arrays in order to analyze only events originating close to the glacier's terminus. These limits were set in Cartesian coordinates as $-3km < x < 3km$ and $-2.5km < y < 2.6km$ (figure 10).

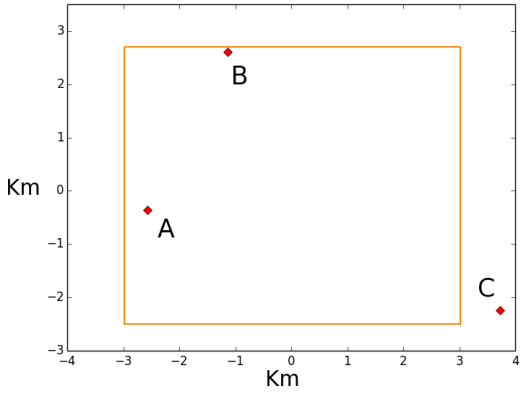

Figure 10: Simple map in Cartesian coordinates, plot only with reference geophones, limits for event separation represented by inner rectangle.

4.3 Event extraction

Events were extracted manually from the seismic record to compile a dataset of events for further analysis and localization. From previous work performed at Kronebreen, the expected signal related to calving should exhibit narrow frequency band in a low frequency range between approximately 2 and 10 Hz (Köhler et al., 2015a). Duration is expected to last approximately 10 seconds but shorter or longer events can also be recorded. Signal should be clear since seismic stations were placed in vicinity of the glacier's terminus. All events exhibiting narrow frequency band (lower frequencies), rather short duration and clear signal were extracted. Events having longer duration or higher content of noise were however chosen for further analysis as well since these can be later filtered out during the processing. Longer duration can represent multiple calving or distant (calving) events and higher noise can be caused by many factors, for example by wind.
Summer season causes more noisy environment due to melting and hence the SNR is expected to decrease in the second half of the recording period. Calving can be distinguished from earthquake signatures as these have higher frequency content, longer duration and clear P and S phases. A number of earthquakes exist in the seismic record in the measuring period and just for comparison few of them are stored for later frequency representation.
To examine season variation, three weeks were chosen from the recording period. First intention was to chose weeks representing different months and those would be the beginning of May, end of June/beginning of July and late August. This had to be however adapted because of geophone

damages and a week in late July was chosen instead of late August. These weeks were named chronologically as week 1 (beginning of May), week 2 (June/July) and week 3 (late July, table 2). During the picking, high-pass filter was applied for all events set to 2 Hz to avoid long periods of

Table 2: List of days.

Day number	Week 1-Date	Day number	Week 2-Date	Day number	Week 3-Date
126	May 06	178	June 27	200	July 19
127	May 07	179	June 28	201	July 20
128	May 08	180	June 29	202	July 21
129	May 09	181	June 30	203	July 22
130	May 10	182	July 01	204	July 23
131	May 11	183	July 02	205	July 24
132	May 12	184	July 03	206	July 25

ocean micro-seismicity disturbing the signal. For some events it was necessary to employ low-pass filter as well (due to noise) and this filter varied from 5 to 30 Hz. Some events exhibited later arrival of acoustic wave with frequency significantly higher than the icequake.
In total, there were 625 events picked in the week 1, 1168 events in the week 2 and 1619 events in the week 3. All events were labeled to distinguish between short duration events (up to 30 seconds) and longer events that are meant to go through a separate analysis as these can represent multiple calving along the terminus. Extra label was added to those events followed by acoustic waves.

4.4 FK processing

Few parameters needed to be set. The slowness grid was set as $s_{x_{min}} = -3.0\ s/km$, $s_{x_{max}} = 3.0\ s/km$, $s_{y_{min}} = -3.0\ s/km$, $s_{y_{max}} = 3.0\ s/km$ with slowness step of 0.03. The sliding window length was set to $1s$ and the shift step to $0.05s$. Frequency band was restricted between 2 and 10 Hz which is the dominant frequency of calving events.
With Obspy package three python scripts were used. The first one is self designed script for calling the functions, storing outputs and plotting relevant data: 'FK_analysis_plot_script.py' (appendix). The script uses list with event time picks saved from Snuffler and processing is done for each of them. The second script loads data and world coordinates of array stations: 'load_SGL.py'. The third script includes functions for array processing of Obspy package and it is called 'array_analysis_new.py'.
Figure 11 represents example of FK analysis output. For each time window along the seismic signal, FK analysis is performed and result is stored as time series with corresponding values of relative power, absolute power, backazimuth and slowness which can be transformed into seismic velocity. Specific value is plotted into each of these four graphs for each time window. Relative power is used for separating the coherent signal from random noise. The first threshold is set to $RP = 0.6$ and all the data above this value is stored in a list. Standard deviation of backazimuth σ_θ of all time windows above this threshold is then computed. In case of too high σ_θ, the threshold is increased gradually by 0.01 until the value drops below 20 degrees. To avoid datasets composed of too few time windows (which can lead into wrong direction estimation) the minimum amount of time windows used for σ_θ computing was decided to be 5. Events having σ_θ below 20 degrees

computed at least from 5 time windows above certain threshold are further analyzed.
The next step in the script was storing the mean of the backazimuth for all available arrays for one event. Backazimuth was obtained either from all three arrays, only two arrays (which can be still usable) or one/none array in case of strong background noise or wrongly picked event with incoherent signal. Events obtaining backazimuths from two or three seismic arrays continue with the script whereas the rest is excluded.
Calculation of crossing point of backazimuths for array A and B is done in order to locate events. Array C was excluded from this step since frequent bias occurred during the examination. This was noticed while plotting backazimuths in a simple sketch with uncertainty range calculated from σ_θ (figure12). The backazimuth obtained for array C often deviates from AB crossing point which is probably caused by location at high elevation. The seismic energy must travel upwards to reach the array and it may cause arrival from different direction due to 3D propagation effects. To support this, representation of all the backazimuths obtained for three weeks are shown in figure 13.
Histograms show clear deviation of array C. Array A has two peaks, the higher one between 50 and 75°. Array B peaks between 150 and 180° giving cross area of A and B located at the glacier's terminus while array C has clear peak between -110 and $-120°$. A simple sketch illustrates the directions of backazimuths in figure 13 (bottom right). To complete successfully the triangulation, the backazimuth of array C needs to be peaking between approximately -80 and $-45°$. For this reason the event location was done with only array A and B as these seem to be more accurate. However, the backazimuth bias of array C could be investigated and corrected in future work.
The last task of the FK script was to select events origination in the area of interest (figure 10). Final number of events located at Kronebreen with use of FK analysis is 217 for week 1, 438 for week 2 and 834 events for week 3.
Uncertainty of the location was calculated from σ_θ while using simple math in Cartesian coordinates (figure 14):
1) compute the crossing point of arrays A and B backazimuths,
2) choose higher value of σ_θ (from array A or B),
3) create imaginary right-triangle with two known points (reference geophone of array and crossing point) and angle ($\sigma_\theta/2$),
4) calculate size of the third side of the triangle (in figure 14 marked as bold line with label '(d)') with simple trigonometry.
Final number was stored for each event and used later for plotting locations with uncertainty.

4.5 SMAB processing

Three scripts were used during the SMAB method processing. The first one was self-designed script for calling the functions and storing data: 'do_diffractionstack_sketch_alldata.py' (appendix). The second one is the same as for FK: 'load_SGL.py' and the third one includes functions of the Obspy package: 'network_analysis.py'.

4.5.1 Script flow

This method has two approaches. One for gradually increasing the threshold of relative power RP to obtain group of corresponding values of latitude and longitude and calculate the mean value

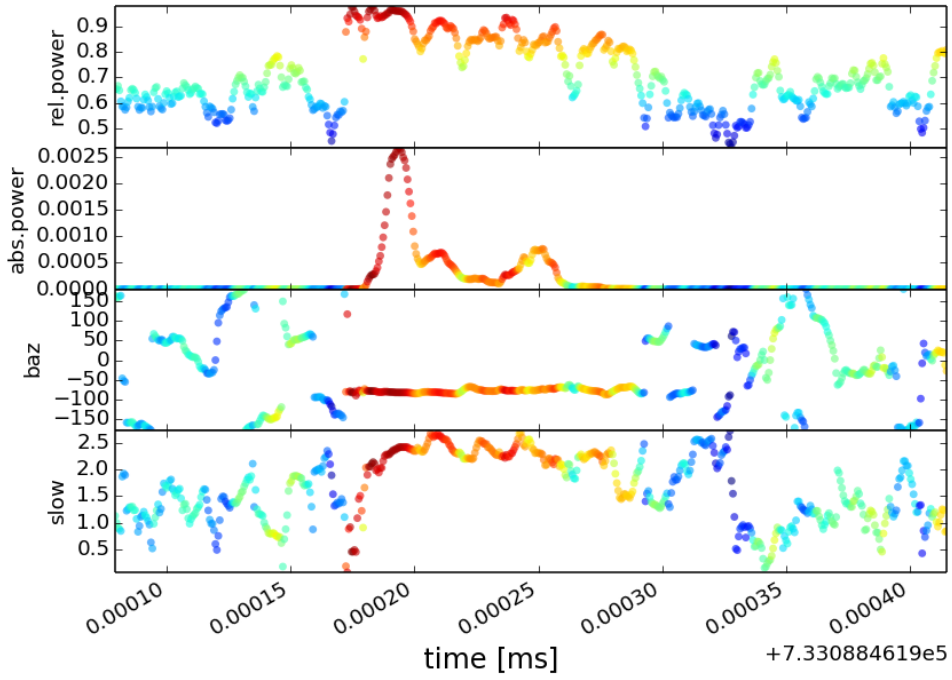

Figure 11: Example of FK analysis output for specific event, from top: relative power, absolute power, backazimuth (in degrees [°]), slowness $[s/km]$. The color gradient represents relative power RP with dark red as maximum and blue-purple as minimum (from http://docs.obspy.org).

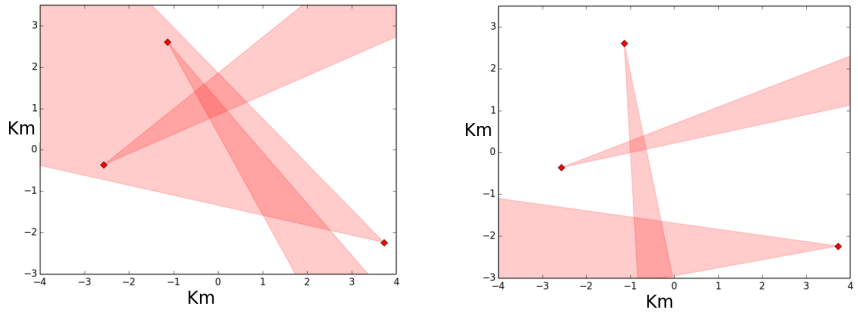

Figure 12: Example of successful (left) and not successful (right) triangulation of FK backazimuths, event from day 126.

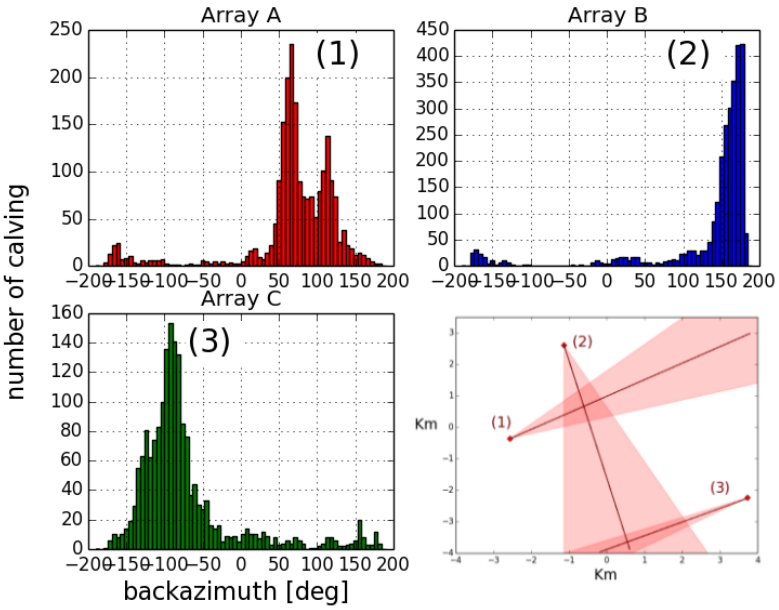

Figure 13: Backazimuth histograms of all analyzed events (FK) and illustration representing peaks of the histograms.

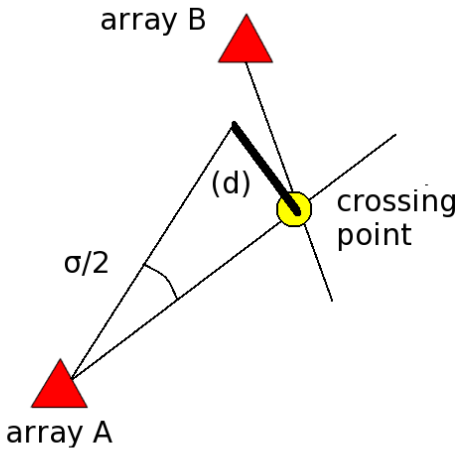

Figure 14: Simple sketch illustrating uncertainty calculation of FK event location.

(*mean location*). The second approach uses the best time window combination from each array (*the best time window location*).
In the *mean location* approach, the FK velocity of arrays A and B is used for SMAB as an input for each array. The area of tested source locations is discretized into bins with 100 meters size spreading 7 kilometers from the center of the geometry in each direction, hence 140 points along each axis. Maps for arrays A and B are created during SMAB analysis showing relative beam-power. These maps are then stacked and normalized (figure 7, equation 20). This normalized map is created for each sliding window and the best location is then stored in a data array and presented as a multiple plot of power, longitude and latitude. The coordinates have approximately constant values in figure 15 during the seismic event. The threshold for separation coherent signal was set again to $RP = 0.6$ and standard deviation is calculated for longitude and latitude values as σ_{lon}, σ_{lat}. If σ reached above $0.5km$ the threshold of RP was increased gradually by 0.01. When both σ_{lon} and σ_{lat} drop below $0.5km$ the process can continue. The standard deviation of latitude or longitude (the greater value) is stored for later map plotting where it is uses as uncertainty. The minimum number of time-windows requirement was not used in this case. Events located by only one time-window were compared with FK and signal characteristics were investigated to exclude incorrectly located events. An example location with standard deviation 0.37 km is displayed in figure 16.

The average of listed coordinate values is used to get *mean location* for each event and final separation based on location is done to exclude events originating from outside the area of interest. The second approach of SMAB method is the *the best time window location* which stores directly longitude and latitude values obtained from the map stack of the best time window for each array.

4.5.2 Method testing and parameter calibration

Both SMAB approaches were tested to figure out which one has less scatter at the glacier terminus and what is the best combination of parameters. The setting was tested for few different combination of time window length and used seismic velocity. Three days were chosen for this testing, one corresponding with each week (210 events in total from days 129, 181 and 203). For each event, two locations were obtained by *mean location* and *the best time window location*. These were plotted into Kronebreen map to examine how the origins scatter around the terminus. Events chosen for this test were previously evaluated as originating from Kronebreen with FK method and hence were expected to have location close to the glacier's terminus. Parameters combinations are listed in table 3. The combinations were first tested for days 126 and 127 (69 events) to find out the

Table 3: Combinations of time window length and velocity values for SMAB.

Combination	Time window length	Velocity	Unsuccessful stacking
1	2 s	3 km/s	4%
2	3 s	3 km/s	5%
3	2 s	4 km/s	16%
4	3 s	4 km/s	19%
5	2 s	FK	0%
6	3 s	FK	0%

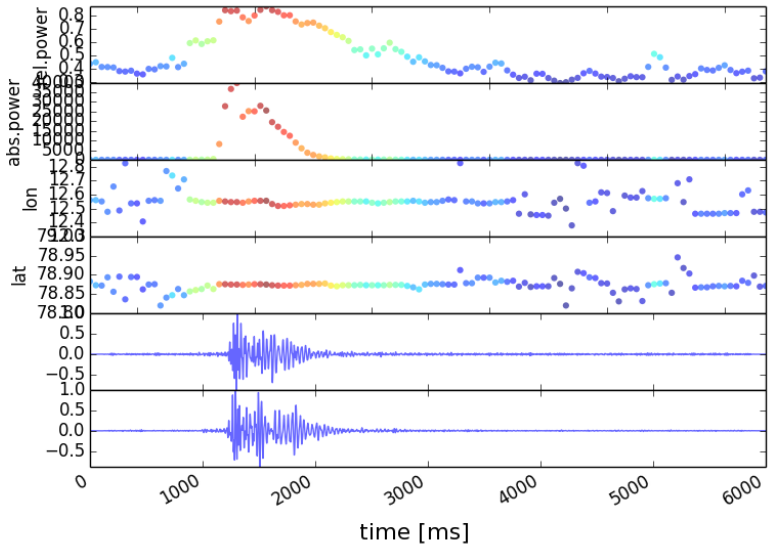

Figure 15: Example of SMAB output figure, from top: relative beampower, absolute beampower, longitude, latitude, signal from array A, signal from array B, example from day 183.

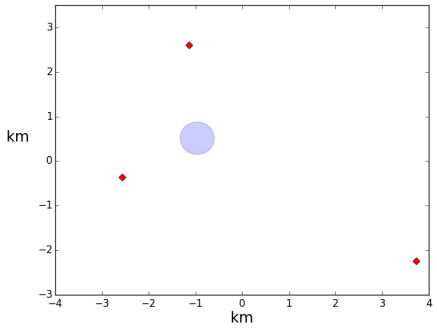

Figure 16: Example of event with standard deviation equal to 0.37 (limit is 0.5) plotted in a simple sketch of the area of interest, scale in kilometers.

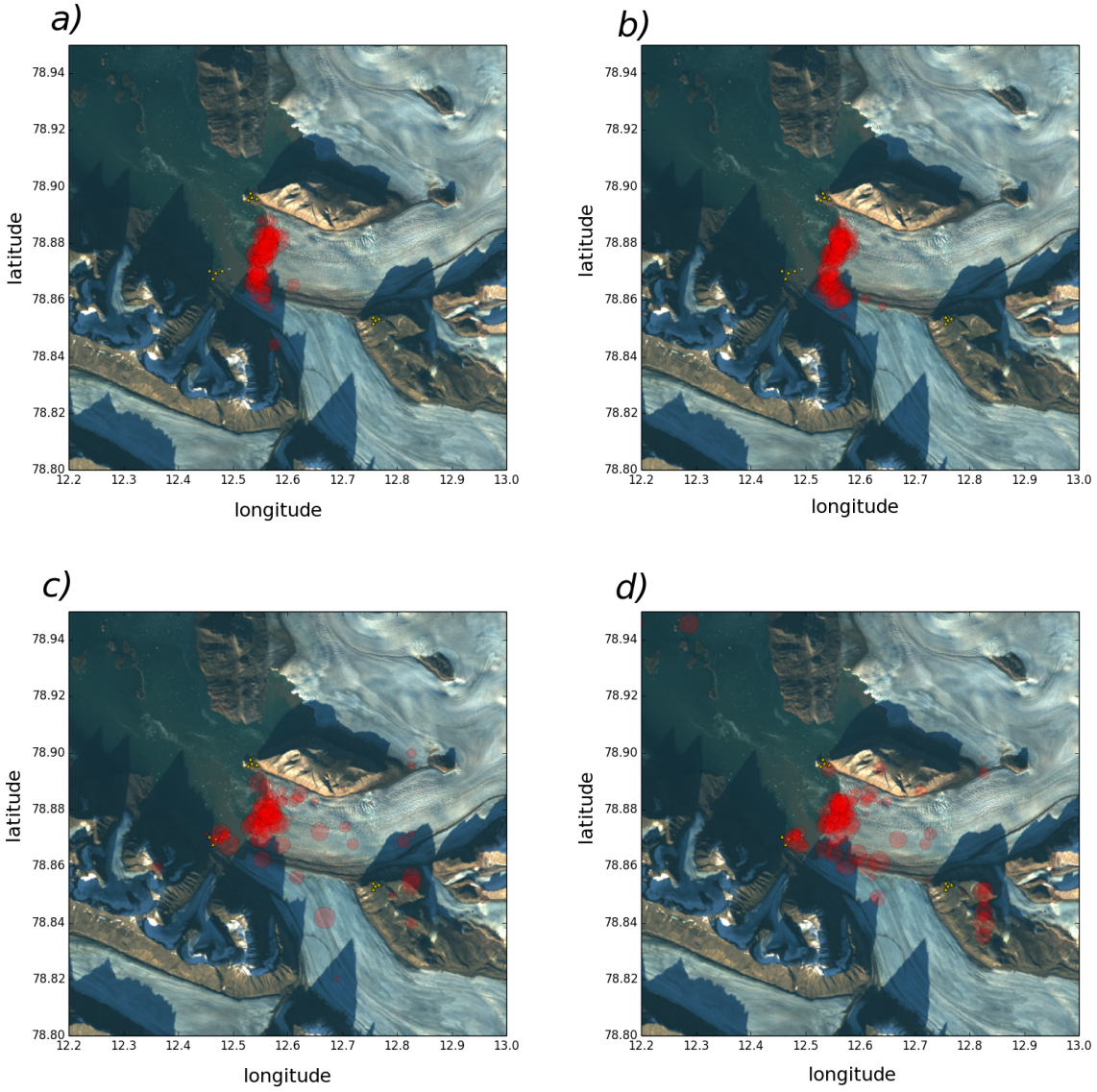

Figure 17: Example of SMAB methods plotted into the map for day number 203, *a) mean location*, parameters: 2 second time window, constant velocity of 3 km/s, *b)*: *mean location*, parameters: 2 second time window and velocity from FK, *c)*: *the best time window location*, parameters: 2 second time window and constant velocity of 3 km/s, *d)*: *the best time window location*, parameters: 2 second time window and velocity from FK. The radius of the plotted circles represent the uncertainty of the location which is obtained from standard deviation of either longitude or latitude.

proportion of successfully located events compared with FK. The last column of table 3 displays the percentage of events that did not reach the needed threshold (with respect to FK). The time shift corresponding with seismic velocity of 4 km/s lead into unsuccessful stacking and hence the relative power was too low for some events. For this reason combinations number 3 and 4 were not used for further analysis.

While using constant velocity of 3 km/s, the number of events not reaching the threshold was lower and combination 1 provided more events reaching the threshold than combination 2. For combinations number 5 and 6 (velocities obtained from FK analysis) all the events reached the threshold. For further analysis combination number 5 was chosen and 210 events were processed to investigate the computed locations for both approaches of SMAB method (combination 6 worked well also but shorter time windows are preferred to avoid mixing phases). All the events were plotted for each of the selected days 129, 181 and 203 into a map. Day number 203 (figure 17) was chosen as an example. It is very obvious that *best time window locations* are much more scattered at the glacier terminus than *mean locations*. The same pattern is found in the other two days plots. The combination using FK velocities was expected to provide the best results since more realistic velocities at each array are used. Constant velocity of 3 km/s results however do not vary significantly from those using FK velocities (figure 17 *a)* and *b)*).
The *mean location* approach is more appropriate and will be applied for the whole dataset. The parameters will be set with time window length of 2 seconds and velocities obtained from FK analysis.

4.6 Phase picking processing

The phase onsets were picked using Snuffler. Only very clear signals can be picked correctly and hence only a fraction of events was possible to chose for this analysis. Events located at Kronebreen with FK were used to pick the phases to allow comparison between found locations. Events exhibiting coherent phase on each array could be selected for picking. From one station of each array the first phase onset was picked as later phases arriving are tricky to pick correctly. In some cases only two arrays were possible to pick because of background noise. These time data were listed in a text file and Python program was made for further calculation (script in appendix).
The elevation difference needed to be included in this method since the distance of the source is crucial for computation. The wave travels upwards to reach the stations of array C and hence the distance between grid point and C station was extended in the script by elevation difference. This is approximately 500 meters and this extension represents the upper limit for distance since signal must travel almost vertically to reach the seismic array. The computation was tested with and without the elevation difference to see how big effect is.
Color gradient map was created as a result and the lowest t_{diff} showed the possible sites of the event origin. In the same figure the FK location was plotted to make direct comparison possible.
This method was tested also for constant velocity to check if it can be used independently without FK analysis. Constant velocity was chosen to be 3 km/s. All the results are presented in the next chapter.

4.7 Event classification

The final separation was based on both location of the event and characteristics of the signal. For each event a map plot is created together with frequency spectrum representing the signal. Both obtained locations, FK and SMAB were plotted together into the Kronebreen map. For this task satellite figure was used captured on 19/9/2013. Even the figure was captured after the monitoring time, the terminus was at a pretty stable position which is later supported by more figures and terminus studies. To analyse the frequency representation, spectrograms are computed along the

events (figures 25, 26, 27).

4.8 Multiple calving and acoustic wave

Multiple calving occurs at the glacier terminus sometimes during the recording period. These events have duration from 30 to 70 seconds and calving signal characteristics. Chosen events were processed with FK analysis to observe possible backazimuth and velocity variations of the signal. Some parameters in the analysis needed to be re-calibrated. Duration of the FK analysis was extended to 70 seconds as the majority of them did not reach 1 minute duration. Longer events were divided into two parts for the analysis (used only twice out of all multiple calvings). Backazimuth standard deviation limit was increased up to thirty degrees since multiple calving may start at one point and continues along the terminus.
The geophones also recorded an acoustic wave in the air which followed some of the icequakes. The air wave contains much higher frequency, has shorter duration and also much lower velocity compared to the seismic wave (around 300 m/s). Total number of events selected was 202 but the air wave is not recorded at all the stations for each event which is crucial for successful beamforming. It can be observed mostly at 2 to 4 stations of array A and sometimes at some stations of array B. Array C seems to be too far to contain air wave for majority of the events. Four representative events were selected with acoustic wave on most of the stations and these were analyzed with both FK and SMAB methods. During the FK processing, maximum slowness value 4.0 s/km in each direction was chosen since $v = \frac{1}{s} = \frac{1}{4} = 0.25km/s$ which is lower than velocity of the acoustic wave. Hence the FK analysis was performed with increased slowness grid up to 4.0 points in each direction. The frequency range was set between 20 and 49 Hz.
For SMAB processing, constant velocity was set to 0.3 km/s and frequency range was set between 20.0 and 49.0 Hz. Length of sliding time window was set to 1 second since longer window did not provide any results. However, time window this short cannot cover the air wave on both arrays (since air wave is slower and must have longer delay between arrays) and hence *the best time window location* is used in this case. Phase picking was tested for acoustic wave as well (see Results).

5 Results

Results are presented in this chapter for each localization method for 21 days and their advantages and drawbacks are analyzed.

5.1 FK localization

Events with clear, coherent signal are expected to have distinctly higher values of relative power than background noise. Backazimuth should have stable value along the coherent signal while velocity (derived from slowness) can vary as different phases occur along the signal. Figure 18 shows seismic signals recorded at array A and B which both exhibit stable backazimuths while velocities start with higher value and slightly decrease. Array C is situated in a noisy environment and hence the signal is often not very clear. This decreased the ability of coherent signal stacking, example can be seen in figure 19 where triangulation was successful but array C (bottom left) has worse signal than other two arrays and the corresponding backazimuth and velocity plots are noisy. Array C often

did not reach either threshold value of relative power RP or narrow standard deviation condition while processing which can be partly caused by further distance from the terminus.
Typical velocities values vary between 2 and 4 km/s, some events exhibit velocities lower than 2 km/s, especially array A. Array C on the contrary demonstrates velocities sometimes higher than 4 km/s (up to 7 km/s) which supports more vertical path of the energy traveling upwards (since apparent velocities get higher with steeper ray path, see equation 1). The real medium velocities are difficult to determine without any subsurface model. In example from figure 19, arrays exhibit mean apparent velocities at arrays A, B and C of 2.7 km/s, 3.0 km/s and 4.5 km/s respectively. Similar values were obtained for most of the events.
The velocity values along the coherent signal is often stable but sometimes more phases with different velocities can be observed. If velocity differs along the signal, it starts often at higher

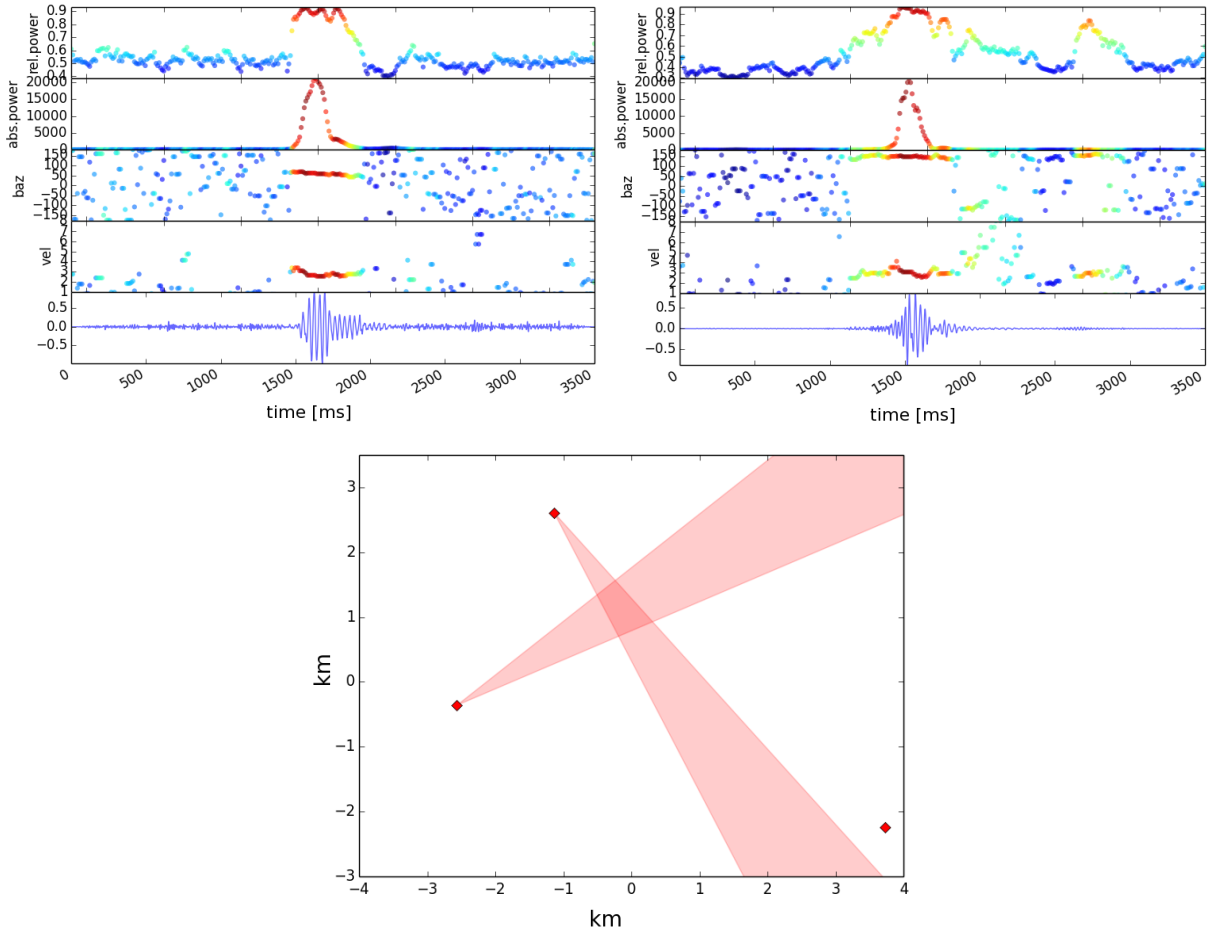

Figure 18: FK analysis example of event from day 202, only arrays A and B available.

values and gradually or steeply drops down (some events however show increase in velocities). This indicates that P and later S or surface waves are present. Events with velocity within narrow range (the value is never completely stable) have probably mixed phases that were not separated by distance yet.
Backzimuth was used to separated events with stable direction of arrival from the rest. This

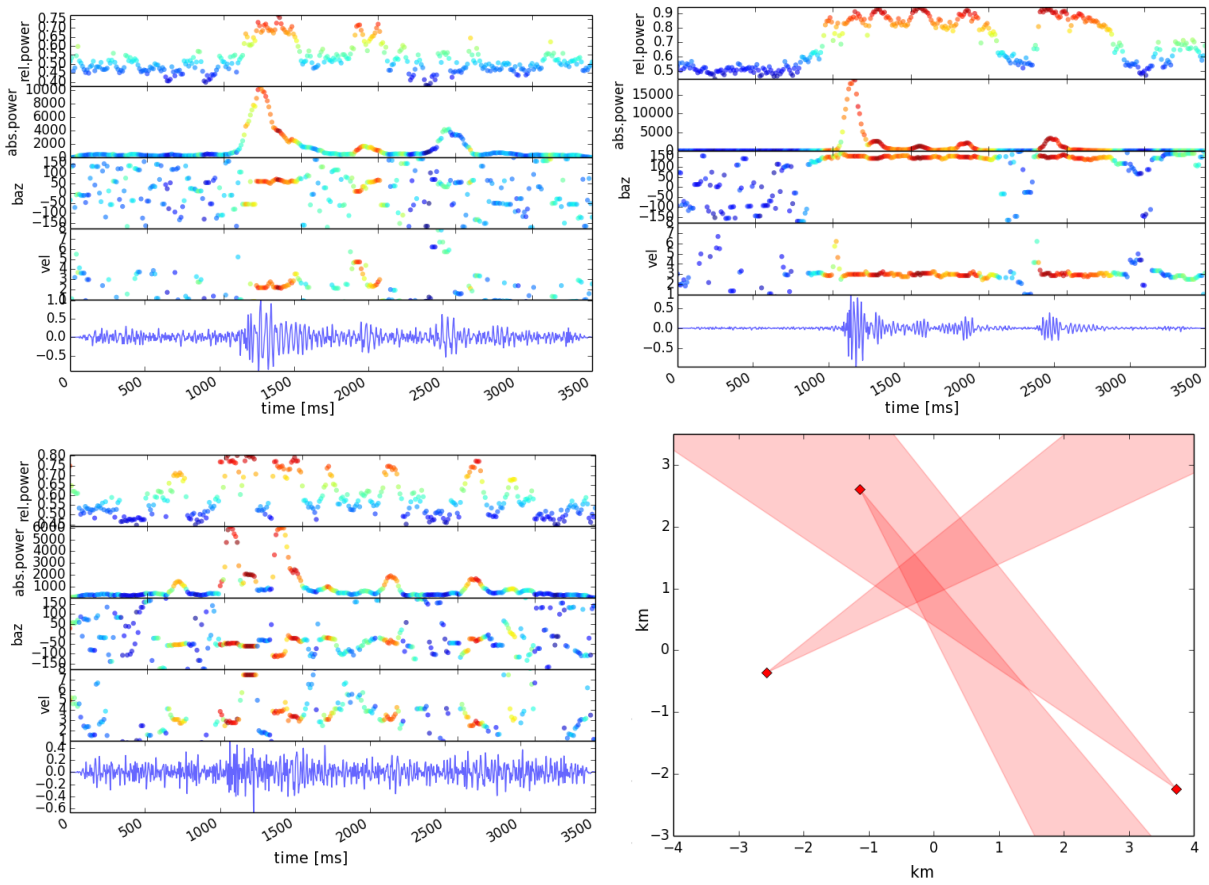

Figure 19: FK analysis example of event from day 126, all arrays available.

was done by setting maximal standard deviation to $\sigma_{\theta max} = 20°$. Array C often obtain higher uncertainty compared to other two arrays. Number of all events originating from Kronebreen area are listed in table 4. Increase of the activity with time is noticeable. All locations before event classification can be seen in figure 20 with one example of localization uncertainty.

Table 4: Events located at Kronebreen with FK analysis.

Day number	Number of events	Day number	Number of evets	Day number	Number of events
126	46	178	41	200	80
127	23	179	76	201	92
128	19	180	65	202	85
129	38	181	53	203	119
130	47	182	52	204	141
131	11	183	89	205	152
132	33	184	62	206	165

5.2 SMAB localization

This method used only arrays A and B. There were slightly more events located in Kronebreen area than with FK method (table 5). Uncertainty varies below 0.5km. All locations originating from Kronebreen were plotted into a map (figure 21) with one example representing standard value of localization uncertainty.
In total there were 226 events located from Kronebreen area for week 1, 487 for week 2 and 862 for week 3. These locations will be further examined and compared with those located by FK.

Table 5: Events located at Kronebreen with SMAB analysis.

Day number	Number of events	Day number	Number of evets	Day number	Number of events
126	48	178	39	200	83
127	26	179	81	201	97
128	19	180	72	202	84
129	39	181	77	203	125
130	48	182	51	204	143
131	11	183	101	205	159
132	35	184	66	206	171

5.3 Phase picking localization

Elevation difference included in the script did not have such a significant impact on the final location. Switching from FK velocities to constant velocity of 3 km/s however showed greater location difference. In the same grid search showing lowest values of t_{diff} (white color) FK location was plotted to make direct comparison possible (figure 22). In total there were 304 events used for phase picking.
In the third week array C contains more noise than the other two arrays and hence FK analysis did not provide velocity for each event. In such a situation constant velocity is a good approximation. Computed locations are compared to FK locations: 122 events demonstrated closer location to FK using FK velocities. 55 events exhibited closer location to FK using constant velocity and 122 showed no effect while switching between velocities.
In table 6 final event numbers are listed. Much more events could be picked on array A and B while array C gave only fraction of visible phases. Events with picked phases only on two arrays have all their possible source locations on a curve (figure 23) and were not used further. All events located with three arrays are plotted into the map (figure 24). It is obvious how small part of events could be located by phase picking. The scatter of the locations from the terminus illustrates that this method does not have very high accuracy due to wrongly picked phases, and higher level of noise.
If only two stations can be used for phase picking, and signal characteristics classify that this is a calving event, the curve of all possible points can intercept with the glacier terminus line and this intercept point can be assumed as location of the event. However, the number of localized events would still provide only a small portion of FK locations.

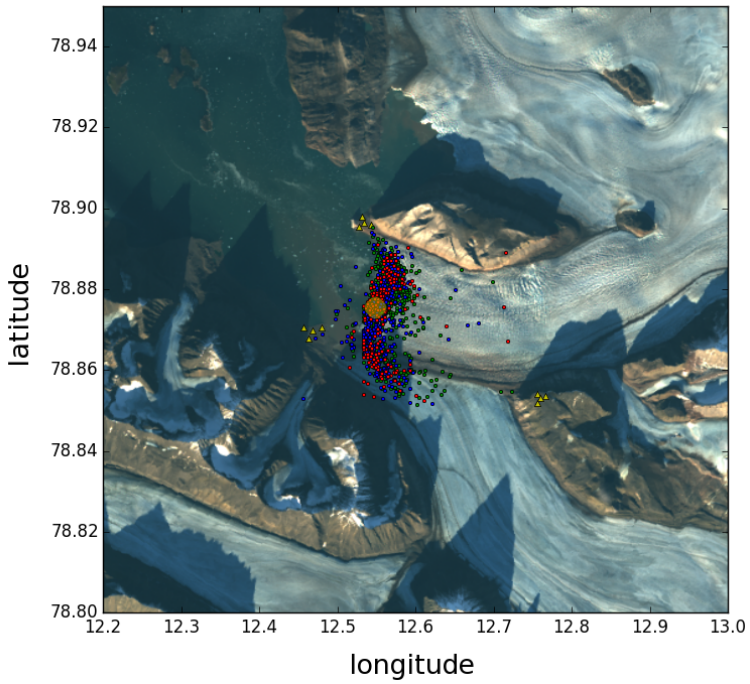

Figure 20: FK locations of all events originating from Kronebreen, week 1 (red color), week 2 (blue color) and week 3 (green color) with one example of uncertainty with radius of 150 meters (yellow color).

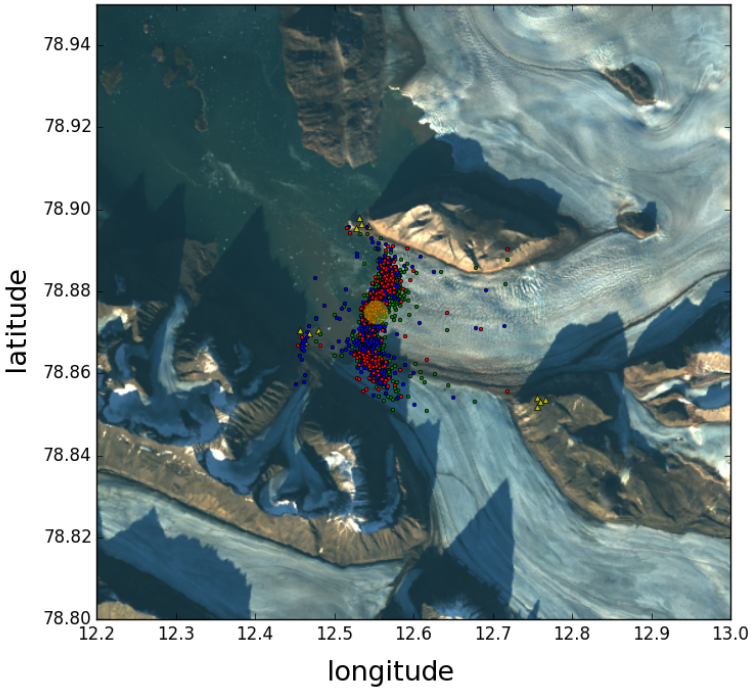

Figure 21: SMAB locations of all events originating from Kronebreen, week 1 (red color), week 2 (blue color) and week 3 (green color) with example of uncertainty with radius of 200 meters (yellow color).

Table 6: Overview of event numbers, weeks 1 - 3.

Week	Number of events	FK located at Kronebreen	Phase picked (2 stations)	Phase picked (3 stations)
1	625	217	22	16
2	1168	438	108	20
3	1619	834	124	14

5.4 Final event classification

Six icequake groups were established:
Group 1 : Location at the terminus (or within 200 meters distance from the terminus), signal with calving characteristics: narrow frequency band, short duration.
Group 2 : Location at the terminus, signal with not clear calving characteristics (with a lot of noise).
Group 3 : 'Bay calving', location in the southern part of the Kronebreen glacier situated further from terminus (explained below), signal with calving characteristics.
Group 4 : Kronebreen - Kongsvegen interaction, location at the boundary line, signal distinct from calving.
Group 5 : Other not interesting events.
Group 6 : Not fitting any of the first four groups, but having special characteristics or location.
Most of the events were located with both FK and SMAB method, some locations were however provided by only one method, this is discussed later. During the classification it was sometimes disputable if the events belong to group 1, 2 or 3.
Most of the events were classified as group 1, example is displayed in figure 25 in the left panel. Group 2 included less events and example is in figure 25 in the right panel.
'Bay calving' (group 3) was suggested to be happening in the southern part of Kronebreen - Kongsvegen system as calving locations seem to be retreating further into the glacier's tongue area (example in figure 26, left panel). In May 2014 there were seven time-lapse cameras installed at Kronebreen glacier to follow the glacier's flow and examine speed. These took picture every 30 minutes during the day light until September 2014 and final movie was made by picking the best picture for each day and showing them in a row as a movie. The result can be found at http://www.youtube.com/watch?v=Llod4k0-1DCY (or just 'Kronebreen time lapse' searched on http://www.youtube.com). In this short movie the terminus position can be observed during the spring and summer. One year earlier the dynamics is expected to be very similar and hence the movie can be compared to the seismology investigation. In these time-lapse figures a bay like structure is gradually created in the southern part of the terminus as the glacier calves away with time. This gave idea for 'bay calving' and it can provide possible explanation for calving like signal coming from inside the glacier in the southern part of the tongue.
Kronebreen and Kongsvegen (group 4) were expected to produce signal resulting from their interaction since Kronebreen is fast moving compared to Kongsvegen and therefore separate group was created for these events. The total amount of these events is only 10 during the investigated weeks. The signal contains high frequencies and exhibit neither clear duration nor phases. The only indications speaking for classifying as glaciers interactions are location on the boundary line and signal which is not like calving but has no specific features. Example can be seen in figure 26 in

the right panel. The signal features of group 2 and group 4 is similar and hence location was used to distinguish between them. However, events from group 4 can also represent calving originating from the front but mis-located while processing as the methods do not work perfectly.
Events classified as group number 5 do not fit any criteria above and for that reason have no important role in this investigation. These events will be excluded from further discussions.
Group number 6 was created to label interesting events while processing the data. These events did not fit in any of the previous groups but for some reason were stored for later discussion if needed. There is for example event cluster very close to array A during the day 30^{th} of June. The record on array B exhibits very noisy signal with unclear onset while array A signal has very short duration (around 3 seconds) and narrow frequency band. This cluster has 17 events that look the same and originate from the same location on the land very close to array A. These are recorded between 5 am and 18 pm and are located only by SMAB analysis. Example is displayed in figure 27. Source is not known but it could be for example a mountain glacier. Such a signal would be however expected to occur during more than just one day and hence it could also indicate human activity.
The rest of the events classified in the group 6 were mostly calving like signals situated far from the terminus or on the rocks with no specific relations. Methods are not working perfectly and these signals can be just incorrectly located calving events. They were however excluded from calving groups since both FK and SMAB methods provided the same locations (or very similar) and hence it could be also different activity which has signal characteristics similar to calving (for example iceberg break-off on the fjord). This type of events apart from cluster during the day 181 occurred 13 times.
Final numbers of all classified events are expressed in table 7 and all locations are plotted in figure 28, bottom right.
As expected the glacier activity was lowest in the first and highest in the third week. Majority of the Kronebreen activity was classified as calving events (groups 1 - 3), exactly it is 1399 calving events during 21 days from total 1604 events located at the glacier's tongue and from totally 3412 events that were picked in the beginning.

6 Discussion

6.1 Method comparison

Phase picking as expected did not provide enough event locations but demonstrated that most of the picked events correspond well with FK locations. This correlation is mostly observed while using specific velocity input obtained from FK. Phase picking used independently with constant velocity estimation did not provide very good results compared to FK locations. Lack of clear phases and lack of velocity model is crucial drawback for this method in the noisy environment with weak signal. Phase picking can however be used in case of not fully working arrays or while using single stations.
Locations obtained from FK analysis were successfully plotted around expected terminus area and corresponding frequency spectrum supported the final classification as calving events. The assumption of planar wavefront is the main drawback for near events. Obtaining slowness of the signal is however advantage of this method even it might contain small errors (because of non planar wavefront).

Table 7: Events located at Kronebreen with both FK and SMAB analysis.

Day number	**Group 1**	**Group 2**	**Group 3**	**Group 4**	**Group 5**	**Group 6**	**SUM**
126	23	6	10	-	11	-	50
127	13	3	2	1	7	-	26
128	11	1	5	1	1	-	19
129	25	3	8	-	5	-	41
130	22	8	15	-	3	2	50
131	8	2	-	-	1	-	11
132	18	3	9	-	5	-	35
sum	**120**	**26**	**49**	**2**	**33**	**2**	**232**
178	24	1	13	1	3	-	42
179	48	4	17	-	12	1	82
180	49	2	10	-	11	2	74
181	33	3	13	-	10	18	77
182	28	6	13	-	4	1	52
183	58	13	17	-	14	1	103
184	44	3	66	-	10	-	67
sum	**284**	**32**	**93**	**1**	**64**	**23**	**497**
200	52	5	17	1	4	1	80
201	54	18	11	2	10	2	97
202	55	11	10	1	10	-	87
203	79	17	17	3	10	-	126
204	93	23	21	-	11	-	148
205	119	20	13	-	9	1	162
206	119	20	21	-	14	1	175
sum	**571**	**114**	**110**	**7**	**68**	**5**	**875**
SUM	**975**	**172**	**252**	**10**	**165**	**30**	**1604**

The distance between arrays A or B and terminus related calving events can become less than 1 km. With respect to the size of the array aperture (150 -500 meters between geophones) the distance is too small to record plane wavefront. SMAB method cannot estimate slowness of the energy but removing the assumption of planar wavefront was expected to provide better results. This method seems to be more accurate as the locations deviate less from the terminus.

All events locations from groups 1 and 2 were plotted for each method to examine scatter from the terminus (figure 29). SMAB locations (right) are grouped denser than FK locations (left) which illustrates more accurate locations obtained with SMAB method since all plotted events are classified as calving front events.

Example of one day plotting into the map can be seen in figure 30 (groups 1 - 3). The scatter around the terminus is greater for FK locations (left) than SMAB (right) which is the general pattern observed in the rest of the day maps (21 examples in total).

Arguments to choose SMAB as the most appropriate method for icequakes localization are: locations demonstrated best grouping around the terminus. This method also provided more events

locations. Exact numbers are:
1327 events located with both FK and SMAB methods,
20 events located only by FK,
45 events located only by SMAB.
SMAB method located 25 more calving events than FK.
Velocities obtained by FK analysis were used for SMAB analysis. However, testing with constant velocity of 3 km/s displayed very similar results and hence SMAB can be used separately with good results. Combination of FK and SMAB seems to work best.

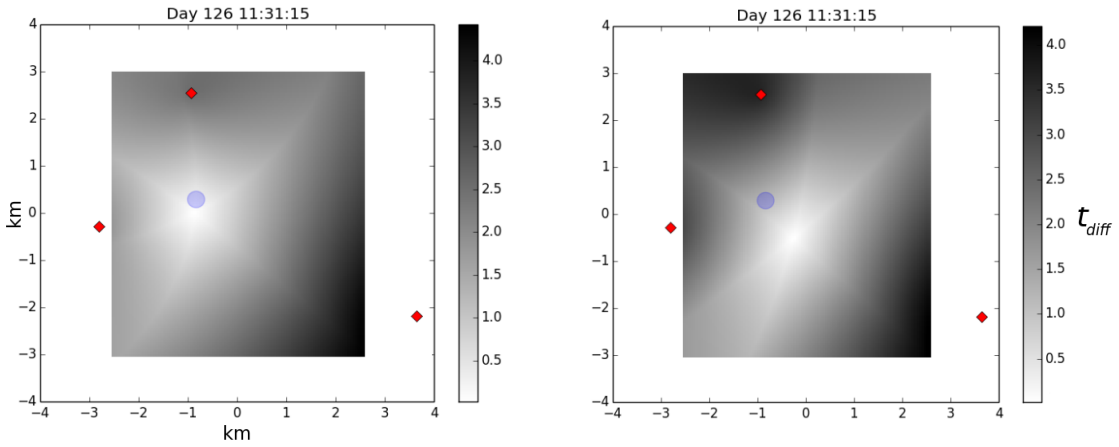

Figure 22: Phase picking location example of event from day 126, left is computation made with FK velocities, right with constant velocity of 3 km/s (blue circle represents the FK location).

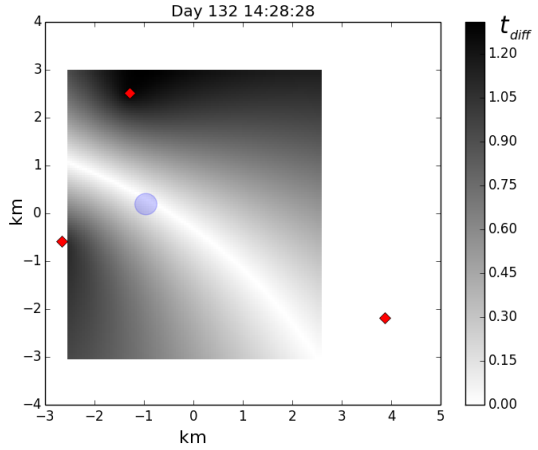

Figure 23: Example of event from day 132 when phase was picked only on station from array A and B.

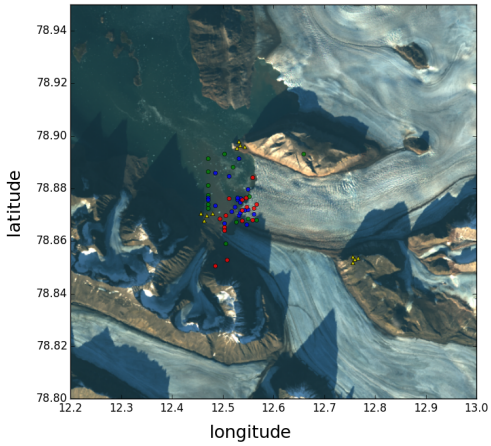

Figure 24: All locations gained by phase picking (phases picked on 3 stations) divided by color into week 1 (red), week 2 (blue), week 3 (green).

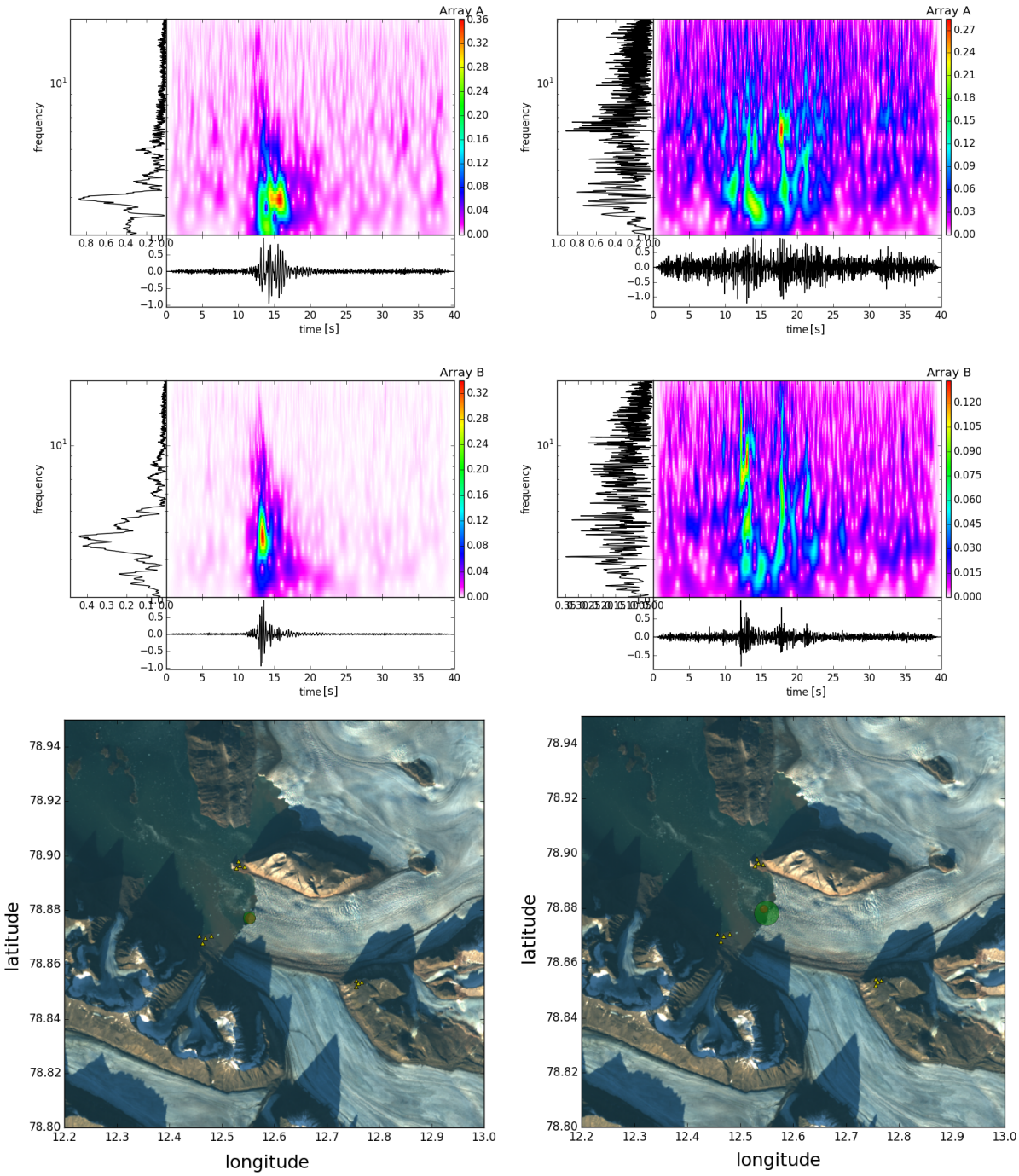

Figure 25: Left panel: example of front calving (group 1), right panel: example of noisy front calving (group 2), both located at the terminus (FK - red circle, SMAB - green circle, the left figure has both circles overlapping with almost the same radius and hence it is difficult to see, the right figure has smaller red circle inside larger green circle, yellow triangles represent the seismic arrays), signal recorded at SGLA1 in the top figures, SGLB1 in the middle figures and map locations in the bottom figures.

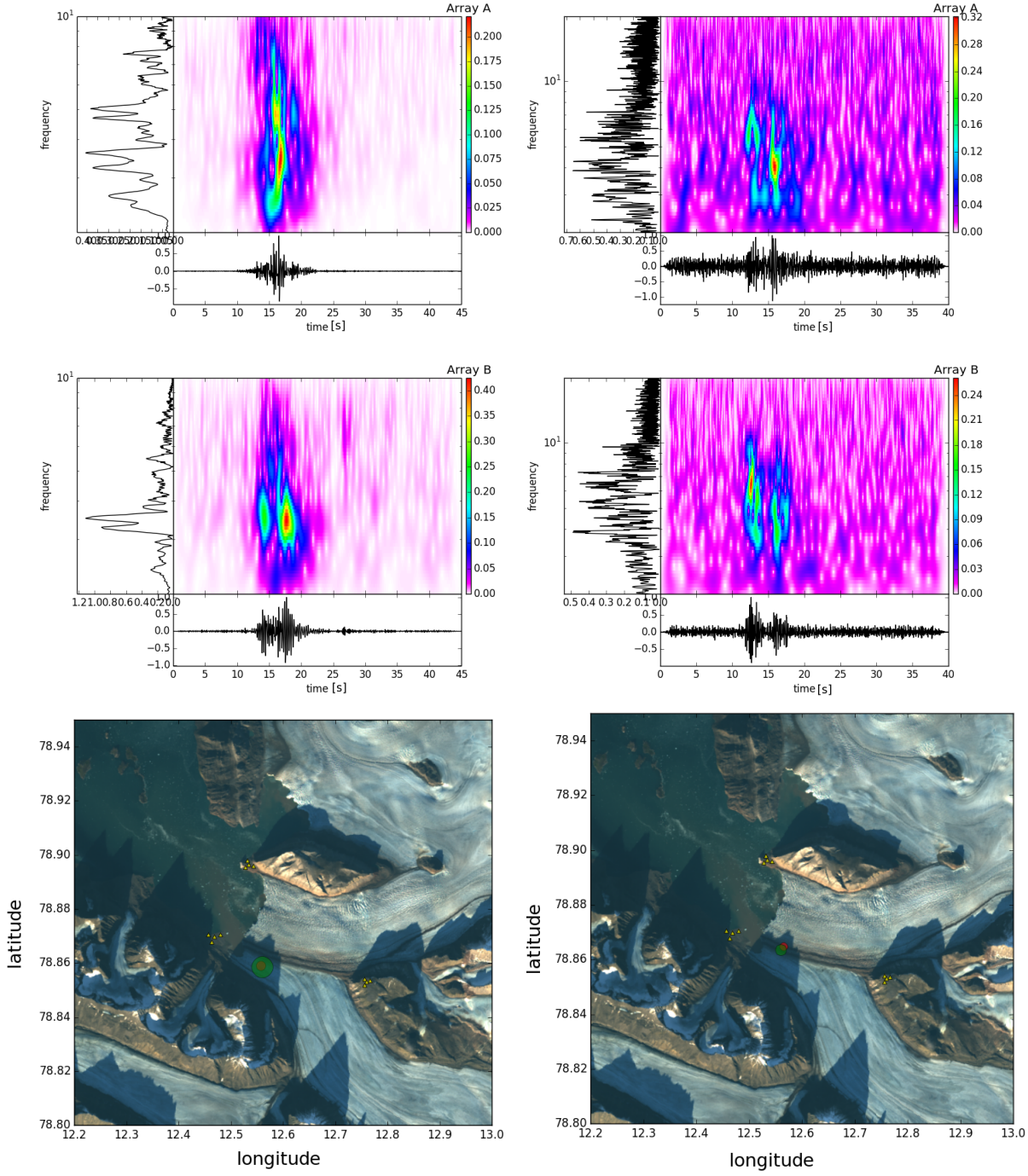

Figure 26: Left panel: example of bay calving (group 3), right panel: example of glaciers interaction event (group 4).

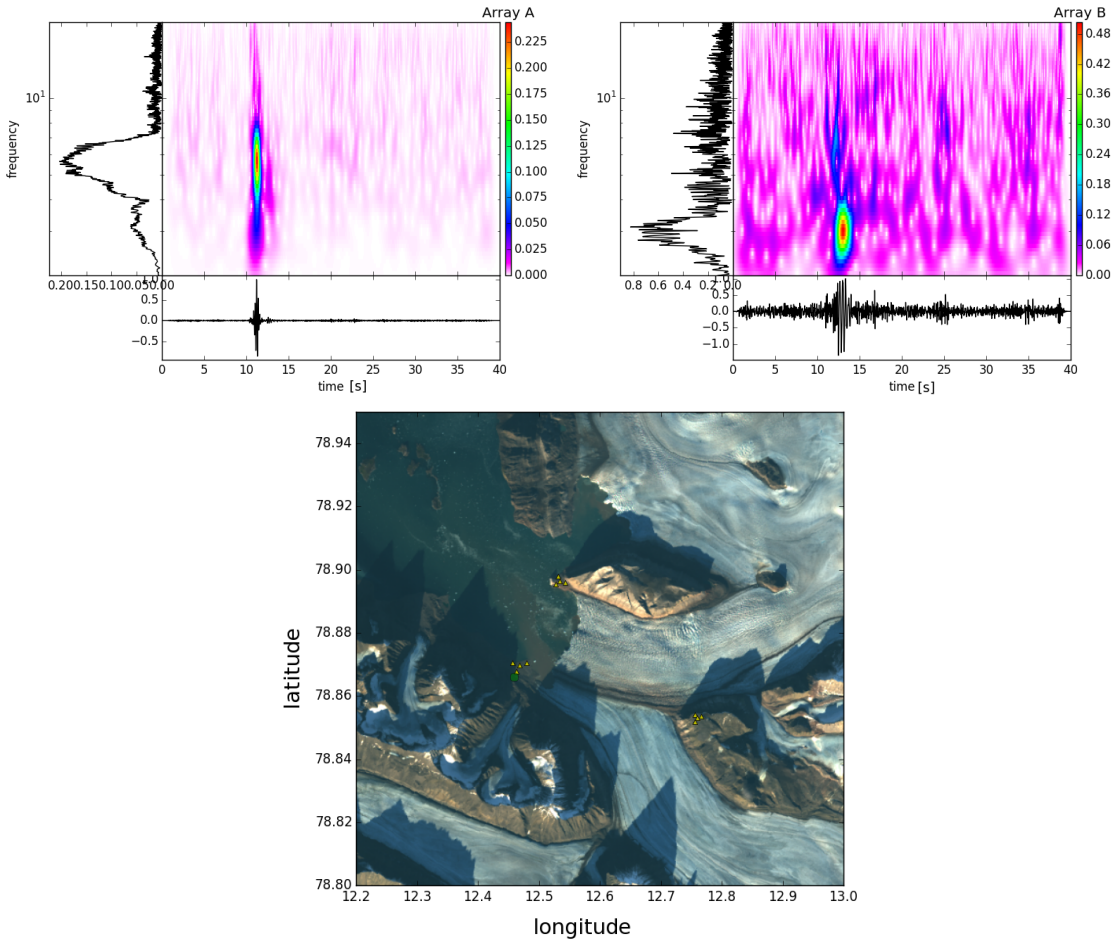

Figure 27: Example of one of events localized close to array A by SMAB method, icequake-like signal (top figures) and location plotted into the map (bottom).

6.1.1 Resolution of the methods and accuracy

The average value of FK backazimuth uncertainty is 9.5° for array A and 10° for array B (calculated as standard deviation of the backazimuth). SMAB method has average uncertainty value of $0.31km$ (calculated as standard deviation of longitude and latitude).
The localization resolution of both methods depends on the distance from both arrays. Simple test was performed to illustrate this (figure 31). Here, the average value of FK backazimuth uncertainty range was used (10°) to calculate crossing area of the two beams for different points of the glacier area. For FK method, an event originating from the central part of the terminus (point 3) has lower uncertainty than event originating from the bay structure (point 5) as uncertainty increases with distance. The beams that are stacked during SMAB analysis have higher inaccuracy with distance away from the array and hence similar trend is expected for this method.
The bay calving was classified depending mainly on the calving signal characteristics which are unlike those for other glacier activity. These locations however seem to be far from the bay cliff,

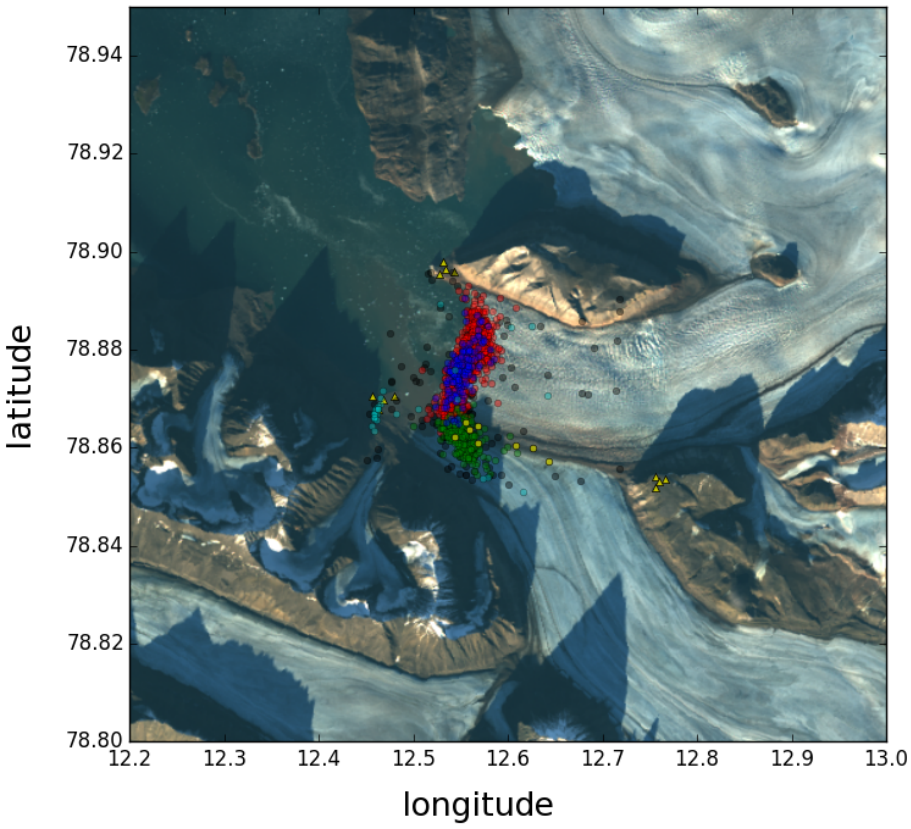

Figure 28: This map illustrates all the classified events locations with different color for each group: Group 1 (red), group 2 (blue), group 3 (green), group 4 (yellow), group 5 (black), and group 6 (turquoise), SMAB.

reaching deeper into the glacier's tongue, see maps in figures 28 and 30. During the recording period, the bay structure cannot perform such a great retreat (which is later illustrated by satellite figures) and hence the further locations from the terminus must be due to the uncertainty of the SMAB method.

Events which originate from an extended line connecting arrays A and B (for example backazimuth of $-160°$) may have much worse resolution for both methods (figure 31, points 3 and 6). This is caused by overlapping beams (and not crossing) which can lead into wrong origins. This is a drawback for both methods and for example the cluster localized close to array A during day 181 can in reality originate from further south. This can be however avoided by using a third seismic array.

The localization accuracy can be further affected by complicated velocity model (as the straight ray path assumption may not be valid). Inhomogeneities below the array aperture is another factor affecting the accuracy.

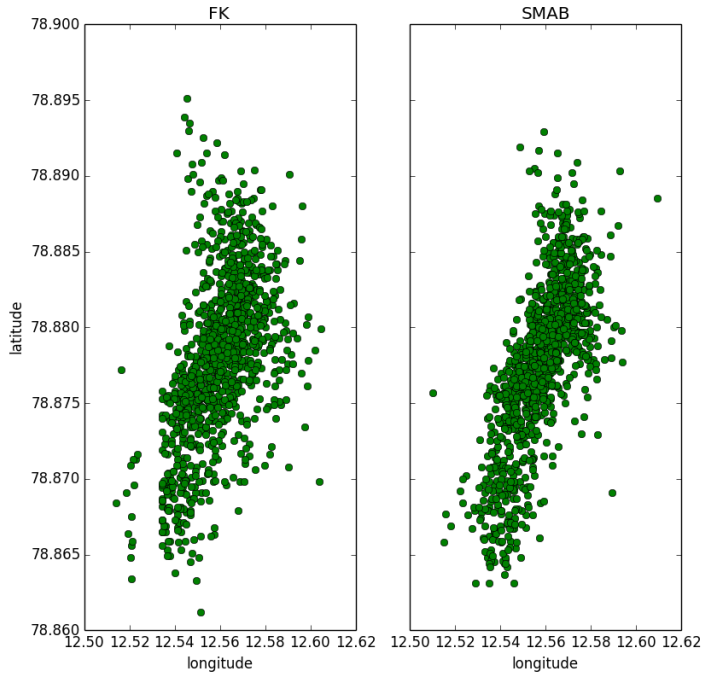

Figure 29: All locations from group 1 and 2 plotted together to illustrate scattering differences between FK (left) and SMAB (right) methods.

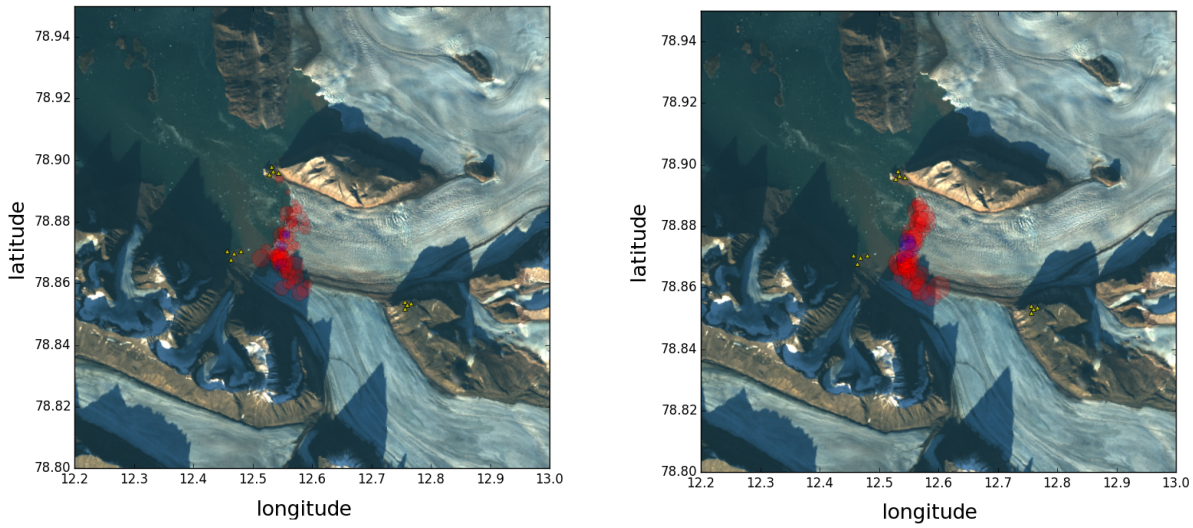

Figure 30: Example of calving locations obtained from FK (left) and SMAB (right) method, day 179. Red color represents clear signal (group 1 and 3) while blue color unclear (group 2, only two events in each map).

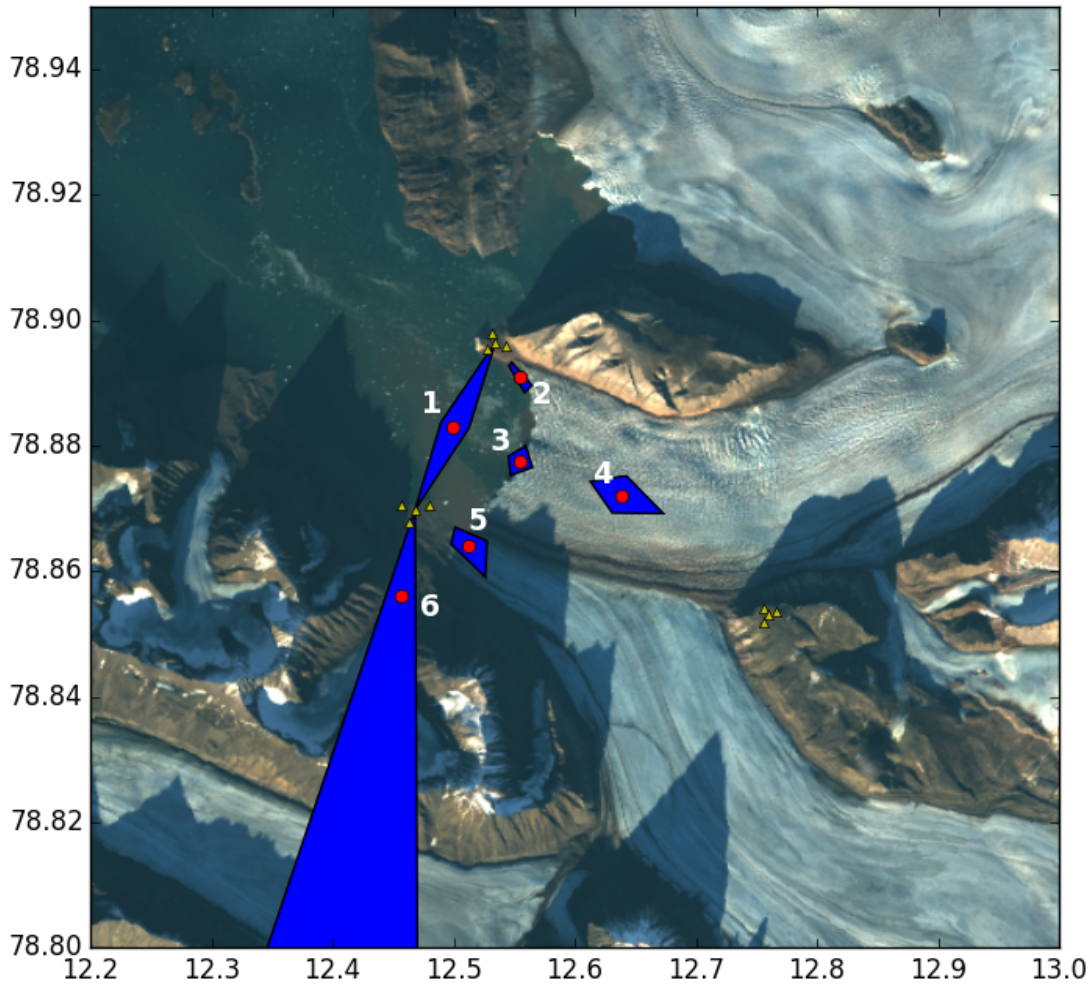

Figure 31: The resolution (blue polygons) is dependent on the location (red points). The north terminus location (point 2) exhibits the highest accuracy while location south from array A (point 6) has high uncertainty and event originating from this area cannot be located correctly.

6.2 Effect of array aperture and network geometry

Two fully working seismic arrays are sufficient for both FK and SMAB methods and for successful localization of icequakes in certain areas. Elevation difference of array C demonstrated failing backazimuth determination due to complicated travel path. Arrays A and B showed no complications as those had no elevation difference between each other and calving events (or very little).
Size of the aperture is different for each array. Array A has the largest size and array C has the smallest one. This has effect on FK analysis as different wave numbers can be resolved and FK diagram sidelobes have different distances from the main lobe. Array A has closest position of side lobes while array C provides windows with larger space between the main and side lobes which indicates less ambiguity (figure 32). However, the larger main lobe gives worse resolution of the backazimuth compared to arrays A and B where the main lobes are narrower. Most of investigated events had the same or very similar features of the ARF and in figure 32 are the most common cases chosen to be displayed for each array.
Array C provided lower ambiguity but worse resolution compared to other arrays. The backazimuths obtained had larger standard deviation. The further distance from the terminus caused

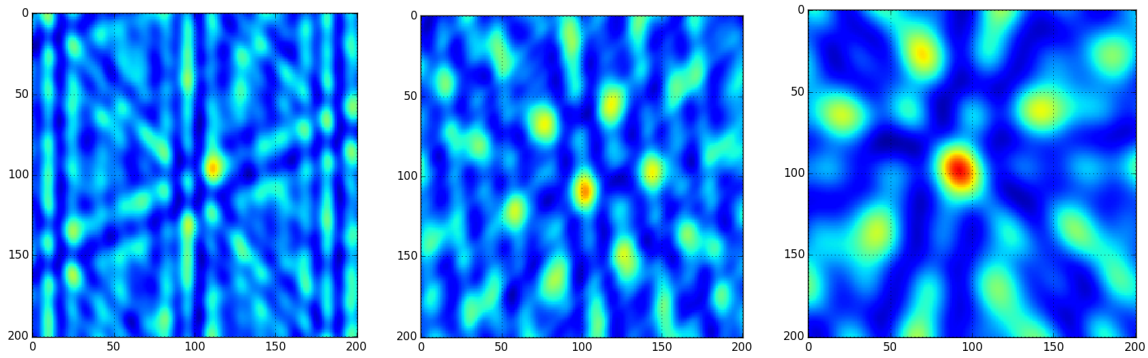

Figure 32: Examples of ARF to illustrate how the size of an array affects FK processing, from left: array A, array B and array C.

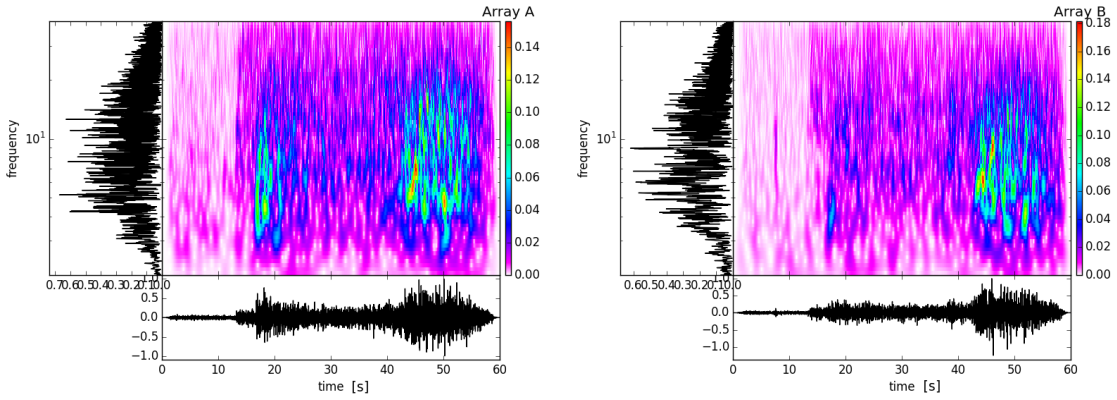

Figure 33: Example of signal and frequency representation from earthquake event, the same event recorded on array A (left) and B (right). The frequency analysis was made for band between 2 and 40 Hz.

noisy environment which lead to lowest proportion of successful stacking while arrays A and B were installed very close to expected events which resulted into good coherent signals for both of them.
For future studies the arrays should be placed close to the glacier terminus with size similar to arrays A and B. They must be placed in such a position to provide simplest possible velocity model for the traveling waves and hence the elevation differences need to be minimal between the arrays and the source. Locations were obtained using only two arrays which worked well but three arrays are recommended in case one array fails and to improve accuracy (in figure 31 the high uncertainty of point 6 could be avoided by using third array).

6.3 Icequake signal characteristics

The signal characteristics were described in previous works (e.g. Köhler et al. 2015a). During this examination the criteria did not change and here will be introduced only supportive examples. Frequency representation was made for few earthquakes picked from the first week to illustrate how distinct the signal is compared to icequakes (figure 33). There is a clear P wave and S wave. The frequency spectrum shows high frequency content (in the plot the frequency analysis was made for band between 2 and 40 Hz).
Very clear signal classified as calving is displayed in figure 34 where frequency band of the analysis is set between 2 and 10 Hz. The signal is short, with weak onset and with lack of clear phases. The frequency representation has narrow band between 2 and 5 Hz. Not all calving events demonstrate these values and many of them have upper limit of the frequency band around 10 Hz which makes the signal less clear but still easily distinguished from other types of events. Most of the events exhibited one peak in the frequency spectrum within the mentioned range while others did not exhibit one single peak. In figure 26 in the left panel the bay calving for array A has several higher values within the frequency range between 2 and 10 Hz while array B has only one clear peak. This could be due to a site effect (amplification at array A). Some events also exhibited two peaks in the frequency spectrum range.
Analyzing the source mechanism is beyond the scope of this thesis but assumed model follows the work of Bartholomaus (2012) who suggested event origin from the interaction between the iceberg and sea water.

6.4 Spatial and temporal distribution of calving

For the icequake distribution only locations obtained by SMAB method were used since it was evaluated as the most appropriate method. In general the frequency of calving events increases with summer time. During a single day the calving activity has slightly higher values in the second half of the day which can be seen from histograms in figure 35 which represents stack of days within each week. Pattern in week 1 deviates from the other two weeks with peaks in the middle of the day while the activity decreases in the second half of the days. Week 2 and 3 have slight growth with later hours and both have peak between hours 19 and 20. This pattern is however not very pronounced. Plot for each week without stacking was made to investigate any periodicity with period longer than 24 hours. In figure 36 the calving rate per hour for week 3 was plotted together with ocean tides. Week 3 is used since it has the highest amount of icequakes and is most likely

to show pattern if any. The calving rate seems to increase and decrease periodically rather than randomly and hence the ocean tides could be affecting the calving rate. This is further discussed in the chapter 6.6.

Spatial distribution of icequakes was examined. All the terminus locations (groups 1 - 3) for each day were plotted into the map as described in previous chapter. Due to the inaccuracy of used methods one cannot expect all sites to be located exactly at the terminus line. Also the terminus is assumed to be slightly moving back and forwards as the calving and sliding of the glacier happens simultaneously. Both of these reasons result into scattering calving locations around the terminus. To examine how accurate the locations are, the possible retreat of the terminus was traced (the retreat of Kronebreen in 2013 was documented by Schellenberger et al, 2014). If the method is accurate enough, the icequakes should exhibit a shift of the locations during investigated weeks. To make this possible the coordinate system was rotated counter clock-wise with angle of 25° to put the terminus in such a position to be parallel with y axis. Groups 1 and 2 (front calving) were used for this investigation (figure 37). The front was divided into six parts, each 500 meters wide. The amount of calving events for part 1 is 107 (7.8%), 276 for part 2 (20%), 336 for part 3 (24.3%), 240 for part 4 (17.4%), 114 for part 5 (8.3%) and 63 for part 6 (4.5%). Bay calving which is not included in this analysis has 243 events (17%). The x coordinate was then plotted for each part with time dependency (figure 38). The blue connecting lines between clusters represent mean value of the x coordinate which should represent the average position along the x axis for each part of the divided terminus and should illustrate movement of the terminus with time. These mean values are plotted together on figure 39 to investigate any trend.

The main calving activity is located in the central part of the terminus (parts 2, 3 and 4) while the side parts are less active. In figure 39 we see that the mean x-values in the central part exhibit the same trend. The average x coordinate increases along the time axis which illustrates a retreat of the terminus. The central part is expected to have mostly accurate locations as discussed before and hence it should exhibit the best indication of retreat if any. The central parts have also highest portion of the calving events which decreases the uncertainty while calculating the average value of x coordinate. Part 1 shows similar trend as the central part but shows also advance between weeks 1 and 2. Parts 5 and 6 show very different trend which can be caused by lower number of events, higer uncertainty of the localization and also worse geometry (as the south part of the terminus is no longer parallel with y axis). This analysis may suggest retreat of the central terminus part around 100 meters (figure 39). This will be later compared with satellite map images but large scatter and high standard deviation make the interpretation difficult.

Bay calving exhibit variations in calving locations with time as well. Longitude development with time was analysed to examine possible retreat while creating the bay structure. This was done without previous rotation of the system (which was not needed in this case as the cluster is in a better position than front calving). In figure 40 the longitude is plotted chronologically as the bay calving was recorded for each week (243 events) with average value computed for each week (red triangles). The average longitude increases with time, which illustrates a retreat of this part of the glacier. The average longitude value for week 1 is 12.546, week 2 12.55 and week 3 12.558. Converted to distance, the retreat is approximately 250 meters between week 1 and week 3. This will be further compared to satellite figures but this distance seems to be too much. Due to high level of uncertainty in this part of the glacier the retreat is probably much smaller in reality. Figure 40 illustrates well how big the inaccuracy of the locations obtained from this part of the glacier is. The maximum in the third week reaches up to longitude value of 12.62 which

is in real distance almost 1.5 km from the average longitude value for this week (measured with http://toposvalbard.npolar.no).

6.5 Multiple calving and acoustic waves

In week 1 there were 12 multiple calvings recorded, 11 in week 2 and 49 in week 3. The FK analysis showed mostly stable backazimuths for array B where all the points of the terminus lies south of the array (approximately between 160° and 180° from north) and hence any calving signals along the terminus arrive from very similar direction. The other two arrays are however placed in such a position that a possible migration along the terminus during calving could be resolved by the backazimuths. Arrays A and C show mostly fluctuating backazimuth with time which could suggest several calvings that overlap. Such an example is displayed in figure 42 where array B has stable backazimuth (value 180 degrees) and also constant velocity while arrays A and C have much less stable values. Most of multiple calving events display the same features.
Chapuis and Tetzlaff (2014) describe one calving triggering another one, which results into multiple calving along the terminus. This suggestion fits well with the seismic measurements on Kronebreen. The temporal distribution did not show any specific pattern. In total there were 72 multiple calvings picked from total 1399 events which makes 5.1% of the amount.
For acoustic waves there were 4 events selected in week 1, 44 events in week 2 and 154 events in week 3 but only 4 of them were chosen for further analysis (as described in processing chapter.)
Frequency spectrum examination was done and some events exhibited clear presence of the air wave with high frequency content, example in figure 41. This example was chosen due to high SNR but majority of the events have air wave mixed with other sources of high frequencies. In this plot, one can clearly observe seismic wave having low frequency which is followed by short duration air wave with corresponding high frequency far above 10 Hz.
After performing FK analysis, only one of the four representative events had usable result as it displayed stable backazimuth for few time windows corresponding with maximum absolute power for each array (figure 43). This event named *air wave 1* went through more detailed analysis. FK showed backazimuths of A and B arrays crossing at glacier's terminus while array C is pointing at opposite direction. Velocity obtained from FK for this acoustic wave was 0.426 km/s which is close to theoretical acoustic velocity. This was used for phase picking. Picking the onset of air wave with Snuffler seemed to be easy as the beginning of much higher frequency signal is very clear. This is displayed in figure 44 where the array B records the air wave first followed by array A with small time delay. The wave arrives at array C with a time delay of around 20 seconds compared to other two arrays. This corresponds well with the distance between the terminus and array C which is around 6 km. Theoretically with velocity in range of 300 - 425 m/s, the travel time should be between 14 and 20 seconds which fits with the observed delay. The time delay within the array itself is however equal to zero in case of array C in figure 44 which indicates arrival of the air wave from above (possible refraction in the atmosphere) while both arrays A and B show usual time delay in between the stations.
Computing of the location by phase picking gave result slightly beyond the terminus (figure 45).
The best time window location was used during SMAB processing. The origin was located and plotted together with FK and phase picking results (figure 45). Here clearly phase picking gave the best result since the location is the closest one to the main event.

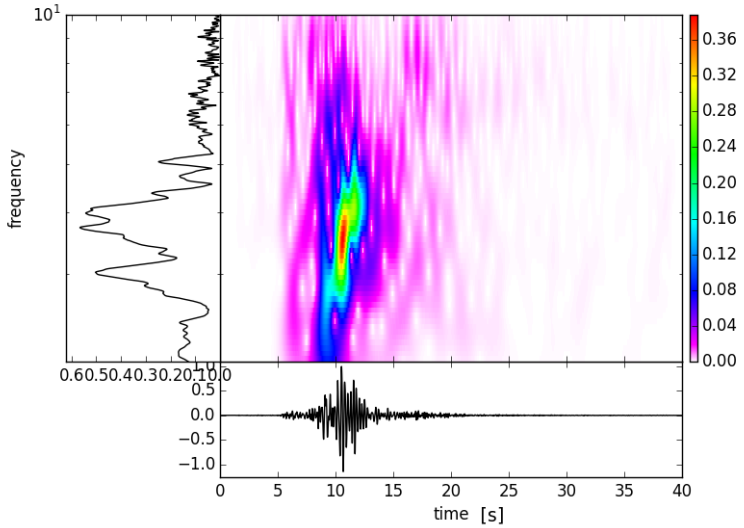

Figure 34: Example of very clear icequake event and its frequency representation.

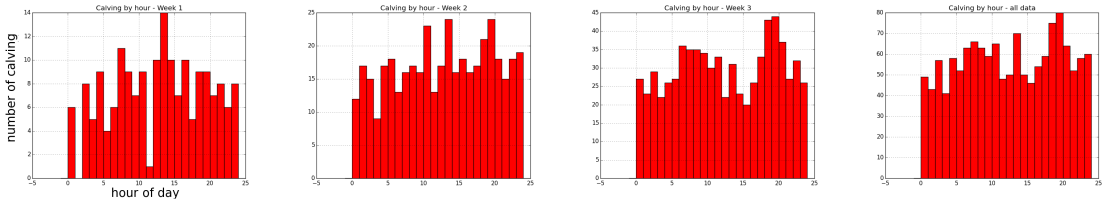

Figure 35: Amount of calving events per hour, from left: week 1, week 2, week 3, sum of three weeks.

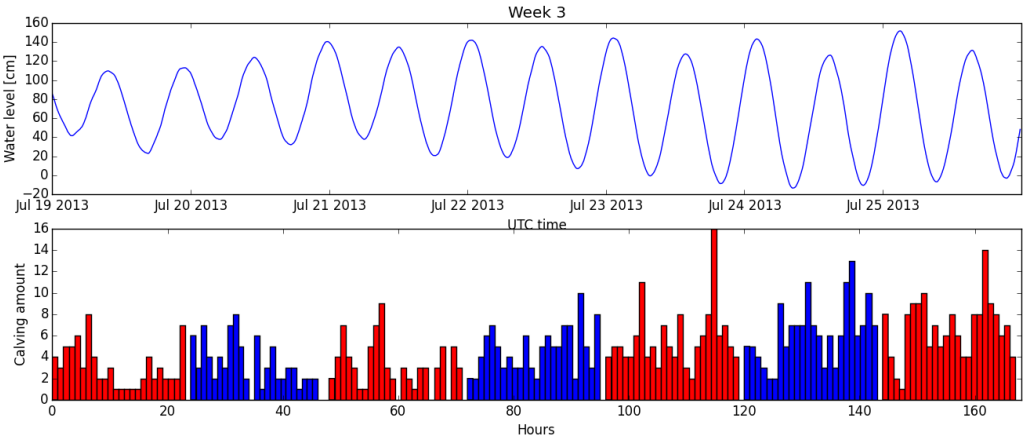

Figure 36: Week 3 calving distribution per hour, colors separate different days, plotted together with ocean tides.

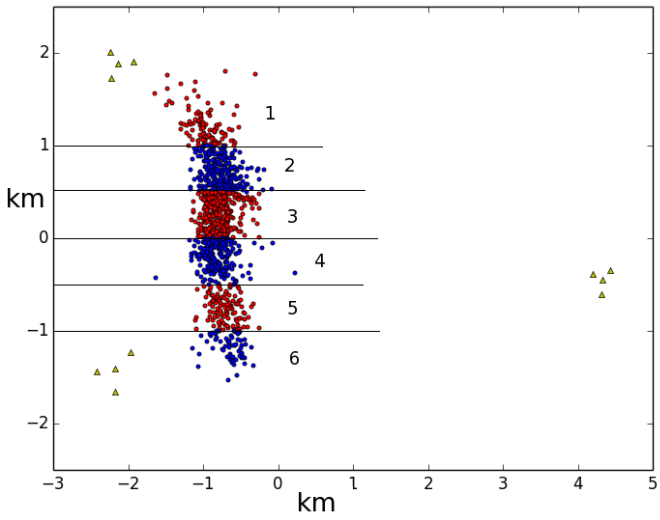

Figure 37: Coordinate system rotated with 25°, plotted calving SMAB locations: group 1 and 2 divided into six parts, triangles represent seismic arrays.

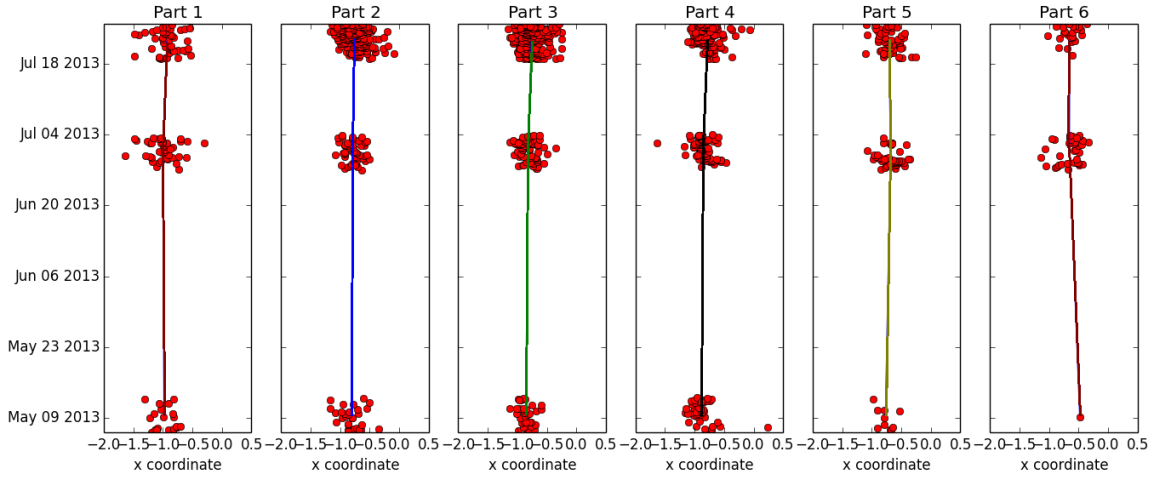

Figure 38: X coordinates in $[km]$ of groups 1 and 2 after rotation of the coordinate system (red dots) with connecting blue line representing the average value for each weak, terminus divided into 6 parts.

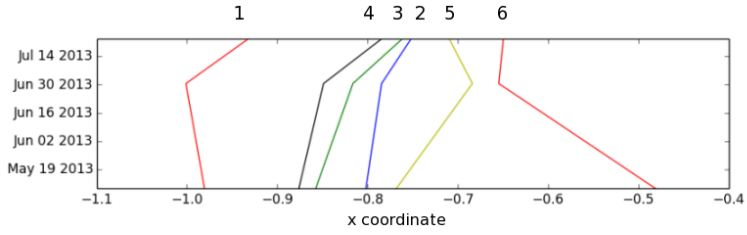

Figure 39: Average x-value for each part of the divided terminus plotted with time, top numbers represent part of the terminus.

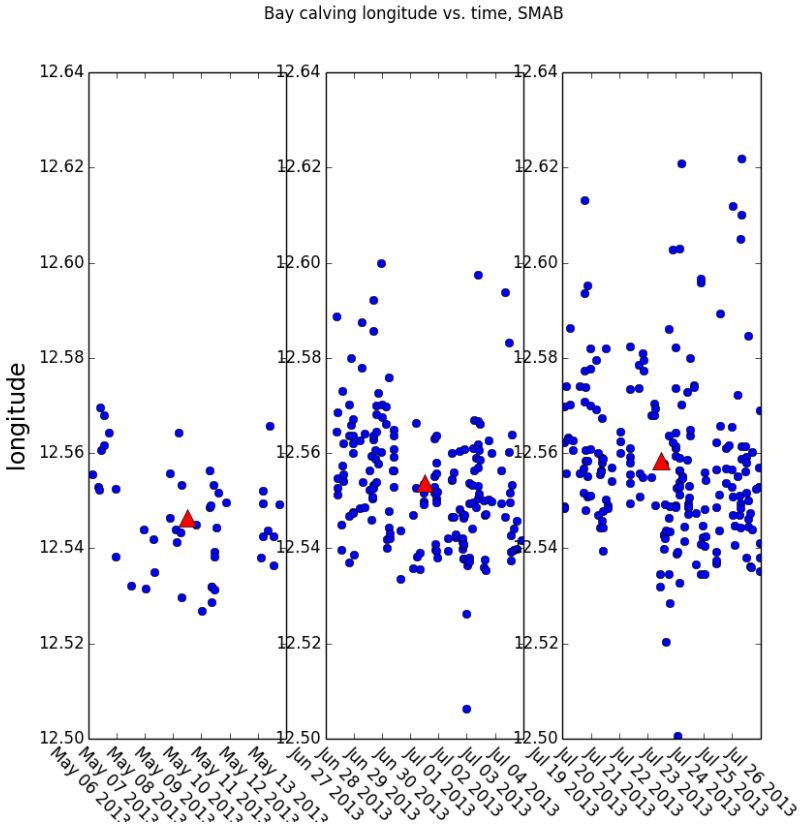

Figure 40: Longitude development with time of group 3, bay calving, red triangle represents the average for each week.

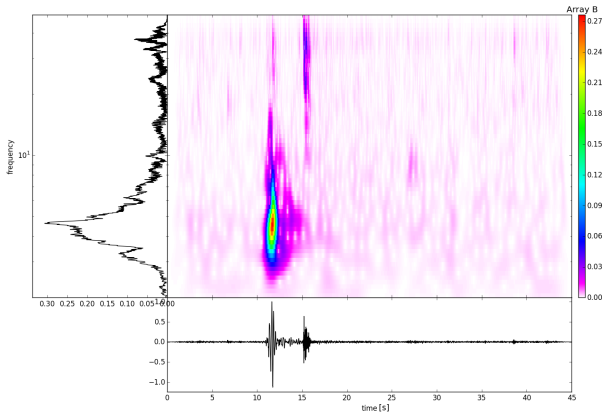

Figure 41: Frequency spectrum of event followed by air wave (array B).

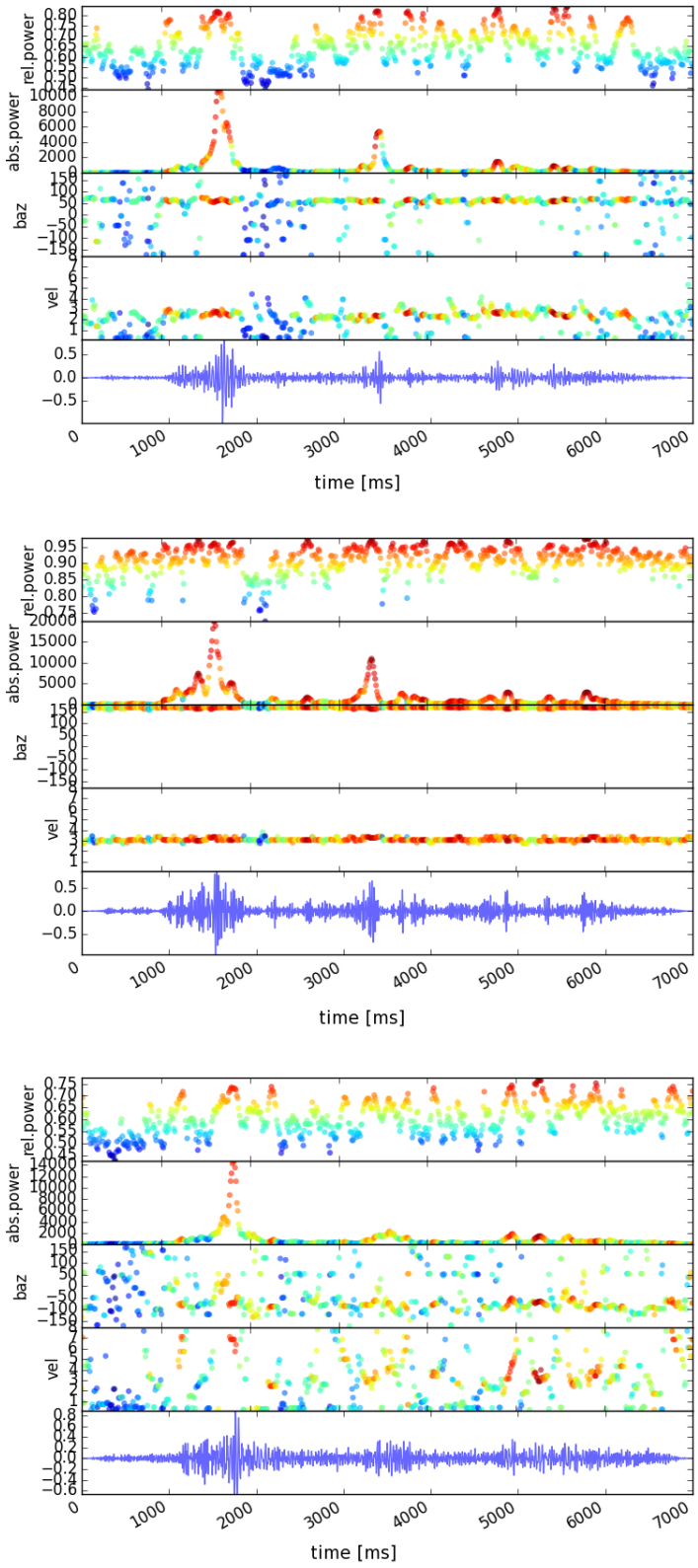

Figure 42: Example of multiple calving event from day 206, array A (top left), array B (top right) and array C (bottom).

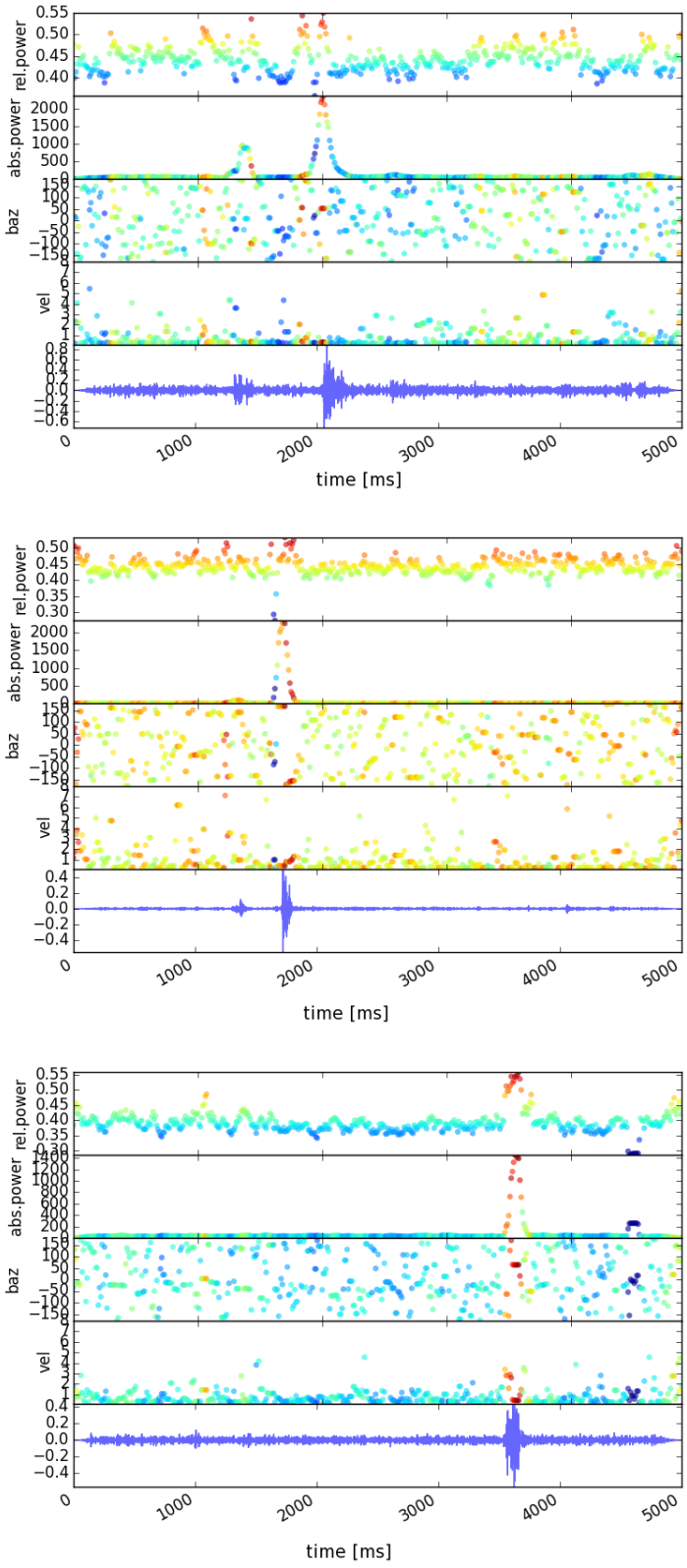

Figure 43: FK analysis of acoustic wave from day number 205, array A (upper left), array B (upper right), and array C (bottom).

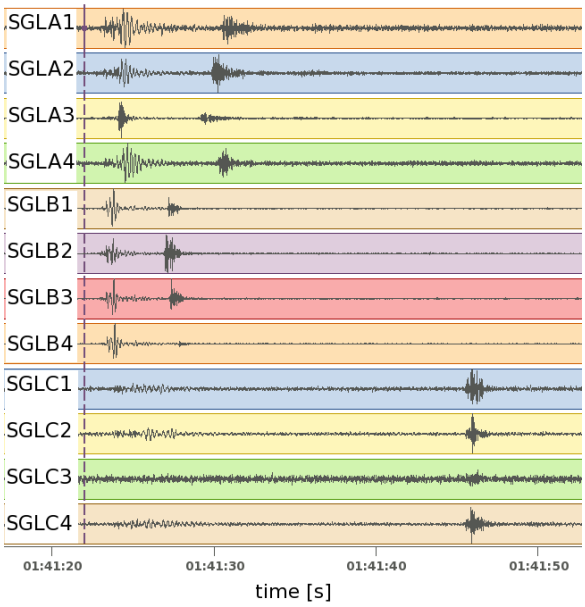

Figure 44: Acoustic wave clearly follows main events, Snuffler.

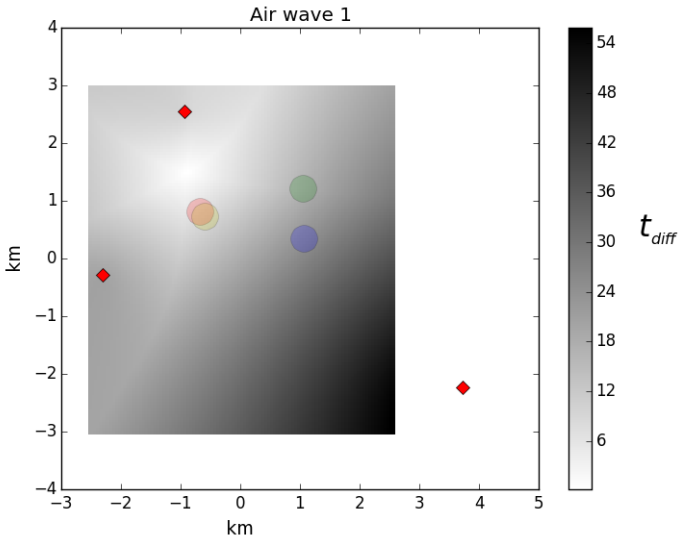

Figure 45: Calving event from day 205, main event located by FK (red circle), SMAB (yellow circle) and acoustic event located by FK (blue circle), SMAB (green circle) on background of grid-search from phase picking of the acoustic wave (where white color shows the best location).

6.6 Relation to independent data

Calving events were compared to ocean tides to investigate if these two phenomena can be correlated. Water level increase happens twice a day by approximately 1.6 meter and this can affect glacier's dynamic due to support difference of the glacier terminus when maximal level of water presses against the wall while minimal water level gives less support. Hence calving rate can possibly rise during minimal water level. In figure 36, we found an indication of periodicity of calving rate following the ocean tides. Calving rate for each hour of the dataset were stacked together to investigate behavior of calving during minima and maxima of the water level. Histograms of each day were shifted so it starts with an hour of minimal water level and then these histograms were stacked together. The final stacked histogram demonstrates increase of the calving rate with minimal water level and decrease with maximal water level. In figure 46 the stacked calving rate is plotted together with the ocean tides maxima and minima.

Another comparison was done between signal quality and wind speed. Wind can get very strong

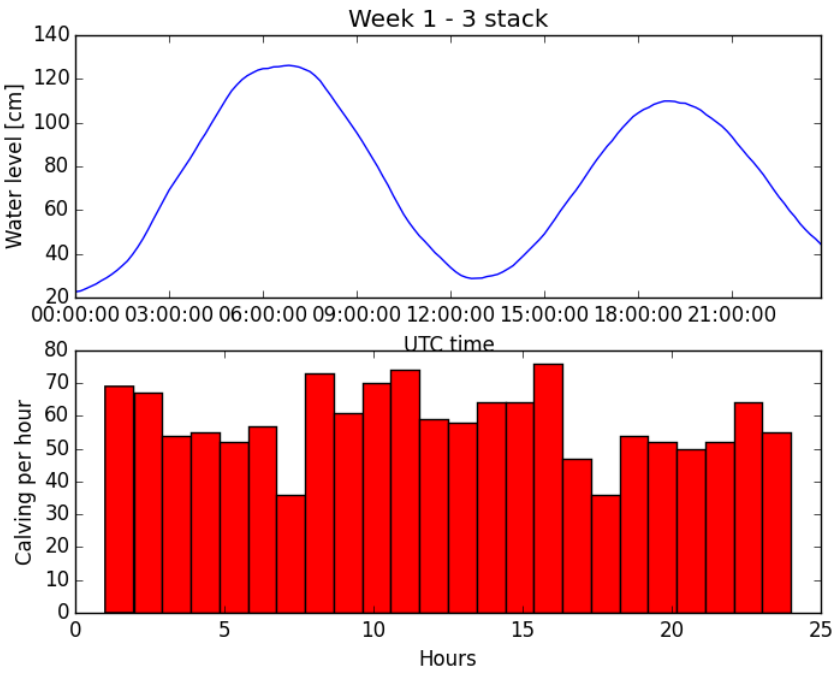

Figure 46: Example of data relation investigation between tides and calving rate per hour, stack of all days.

in Svalbard and can decrease quality of the seismic record by increasing seismic noise significantly. With too high noise, coherent signal of icequakes can become hidden. This would lead into an apparent decrease of calving rate as the signal would stay unrevealed and events classified as group 2 would have higher rate.

Average wind speed per hour data was obtained from Pynten station (situated on the coast between Ny Ålesund and Kronebreen) and plotted together with calving rate values (figure 47). Week 3 was chosen as an example but none of the three weeks showed any correlation between wind speed and

calving rate. The independency of the wind speed can be due to the close location of the geophones from the source. This indicates that the noise level does not affect detectability of the icequakes and hence FK and SMAB methods are not significantly affected by worse wind conditions.

Calving rate is expected to increase with higher water input and hence the data is further com-

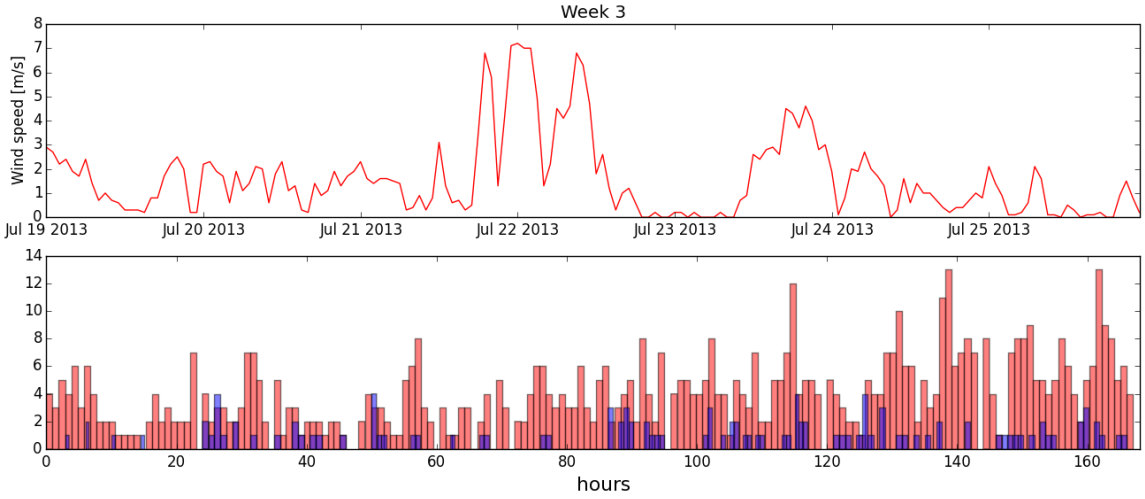

Figure 47: Example of data relation investigation between wind speed from Pynten and calving rate per hour, group 1 (red) and group 2 (blue).

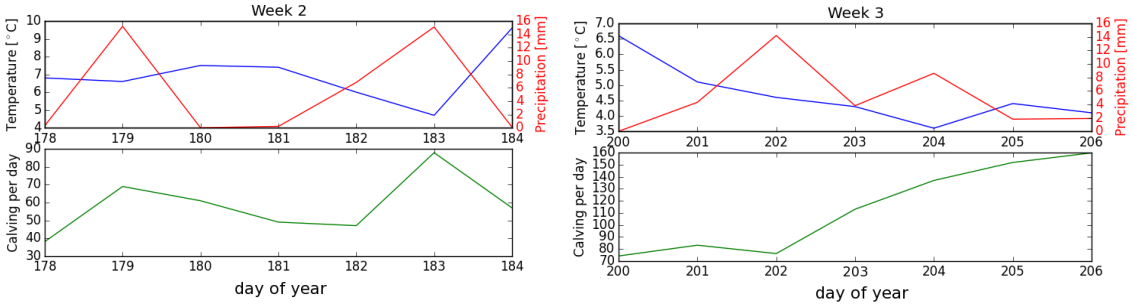

Figure 48: Relation of calving rate (green curve) per day to temperature (blue curve) and precipitation (red curve) together with calving rate per hour.

pared with both temperature variations and precipitation. Temperature rise contributes to melting which increases also water under the glacier. This lubricates the bed and glacier starts sliding faster. Such an advancing can be balanced with more frequent calving. This reaction to water increase can take several days while precipitation increase can lead into higher calving rate with no delay. Both temperature and precipitation were examined and plotted together with calving rate. This was done only for week 2 and 3 since there was very little precipitation during week 1 and temperature stayed below zero. Plots of weeks 2 and 3 are represented in figure 48. In week 2 the calving rate increases with both precipitation maximums in days 179 and 183 which illustrates no delay in reaction of the glacier. Temperature decreases slightly about 2°C and this seems to have no effect on calving rate. In week 3 the temperature decreases gradually while calving increases each day and precipitation increases in the first three days and then varies until it decreases in the

end of this week. The calving rate responds to both higher temperature in the beginning of the week (almost 7°C) with delay of a few days while precipitation in this week has delay of one day. Both weeks show very fast reaction to the precipitation increase while temperature seems to influence calving rate only in the week 3 with some delay. This demonstrates that calving event record is complete enough and usable for calving monitoring.

6.7 Glacier dynamics

The locations of the SMAB method are compared to glacier dynamics to examine if the locations are accurate enough to trace the terminus position and satellite figures are used for this.
The terminus exhibited retreat which was documented by satellites. A map was created by overlapping figures captured on 28^{th} of May and 19^{th} of September 2013 (figure 49, left). The retreat is roughly about 400 meters in the middle part of the terminus. The retreat between week 1 and week 3 (beginning of May to end of July) could be estimated as portion from the total retreat of 400 meters and hence could be between 100 and 200 meters. The icequakes originating from the central part of the terminus indicated retreat between week 1 and week 3 around 100 meters. The retreat is more significant between weeks 2 and 3 compared to difference between weeks 1 and 2 (as in figure 39). This indicates a speeding up of the glacier retreat during summer season which is due to higher temperature, larger water input and enhanced lubrication of the glacier bottom which enables easier sliding over the bed and leading into more frequent calving.
The glacier surface velocities from 2007 and 2012 are compared with the results (figure 50, Kohler, Schellenberg at al., 2014). The south half of the terminus exhibits higher surface speed in both studies. This corresponds with parts 4 - 6 from the divided terminus (division in figure 37). Higher velocity should result into higher calving rate while lower velocity should result into decreased calving rate (if we assume stable terminus or the same retreat distance along the terminus). In the map in figure 49 the retreat seems to be approximately equal along the terminus, but this is between May and September 2013 and hence the retreat could behave in various ways in between. However, the seismic record showed that the amount of calving is higher in the north half of the glacier terminus than in the south part and hence the surface velocity do not fit well with the seismic monitoring.
In the time-lapse video from 2014 both terminus and bay structure exhibited very slow retreat in the beginning of the video (May 2014) and later speed up (approximately June and July 2014) which corresponds well with the seismic recording of the central terminus in 2013 (as we assume similar behavior of the glacier retreat in 2013 and 2014). The bay structure located in the southern part of the Kronebreen-Kongsvegen system however almost did not experience any retreat between May and September 2013 (figure 49, right). This does not correlate well with the bay calving locations provided by SMAB method and it indicates higher uncertainty in this area. This is caused by increasing distance from seismic arrays.
Calving exhibited partly correlation with higher temperature values but this would have to be examined over longer period as the glacier has few days delay in responding to the temperature increase. Precipitation however showed immediate effect on calving rate during both weeks 2 and 3. This is due to direct input of liquid water while melting due to increased temperature takes time.
Tides correlation showed that calving events become more frequent with tides minima. The water level difference seems to be small compared to the size of Kronebreen (the highest point of the

terminus is around 60 meters above the water while tides change water level by 1.6 meter). The difference between maximal and minimal calving rates is not very significant. However this illustrates that terminus and also dynamics of the whole glacier can be affected by small environment changes.
To sum up, the calving events seem to be influenced by several factors. The tides cause semidiurnal variation of the calving rate. Another effect is caused by precipitation (immediate effect) and temperature (delayed effect) which both result into increasing of the calving activity. Calving also demonstrated higher values during the second half of the day which could be however an effect of the tides as this trend was not really clear (figure 35). In a period greater than a single day the frequency of calving increases significantly from May to July. The occurrence of calving events is resulting from combination of all these factors.

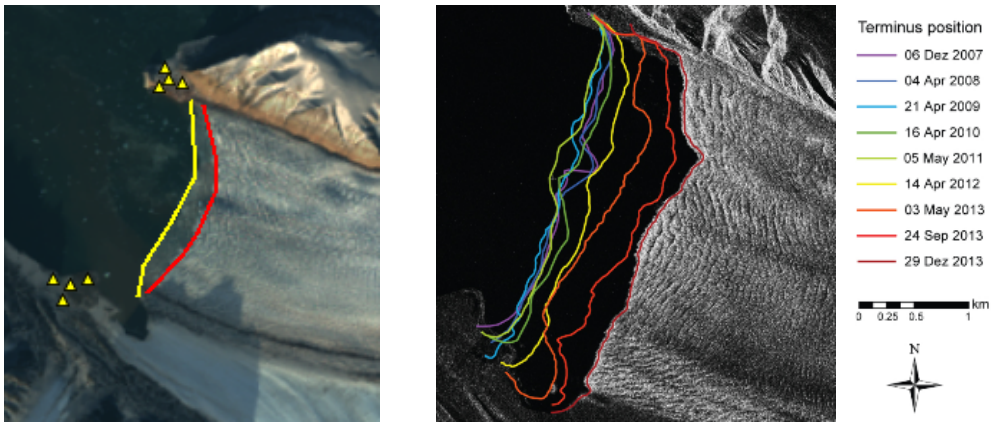

Figure 49: Left: satellite retreat difference of the terminus position between 28/5/2013 (yellow line) and 19/9/2013 (red line), right: terminus positioning between December 2007 and December 2013 (Schellenberger et al., 2014).

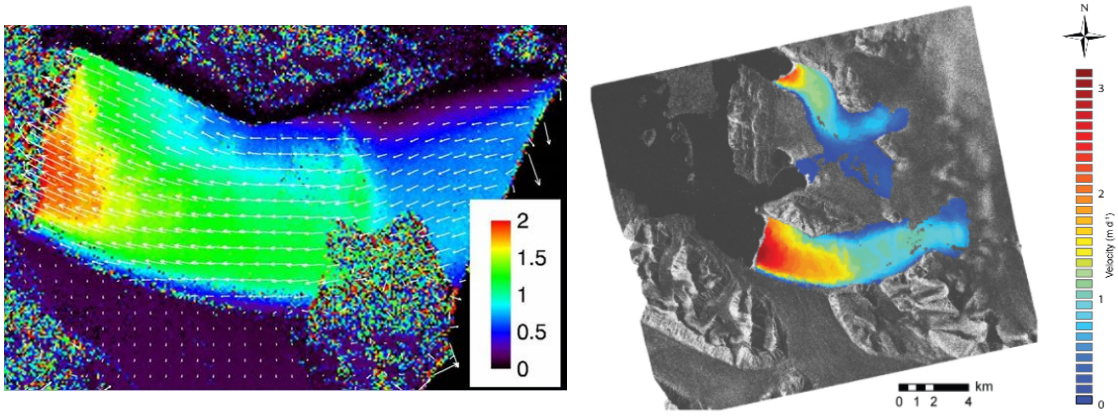

Figure 50: Left: surface velocity obtained from 2007 (Kohler, personal communication), right: surface velocity from 25 June - 19 July 2012 from RADARSAT (Schellenberger et al., 2014).

7 Conclusion

In this thesis continuous seismic records from seismic arrays located close to the terminus of Kronebreen were analyzed. Seismic events related to calving were picked and processed with three different methods to obtain source locations. These methods were compared with each other and related to independent data to decide which method is most suitable for cryo-seismology targeted on locating calving-related events with seismic arrays.

More events were successfully localized with SMAB method and less scatter around the glacier terminus showed better accuracy of the localizations which makes SMAB method more appropriate for calving-related seismicity. FK method is however needed for obtaining velocities and hence combination of both methods seems to work best. Phase picking method did not provide enough locations and was mostly limited by visual picking of the same phase at each array (due to noise). SMAB method locations indicated retreat of the central terminus in time which was positively correlated with satellite pictures. This illustrates successful localization with high accuracy in the central part of the terminus.

A bay-like structure was created in the southern part of the terminus. Calving originating from this area tend to retreat with time. However, due to poorer accuracy of the localization, this retreat was evaluated as uncertain. Compared to independent data and studies, no significant retreat was measured in this area in the satellite pictures or by the terminus position monitoring by Schellenberger (2014). The north part of the glacier exhibited smaller scatter away from the terminus than calving originating from the bay structure.

Temporal distribution of calving was related to weather data and ocean tides. Calving rate is affected by several factors: rise of temperature leads into calving increase. This has however a few days delay (here 2 - 3 days) but it could not be investigated into more details. Rain increase showed immediate effect on calving rate which increases without delay. Ocean tides has semidiurnal cycle on Svalbard. During two maxima in a single day the calving rate decreases while the minima cause increase of the calving rate. This can be caused by pressure of the water against the glacier cliff wall during the tide maxima and releasing it during the minima.

For future studies the calving-related seismicity can be automatized using automatic event detection (STA/LTA) which can be applied for large datasets without manual picking and events can further go through processing similar to this thesis: use of FK method for revealing the seismic velocity for each array, than use SMAB method for localization of the events. Additionally, the automatic processing should restrict the area of interest to smaller part covering only the terminus area and automatic classify events exhibiting narrow, low frequencies (in case of targeting only calving icequakes).

Processing in this thesis also showed that both methods can be applied with only two fully working arrays. Aperture size was good enough for icequakes as the distances between geophones were chosen correctly to target lower frequencies. In future studies the aperture size and its location should be similar to arrays A and B as those provided higher accuracy of localization and also higher SNR. Array C was placed further and the proportion of successfully stacked events was lower than arrays A and B. Array C was also located with elevation difference causing backazimuth bias and smaller size of the array provided worse resolution. The elevation difference between arrays can make localization complicated since it affects the direction of the signal due to reflections and hence for future studies the arrays should stay within small elevation difference range.

The seismic arrays were placed close to the terminus and detection was not significantly affected by wind speed (which causes noise with greater distance as the SNR gets lower) and hence for the

future work, we recommend similar distance between source and stations as here.
To sum up, SMAB method should be used together with FK to minimize the uncertainty of the locations. The accuracy of the method is highest in this study in the middle between the two seismic arrays (located on the glacier terminus) where we could also measure the retreat of the glacier well-correlated with satellite figures.
Calving monitoring helps understanding of the glacier dynamics response to the changing environmental conditions. This is important in forecasting the future behavior of the glaciers in general and the impact to the world sea level rise. SMAB in combination with FK method can be used for calving monitoring in the future and also calving data can be obtained from regional seismic record from the past (on Svalbard for example from NORSAR). This can be used to create long period catalog of glacier-related seismicity and to relate these data to changing weather conditions from a long term perspective.

8 References

- Bartholomaus, T. C., Larsen, C.F., ONeel, S., West, M.E. 2012. Calving seismicity from icebergsea surface interactions, J. Geophys. Res., 117, F04029, doi:10.1029/2012JF002513.
- Beyreuther, M., Barsch, R., Krischer, L., Megies, T., Behr, Y., Wassermann, J. 2010. ObsPy: A Python toolbox for seismology, Seismol. Res. Lett., 81, 530-533.
- Bormann, P. 2012. New Manual of Seismological Observatory Practice (NMSOP-2), IASPEI, GFZ German Research Centre for Geosciences, Potsdam; http://nmsop.gfz-potsdam.de; DOI: 10.2312/GFZ.NMSOP-2 urn:nbn:de:kobv:b103-NMSOP-2.
- Chapuis, A., Rolstad, C., Norland, R. 2010. Interpretation of amplitude data from a ground-based radar in combination with terrestrial photogrammetry and visual observations for calving monitoring of Kronebreen, Svalbard, Ann. Glaciol., 51, 3440, doi:10.3189/172756410791392781.
- Chapuis, A., Tetzlaff, T. 2014. The variability of tidewater-glacier calving: origin of event-size and interval distributions, Journal of Glaciology 60(222):622634, doi:10.3189/2014JoG13J215.
- Hagen, J.O., Melvold, K., Pinglot, F., Dowdeswell, J.A. 2003. On the net mass balance of the glaciers and ice caps in Svalbard, Norwegian Arctic. Arctic, Antarctic, and Alpine Research,35, 264270.
- Harjes, H.-P., Henger, M. 1973. Array-Seismology,Z. Geophs.,39, 865905.
- Heimann, S. Snuffler Tutorial 2012. Available at: http://emolch.github.io/pyrocko/current/snuffler_tutorial.html (Accessed: 27.04.2015).
- Kelly, E. J. 1967. Response of seismic signals to wide-band signals, Lincoln Lab. Tech. Note 1967 30, Lincoln Lab., Mass. Inst.of Technol., Lexington, Mass.
- Kohler, J., Norwegian Polar Institute, personal communication (in 2015).
- Kääb, A., Lefauconnier, B., Melvold, K. 2005. Flow field of Kronebreen, Svalbard,using repeated Landsat and ASTER data. Ann. Glaciol.,42,713.
- Köhler, A., Chapuis, A., Nuth, C., Kohler, J., Weidle, C., 2012. Autonomous detection of calving-related seismicity at Kronebreen, Svalbard. The Cryosphere, 6,393-406, doi:10.5194/tc-6-393-2012.
- Köhler, A., Nuth, C., Weidle, C., Schweitzer, J., Gibbons, S. 2015a. Dynamic glacier activity revealed through passive regional seismic monitoring on Spitsbergen, Svalbard. Submitted to Polar Research, in review.
- Köhler, A., Nuth, C., Weidle, C., Schweitzer, J. 2015b. On the calving history of Kronebreen, Svalbard, observed through 14 years of seismic monitoring. In preparation.
- Nuth, Ch., Schuler, T.V., Kohler, J., Altena, B., Hagen, J.O., 2012. Estimating the long-term calving flux of Kronebreen, Svalbard, from geodetic elevation changes and mass-balance modelling. Journal of Glaciology, Vol. 58, No. 207, 2012 doi:10.318.

- Ohrnberger, M., Schissele, E., Cornou, C., Bonnefoy-Claudet, S., Wathelet, M., Savvaidis, A., Scherbaum, F., Jongmans, D., 2004. Frequency wavenumber and spatial autocorrelation methods for dispersion curve determination from ambien vibration recording. Proceedings of the 13th World Conference on Earthquake Engineering. Vancouver, Canada. Paper 946.

- O'Neel, S., Marshall, H.P., McNamara, D.E., Pfeffer, W.T. 2007. Seismic detection and analysis of icequakes at Columbia Glacier, Alaska, J. Geophys. Res., 112, F03S23, doi:10.1029/2006JF000595.

- Richardson, J.P., Waite, G.P., FitzGerald, K.A., Pennington, W.D. 2010. Characteristics of seismic and acoustic signals produced by calving, Bering Glacier, Alaska, Geophys. Res. Lett.,37, L03503,doi:10.1029/2009GL041113.

- Rost, S. and Thomas C. 2002. Array seismology: Methods and applications, Rev. Geophys., 40(3), 1008, doi:10.1029/2000RG000100.

- Schellenberger, T., Dunse, T., Kääb, A., Kohler, J., Reijmer, C.H. 2014. Surface speed and frontal ablation of Kronebreen and Kongsbreen, NW-Svalbard, from SAR offset tracking, The Cryosphere Discuss., 8, 61936233, doi:10.5194/tcd-8-6193-2014.

- Trusel, L.D., Powell, R.D., Cumpston, R.M., Brigham-Grette, J. 2010. Kronebreen and Kongsvegen polythermal tidewater glaciers, Kongsforden, Svalbard. Geological Society, London, Special Publications 2010; v. 344; p. 89-102 doi:10.1144/SP344.9.

- Walter, F., Amundson, J.M., ONeel, S., Truffer, M., Fahnestock, M., Fricker, H.A. 2012. Analysis of low-frequency seismic signals generated during a multiple-iceberg calving event at Jakobshavn Isbræ, Greenland, J. Geophys. Res., 117, F01036, doi:10.1029/2011JF002132.

A Appendix

A.1 FK analysis script

```
#!/usr/bin/env python

from obspy.core import read, UTCDateTime, AttribDict
from obspy.signal import cornFreq2Paz
import obspy.signal
from array_analysis_new import array_processing
import matplotlib.pyplot as plt
from load_SGL import load_SGL
import linecache
from obspy import read
import numpy as np
import os
import math
import scipy.optimize as opt
from matplotlib.patches import Wedge
import matplotlib
from collections import deque

d126 = '126_all_Z_groups'
d127 = '127_all_Z_groups'
d128 = '128_all_Z_groups'
d129 = '129_all_Z_groups'
d130 = '130_all_Z_groups'
d131 = '131_all_Z_groups'
d132 = '132_all_Z_groups'

d178 = '178_all_Z_groups'
d179 = '179_all_Z_groups'
d180 = '180_all_Z_groups'
d181 = '181_all_Z_groups'
d182 = '182_all_Z_groups'
d183 = '183_all_Z_groups'
d184 = '184_all_Z_groups'

d200 = '200_all_Z_groups'
d201 = '201_all_Z_groups'
d202 = '202_all_Z_groups'
d203 = '203_all_Z_groups'
d204 = '204_all_Z_groups'
d205 = '205_all_Z_groups'
d206 = '206_all_Z_groups'
corr = 'correction.dat'

day_1 = input('Choose day: ')
day = open(day_1, 'r')

### number of lines in the file = counts
```

```
count = 0
for lines in day:
 if lines.strip():
  count +=1

event_number = (count-1)

print('Number of events: ', event_number)

### selection of events to display in a range

beg = input('Starting event: ')
true_beg = beg + 1
end = input('Ending event: ')
true_end = end + 2

### starting loop for all selected event

for i in range(true_beg, true_end):
 try:
  d=linecache.getline(day_1, i)
  start = d[0:10] + 'T' + d[11:19]
  starttime = UTCDateTime(start)
  start_minus = starttime - 10
  tp_ev = d[26]
  if tp_ev == 3:
    end_time = UTCDateTime(starttime + 50)
  else:
    end_time = UTCDateTime(starttime + 30)

  ### selection of stations to display


  a = 'SGLA1', 'SGLA2', 'SGLA3', 'SGLA4'
  b = 'SGLB1', 'SGLB2', 'SGLB3', 'SGLB4'
  c = 'SGLC1', 'SGLC2', 'SGLC3', 'SGLC4'
  n = 'n'

  ### printing data during the process

  X = i - 1
  percentage = (X*100/event_number)

  print('Date:', d[0:19], 'event number', X, 'from', event_number, '—',
    percentage, '%' )

  ### coordinates of array stations

  a_x = -2.5621
  a_y = -0.3610
```

```
b_x = -1.1337
b_y = 2.6089
c_x = 3.7285
c_y = -2.2368

#a_x = 1387968.8
#a_y = 8720415.9
#b_x = 1395338.2
#b_y = 8723357.0
#c_x = 1420441.0
#c_y = 8718558.4

### lists for later plotting of crossing points
vel_adding = []
a_av_range_list = []
b_av_range_list = []
c_av_range_list = []
a_wedge_list = []
b_wedge_list = []
c_wedge_list = []
ax_plot_list = [a_x]
ay_plot_list = [a_y]
bx_plot_list = [b_x]
by_plot_list = [b_y]
cx_plot_list = [c_x]
cy_plot_list = [c_y]
range_a_b_list = []

ab_list = []
bc_list = []
ac_list = []

ab_x_y = []
list_total = []
inn = [a, b, c]
inn_list = 'abc'

dir_name = day_1[0:3]
os.chdir(dir_name)

if inn == n:
  continue
else:

### FK processing (obspy)

 for x in range(0, len(inn)):
  print 'ARRAY', inn[x]

  stations = (inn[x])
  st=load_SGL(start_minus,end_time,stations)
```

```
for tr in st:
  tr.detrend()
  tr.taper(max_percentage=0.05, type='cosine')
  tr.data = obspy.signal.bandpass(tr.data, 2.0, 49.0, zerophase=True,
    df=tr.stats.sampling_rate)
  tr.data = tr.data/max(tr.data)

kwargs = dict(
  # slowness grid: X min, X max, Y min, Y max, Slow Step
  sll_x=-3.0, slm_x=3.0, sll_y=-3.0, slm_y=3.0, sl_s=0.03,
  # sliding window properties
  win_len=1.0, win_frac=0.1,
  # frequency properties
  frqlow=2.0, frqhigh=10.0, prewhiten=0,
  # restrict output
  semb_thres=-1e9, vel_thres=-1e9, timestamp='julsec',
  stime=start_minus+0.01, etime=end_time-0.01
)
out = array_processing(st, **kwargs)


### creating tab of output

name = day_1[0:3] + '_' + d[0:19] + '_' + inn_list[x] + '.dat'
name2 = day_1[0:3] + '_' + d[0:19] + '_' + inn_list[x] + 'BAZ.txt'

threshold = 0.6

fout = open(name, "w")
vel_list = []
list_range = []
x_slow = []
y_slow = []
rel_p = []
baz_list = []
for twin in out:
    text = "%s %10.6f %10.6f %15.6f %15.3f %10.2f %10.2f %10.2f\n" %
        ( UTCDateTime(twin[0]),twin[1],twin[2],twin[3],1/twin[4],
        twin[5],twin[6],twin[7])
    fout.write(text)
    if twin[1]>threshold:
      x_slow.append(twin[5])
      y_slow.append(twin[6])
      rel_p.append(twin[1])
      vel_list.append(1./twin[4])
      list_range.append(twin[7])
fout.close()

### increasing of threshold and computation of standart deviation
   (np.std) and average (x_av, y_av)
```

```
for _ in range(0, 40):
        for p in range(0, len(x_slow)):
             az_1 = 180 * math.atan2(x_slow[p], y_slow[p]) / math.pi
             baz_1 = az_1 % -360 + 180
             baz_list.append(baz_1)


        if len(x_slow) == 0:
             break

        xx = np.std(baz_list)
        x_av = sum(x_slow) / float(len(x_slow))
        y_av = sum(y_slow) / float(len(y_slow))
        azimut = 180 * math.atan2(x_av, y_av) / math.pi
        baz = azimut % -360 + 180

        if xx > 20:
           baz_list = []
           y = 0
           threshold = threshold + 0.01
           while y < len(rel_p):
              if rel_p[y] < threshold:
                 rel_p.pop(y)
                 x_slow.pop(y)
                 y_slow.pop(y)
                 list_range.pop(y)
                 vel_list.pop(y)
              else:
                 y += 1

        if xx <= 20:
           break

### making BAZ overview file

if len(baz_list) >= 5:

  av_range = float(sum(list_range) / float(len(list_range)))
  cislo = len(baz_list)
  av = float(baz)
  av_str = str(baz)
  aa = float(xx)
  end = '\n'
  vel_average = float(sum(vel_list) / float(len(vel_list)))

  trs = float(threshold)
  listik = [av, aa, trs]
  baz = open('baz_overview.dat', 'a')
  name4 = '%10.3f %10.2f %10.3f %10.0f %10.3f %10.2f\t' % (listik [0],
      listik [2], listik [1], cislo, av_range, vel_average)
  name5 = day_1[0:3] + '_' + d[0:19] + '  ' + inn_list[x] + '  '
```

```
text3 = name5 + name4 + end
baz.write(text3)
range_a_b_list.append(av_range)

### Adding values into lists for calculation of crossing point and
    plotting wedges

if av < 0:
    if av >= -90:
        x_vec = 10*(math.sin(math.radians(av)))
        y_vec = 10*(math.cos(math.radians(av)))
        mid_angle = (av-90.0)*(-1)
    if av < -90:
        x_vec = -10*(math.cos(math.radians(av+90)))
        y_vec = 10*(math.sin(math.radians(av+90)))
        mid_angle = (av-90.0)*(-1)
if av >= 0:
    if av <= 90:
        x_vec = 10*(math.sin(math.radians(av)))
        y_vec = 10*(math.cos(math.radians(av)))
        mid_angle = (90.0-av)
    if av > 90:
        x_vec = 10*(math.cos(math.radians(av-90)))
        y_vec = -10*(math.sin(math.radians((av-90))))
        mid_angle = (450.0-av)

if inn_list[x] == 'a':
    bod_ax = a_x + x_vec
    bod_ay = a_y + y_vec
    ab_list.append(x_vec)
    ab_list.append(y_vec)
    ac_list.append(x_vec)
    ac_list.append(y_vec)
    a_wedge_list.append(mid_angle)
    a_av_range_list.append(av_range)
    vel_adding.append(vel_average)

if inn_list[x] == 'b':
    bod_bx = b_x + x_vec
    bod_by = b_y + y_vec
    ab_list.append(x_vec)
    ab_list.append(y_vec)
    bc_list.append(x_vec)
    bc_list.append(y_vec)
    b_wedge_list.append(mid_angle)
    b_av_range_list.append(av_range)
    vel_adding.append(vel_average)

if inn_list[x] == 'c':
    bod_cx = c_x + x_vec
    bod_cy = c_y + y_vec
```

```
    ac_list.append(x_vec)
    ac_list.append(y_vec)
    bc_list.append(x_vec)
    bc_list.append(y_vec)
    c_wedge_list.append(mid_angle)
    c_av_range_list.append(av_range)
    vel_adding.append(vel_average)

### Calculating crossing point AB, BC, AC

if inn_list[x] == 'b':
 if len(ab_list) == 4:
     def f (variables):
       (x,y) = variables
       first_eq = a_x + ab_list[0] * x - b_x - ab_list[2] * y
       second_eq = a_y + ab_list[1] * x - b_y - ab_list[3] * y
       return [first_eq ,second_eq]
     if __name__=='__main__':
       solution = opt.fsolve(f,(0.1,0))
       ab_x = a_x + ab_list[0] * solution[0]
       ab_y = a_y + ab_list[1] * solution[0]
       print 'A and B crossing point is:', ab_x, ab_y
       ab_x_y.append(float(ab_x))
       ab_x_y.append(float(ab_y))
       if len(ax_plot_list) == 1:
         ax_plot_list.append(bod_ax)
         ay_plot_list.append(bod_ay)
       if len(bx_plot_list) == 1:
         bx_plot_list.append(bod_bx)
         by_plot_list.append(bod_by)

if inn_list[x] == 'c':
 if len(bc_list) == 4:
     print bc_list
     def f (variables):
       (f,g) = variables
       first_eq = b_x + bc_list[0] * f - c_x - bc_list[2] * g
       second_eq = b_y + bc_list[1] * f - c_y - bc_list[3] * g
       return [first_eq ,second_eq]
     if __name__=='__main__':
       solution = opt.fsolve(f,(0.1,0))
       F = b_x + bc_list[0] * solution[0]
       G = b_y + bc_list[1] * solution[0]
       print 'B and C crossing point is:', F, G
       if len(cx_plot_list) == 1:
         cx_plot_list.append(bod_cx)
         cy_plot_list.append(bod_cy)
       if len(bx_plot_list) == 1:
         bx_plot_list.append(bod_bx)
         by_plot_list.append(bod_by)
```

```
if inn_list[x] == 'c':
 if len(ac_list) == 4:
     print ac_list
     def g (variables):
       (s,t) = variables
       first_eq = a_x + ac_list[0] * s - c_x - ac_list[2] * t
       second_eq = a_y + ac_list[1] * s - c_y - ac_list[3] * t
       return [first_eq ,second_eq]
     if __name__=='__main__':
       solution = opt.fsolve(g,(0.1,0))
       S = a_x + ac_list[0] * solution[0]
       T = a_y + ac_list[1] * solution[0]
       print 'A and C crossing point is:', S, T
       if len(ax_plot_list) == 1:
         ax_plot_list.append(bod_ax)
         ay_plot_list.append(bod_ay)
       if len(cx_plot_list) == 1:
         cx_plot_list.append(bod_cx)
         cy_plot_list.append(bod_cy)


### Plot

labels = ['rel.power', 'abs.power', 'baz', 'vel']

fig = plt.figure()
for i, lab in enumerate(labels):
  ax = fig.add_subplot(5, 1, i + 1)
  if lab == 'vel':
    ax.scatter(out[:, 0], 1./out[:, i + 1], c=out[:, 1], alpha=0.6,
        edgecolors='none')
  else:
    ax.scatter(out[:, 0], out[:, i + 1], c=out[:, 1], alpha=0.6,
        edgecolors='none')
  ax.set_ylabel(lab)
  ax.set_xlim(out[0, 0], out[-1, 0])
  if lab == 'baz':
    ax.set_ylim(-180,180)
  elif lab == 'vel':
    ax.set_ylim(1.0 , 8.0)
  else:
    ax.set_ylim(out[:, i + 1].min(), out[:, i + 1].max())

#name_pic3 = day_1[0:3] + '_' + d[0:19] + '_' + inn_list[x] +
    '_distribution.png'
#os.rename('haha.png', name_pic3)
tr = st[0]
tr.filter('bandpass', freqmin=2, freqmax=10)
ax = fig.add_subplot(5, 1, i + 2)
ax.plot(xrange(len(st[0].data)),st[0].data,alpha=0.6)
ax.set_xlim(0, len(st[0].data)-1)
```

```
ax.set_ylim(st[0].data.min(), st[0].data.max())
fig.autofmt_xdate()
fig.subplots_adjust(top=0.95, right=0.95, bottom=0.2, hspace=0)
name_pic = day_1[0:3] + '_' + d[0:19] + '_' + inn_list[x] + '.png'
fig1 = plt.gcf()
#plt.show()
#plt.draw()
fig1.savefig(name_pic)
plt.close('all')

### separating events originating from Kronebreen

#if inn_list[x] == 'b':
if len(ab_x_y) == 2 and -3 < ab_x_y [0] < 3 and -2.5 < ab_x_y[1] < 2.6:

    fig4 = plt.figure()
    ax=fig4.add_subplot(111)
    ax.set_xlim([-4, 4])
    ax.set_ylim([-3, 3.5])
    #ax.set_xlim([1387929.0, 1420490.0])
    #ax.set_ylim([8718510.0, 8723400.0])
    x1 = [a_x, b_x, c_x]
    y1 = [a_y, b_y, c_y]
    plt.plot(x1, y1, 'rD')
    if len(a_wedge_list) == 1:
      mid1 = a_wedge_list[0]
      av1 = a_av_range_list[0]
      angle1 = mid1-(av1/2)
      angle2 = mid1+(av1/2)
      fov1 = Wedge((a_x,a_y), 10000.0, angle1, angle2, color="r",
        alpha=0.2)
      ax.add_artist(fov1)

    if len(b_wedge_list) == 1:
      mid2 = b_wedge_list[0]
      av2 = b_av_range_list[0]
      angle3 = mid2-(av2/2)
      angle4 = mid2+(av2/2)
      fov2 = Wedge((b_x,b_y), 10000.0, angle3, angle4, color="r",
        alpha=0.2)
      ax.add_artist(fov2)

    if len(c_wedge_list) == 1:
      mid3 = c_wedge_list[0]
      av3 = c_av_range_list[0]
      angle5 = mid3-(av3/2)
      angle6 = mid3+(av3/2)
      fov3 = Wedge((c_x,c_y), 10000.0, angle5, angle6, color="r",
        alpha=0.2)
      ax.add_artist(fov3)
```

```
            name_fig4 = day_1[0:3] + '_' + d[0:19] + '_wedge.png'
            fig4.savefig(name_fig4)
            if inn_list[x] == 'b':
             list_total = [range_a_b_list[0], range_a_b_list[1], ab_x_y[0],
                 ab_x_y[1], vel_adding[0], vel_adding[1]]
            if inn_list[x] == 'c':
             list_total.append(vel_adding[2])
        else:
            print('neni splnena prvni podminka')
    kron_ev = open('Kronebreen_events.txt', 'a')
    if len(list_total)==6:
            text02 = '%.2f %.2f %.5f %.5f %.3f %.3f\t' % (list_total[0],
              list_total[1], list_total[2], list_total[3], list_total[4],
              list_total[5])
    if len(list_total)==7:
            text02 = '%.2f %.2f %.5f %.5f %.3f %.3f %.3f\t' % (list_total[0],
              list_total[1], list_total[2], list_total[3], list_total[4],
              list_total[5], list_total[6])
    if len(list_total)==6 or len(list_total)==7:
     text01 = day_1[0:3] + '_' + d[0:19] + ' '
     text03 = '\n'
     text04 = text01 + text02 + text03
     kron_ev.write(text04)
    os.chdir('/uio/hume/student-u10/hanakou/Snuffpick')
 except IndexError:
        os.chdir('/uio/hume/student-u10/hanakou/Snuffpick')
        continue
```

A.2 SMAB analysis script

```
#!/usr/bin/env python

from obspy.core import read, UTCDateTime, AttribDict
from obspy.signal import cornFreq2Paz
import obspy.signal
import matplotlib.pyplot as plt
from load_SGL import load_SGL
import linecache
from obspy import read
import numpy as np
import os
import math
import scipy.optimize as opt
from matplotlib.patches import Circle
import matplotlib
import network_analysis
from obspy.signal.util import utlLonLat, utlGeoKm


d126 = '126_all_Z_groups'
d127 = '127_all_Z_groups'
d128 = '128_all_Z_groups'
```

```
d129 = '129_all_Z_groups'
d130 = '130_all_Z_groups'
d131 = '131_all_Z_groups'
d132 = '132_all_Z_groups'

d178 = '178_all_Z_groups'
d179 = '179_all_Z_groups'
d180 = '180_all_Z_groups'
d181 = '181_all_Z_groups'
d182 = '182_all_Z_groups'
d183 = '183_all_Z_groups'
d184 = '184_all_Z_groups'

d200 = '200_all_Z_groups'
d201 = '201_all_Z_groups'
d202 = '202_all_Z_groups'
d203 = '203_all_Z_groups'
d204 = '204_all_Z_groups'
d205 = '205_all_Z_groups'
d206 = '206_all_Z_groups'
corr = 'correction.dat'

a_x = -2.5621
a_y = -0.3610
b_x = -1.1337
b_y = 2.6089
c_x = 3.7285
c_y = -2.2368


day_1 = input('Choose day: ')
dir_name = day_1[0:3] + '_diff'
os.chdir(dir_name)

day1 = open('baz_overview.dat', 'r')


### number of lines in the file = counts

count = 0
count2 = 0
count3 = 0
for lines in day1:
 if lines.strip():
  count +=1

lines_number = (count)
for b in range(1, lines_number+1):
  c = linecache.getline('baz_overview.dat', b)
  cc = linecache.getline('baz_overview.dat', b+1)
  if c[25] =='a' and cc[25]=='b':
```

```
    count2 +=1

print('Number of events: ', count2)

### selection of events to display in a range

#beg = input('Starting event: ')
#true_beg = beg
#end = input('Ending event: ')
#true_end = end + 1

### starting loop for all selected event

final_out = open('out_testing.txt', 'w')
final_outbest = open('outbest_testing.txt', 'w')

for i in range(1, count+1):
 try:
  d=linecache.getline('baz_overview.dat', i)
  e=linecache.getline('baz_overview.dat', i+1)
  start1 = d[4:23]
  start2 = d[4:23]
  if start1 == start2 and d[25] =='a' and e[25]=='b':
   vel_a = float(d[89:93])
   vel_b = float(e[89:93])
   starttime = UTCDateTime(start1)
   start_minus = starttime - 10
   end_time = UTCDateTime(starttime + 50)
   count3 +=1

   ### printing data during the process

   X = count3 - 1
   percentage = (X*100/count2)

   print('Date:', d[4:23], 'event number', X, 'from', count2,
       '--', percentage, '%' )


   statlist=[['SGLA1','SGLA2','SGLA3','SGLA4'],['SGLB1','SGLB2','SGLB3',
      'SGLB4']]
   st=load_SGL(start_minus,end_time,statlist[0])
   st2=load_SGL(start_minus,end_time,statlist[1])


   i=0
   for tr in st:
    tr.detrend()
    tr.taper()
    tr.data = obspy.signal.bandpass(tr.data, 2.0, 10.0, zerophase=True,
       df=tr.stats.sampling_rate)
```

```
 # scale amplitudes
 tr.data = tr.data / max(tr.data)
#st.plot()
for tr in st2:
 tr.detrend()
 tr.taper()
 tr.data = obspy.signal.bandpass(tr.data, 2.0, 10.0, zerophase=True,
     df=tr.stats.sampling_rate)
 # scale amplitudes
 tr.data = tr.data / max(tr.data)
#st2.plot()

kwargs = dict(
    # location grid around center of loaded stations: X min in km,
       X max, Y min, Y max, Step
    #grd_x=-10.0, grdm_x=10.0, grd_y=-10.0, grdm_y=10.0, grd_s=0.1,
    grd_x=-7.0, grdm_x=7.0, grd_y=-7.0, grdm_y=7.0, grd_s=0.1,
    # sliding window properties
    win_len=2.0, win_frac=0.25,
    # frequency properties
    frqlow=2.0, frqhigh=10.0, prewhiten=0,
    # restrict output
    semb_thres=-1e9, vel_thres=-1e9, timestamp='julsec',
    # time window and velocity
    stime=start_minus+0.01, etime=end_time-0.01, vel1=vel_a, vel2=vel_b
)

# plot all maps (individual and stacked) for each time window
#out, outbest = network_analysis.diffraction_stack_II(st, st2,
     verbose2=True,**kwargs)

# plot best maps, individual and stacked
out,outbest = network_analysis.diffraction_stack_II(st,st2,
     verbose=True,**kwargs)

# no plot
#out, outbest = network_analysis.diffraction_stack_II(st, st2,
     **kwargs)

# out: locations from all time windows (map stack of same time windows)
# outbest: location from map stack of best time window for both arrays

lons_list = []
lats_list = []
rel_pow_list = []
threshold = 0.6

## getting out in txt file

name = d[0:23] + '_diffraction.dat'
diff_txt = open(name, 'w')
```

```
for twin in out:
 text = "%s %.3f %.3f %.4f %.4f\n" % ( UTCDateTime(twin[0]),twin[1],
     twin[2],twin[3],twin[4])
 diff_txt.write(text)
 if twin[1]>threshold:
        lon, lat = utlGeoKm(12.58705833, 78.87303333, twin[3],
            twin [4])
        rel_pow_list.append(twin[1])
        lons_list.append(lon)
        lats_list.append(lat)
diff_txt.close()
best_res = [outbest[3], outbest[4]]
lon_best, lat_best = utlGeoKm(12.58705833, 78.87303333, outbest[3],
     outbest[4])

##increasing the threshold

for _ in range(0, 40):

    if len(rel_pow_list) == 0:
            break

    lons_deviation = np.std(lons_list)
    lats_deviation = np.std(lats_list)

    y = 0

    if lons_deviation > 0.5 or lats_deviation > 0.5:
       threshold = threshold + 0.01
       while y < len(rel_pow_list):
              if rel_pow_list[y] < threshold:
                 lons_list.pop(y)
                 lats_list.pop(y)
                 rel_pow_list.pop(y)
              else:
                 y += 1

    if  lons_deviation <= 0.5 and lats_deviation <= 0.5:
          break

###  separating events originating from Kronebreen

if len(rel_pow_list) > 0:
 lon_av = sum(lons_list) / float(len(lons_list))
 lat_av = sum(lats_list) / float(len(lats_list))
 print lon_av, lat_av

 if -3 < lon_av < 3 and -2.5 < lat_av < 2.6:
   s, t = utlLonLat(12.58705833, 78.87303333, lon_av, lat_av)
   #print s, t
   if lons_deviation < lats_deviation:
```

```
 resolution = lats_deviation
else:
 resolution = lons_deviation
if resolution == 0:
  resolution = 0.1
final_txt = start1 + ' ' + '%.4f %.4f %.2f\n' % (s, t, resolution)
final_out.write(final_txt)
final_txt2 = '%.4f %.4f %.2f\n' % (outbest[3], outbest[4], resolution)
final_outbest.write(final_txt2)

fig4 = plt.figure()
ax=fig4.add_subplot(111)
ax.set_xlim([-4, 4])
ax.set_ylim([-3, 3.5])
x1 = [a_x, b_x, c_x]
y1 = [a_y, b_y, c_y]
plt.plot(x1, y1, 'rD')
circle1=Circle((lon_best, lat_best), radius=resolution, color='b',
    alpha=0.2)
#circle2=Circle((x_cross, y_cross), radius=c_distance, color='r',
    alpha=0.2)
#circle3=Circle((lon_best, lat_best), radius = resolution,
    color = 'g', alpha=0.2)
ax.add_artist(circle1)
#ax.add_artist(circle2)
#ax.add_artist(circle3)
fig4name = d[0:23] + 'c_outbest.png'
fig4.savefig(fig4name)



# plot locations for time windows
labels = ['rel.power', 'abs.power', 'lon', 'lat']

fig = plt.figure()
for i, lab in enumerate(labels):
    ax = fig.add_subplot(6, 1, i + 1)
    ax.scatter(out[:, 0], out[:, i + 1], c=out[:, 1], alpha=0.6,
           edgecolors='none')
    ax.set_ylabel(lab)
    ax.set_xlim(out[0, 0], out[-1, 0])
    if lab == 'baz':
      ax.set_ylim(-180,180)
    elif lab == 'lon':
      ax.set_ylim(12.3 , 12.85)
    elif lab == 'lat':
      ax.set_ylim(78.8 , 79.0)
    else:
      ax.set_ylim(out[:, i + 1].min(), out[:, i + 1].max())
ax = fig.add_subplot(6, 1, i + 2)
ax.plot(xrange(len(st[0].data)),st[0].data,alpha=0.6)
```

```
        ax.set_xlim(0, len(st[0].data)-1)
        ax.set_ylim(st[0].data.min(), st[0].data.max())
        fig.autofmt_xdate()
        fig.subplots_adjust(top=0.95, right=0.95, bottom=0.2, hspace=0)
        ax = fig.add_subplot(6, 1, i + 3)
        ax.plot(xrange(len(st2[0].data)),st2[0].data,alpha=0.6)
        ax.set_xlim(0, len(st2[0].data)-1)
        ax.set_ylim(st2[0].data.min(), st2[0].data.max())
        fig.autofmt_xdate()
        fig.subplots_adjust(top=0.95, right=0.95, bottom=0.2, hspace=0)
        namefig = d[0:23] + 'a_stack.png'
        namefig2 = d[0:23] + 'b_spectrum.png'
        fig.savefig(namefig)
        os.rename('fig.png', namefig2)
        #plt.show()
    except IndexError:
     continue
    except ValueError:
     continue
```

A.3 Phase picking script

```
#!/usr/bin/env python

import matplotlib.pyplot as plt
import matplotlib.cm as cm
import linecache
import numpy as np
import os
import math
from matplotlib.patches import Circle
from obspy.core import read, UTCDateTime
from obspy.signal.util import utlLonLat, utlGeoKm

d126 = '126'
d127 = '127'
d128 = '128'
d129 = '129'
d130 = '130'
d131 = '131'
d132 = '132'

d178 = '178'
d179 = '179'
d180 = '180'
d181 = '181'
d182 = '182'
d183 = '183'
d184 = '184'

d200 = '200'
d201 = '201'
```

```
d202 = '202'
d203 = '203'
d204 = '204'
d205 = '205'
d206 = '206'
ac = 'acoustic_test'
allday = ['126/', '127/', '128/', '129/', '130/', '131/', '132/',
          '178/', '179/', '180/', '181/', '182/', '183/', '184/',
          '200/', '201/', '202/', '203/', '204/', '205/', '206/']

### array coordinates

orig_lon = 12.58705833
orig_lat = 78.87303333


a_x1 = -2.66792194
a_x = -2.5621                ###reference geophone
a_x3 = -2.30547969
a_x4 = -2.80124315
a_y1 = -0.58431406
a_y = -0.3610
a_y3 = -0.28285267
a_y4 = -0.28285267

b_x1 = -1.29096513
b_x2 = -0.94214977
b_x = -1.13374325            ###reference geophone
b_x4 = -1.18103624
b_y1 = 2.50845653
b_y2 = 2.54195224
b_y = 2.60894366
b_y4 = 2.76525698

c_x1 = 3.65317489
c_x2 = 3.6485046
c_x3 = 3.87076867
c_x = 3.72848148             ###reference geophone
c_y1 = -2.37075195
c_y2 = -2.18094292
c_y3 = -2.18094292
c_y = -2.2367691

day_1 = input('Choose day: ')
os.chdir(day_1)

pick_locations = open('/uio/hume/student-u10/hanakou/Snuffpick/
     pick_locations.txt', 'w')

#day = open('Kronebreen_events.txt', 'r')
#phases = open('phases', 'r')
```

```
for x in range(0, len(allday)):
 adress1 = '/uio/hume/student-u10/hanakou/Snuffpick/' + allday[x] +
     'Kronebreen_events.txt'
 adress2 = '/uio/hume/student-u10/hanakou/Snuffpick/' + allday[x] +
     'phases'
 print adress1
 file1 = open(adress1, 'r')
 file2 = open(adress2, 'r')

 #day = open('acoustic_snuffler', 'r')
 #phases = open('phase_pick', 'r')

 count = 0
 for lines in file1:                    ###number of Kronebreen events
  if lines.strip():
   count +=1
 #print count

 count2 = 0
 for lines in file2:                  ### numbern of phases picked events
  if lines.strip():
   count2 +=1
 #print count2


 for i in range(1, count+1):
  list_a = []
  list_b = []
  list_c = []
  d = linecache.getline(adress1, i)
  #text1 = 'Day ' + d[0:3] + ' ' + d[11:19]
  a = d[24:90]
  time1 = UTCDateTime(d[4:14] + 'T' + d[15:23])
  time = d[0:23]
  print time1
  b = a.split()
  t_diff_list = []
  for a in range(2, count2+1):
    e = linecache.getline(adress2, a)
    #f = e[0:10] + 'T' + e[11:19]
    time2 = UTCDateTime(e[0:10] + 'T' + e[11:24])
    difference = math.sqrt((time1 - time2)**2)
             ### dividing lines into evets groups
    if difference < 20:
     print time2
     print difference
     if e[32] == 'A':
             ### changing coordinates to the coresponding geophone picked
                 from snuffler
        list_a.append(time2)
        #print list_a
```

```
        if e[33]=='1':
          a_x = a_x1
          a_y = a_y1
        if e[33]=='3':
          a_x = a_x3
          a_y = a_y3
        if e[33]=='4':
          a_x = a_x4
          a_y = a_y4
    if e[32] == 'B':
        list_b.append(time2)
        #print list_b
        if e[33]=='1':
          b_x = b_x1
          b_y = b_y1
        if e[33]=='2':
          b_x = b_x2
          b_y = b_y2
        if e[33]==4:
          b_x = b_x4
          b_y = b_y4
    if e[32] == 'C':
        list_c.append(time2)
        #print list_c
        if e[33]=='1':
          c_x = c_x1
          c_y = c_y1
        if e[33]=='2':
          c_x = c_x2
          c_y = c_y2
        if e[33]=='3':
          c_x = c_x3
          c_y = c_y3

    ### calculating time shift between phases

if len(list_a)==1 and len(list_b)==1:
      obs_diff_ab = (UTCDateTime(list_a[0]) - UTCDateTime(list_b[0]))
      print 'ab', obs_diff_ab
if len(list_a)==1 and len(list_c)==1:
      obs_diff_ac = (UTCDateTime(list_a[0]) - UTCDateTime(list_c[0]))
      print 'ac', obs_diff_ac
if len(list_b)==1 and len(list_c)==1:
      obs_diff_bc = (UTCDateTime(list_b[0]) - UTCDateTime(list_c[0]))
      print 'bc', obs_diff_bc

list1 = []
for x in range(0,len(b)):
    x = float(b[x])
    list1.append(x)
#print list1
```

```
if len(list_a)==1 and len(list_b)==1 and len(list_c)==1 and len(list1) ==7:
#if len(list_a)==1 and len(list_b)==1 or len(list_b)==1 and len(list_c)==1
    or len(list_a)==1 and len(list_c)==1:

 a_range = list1[0]
 b_range = list1[1]
 x_cross = list1[2]
 y_cross = list1[3]
 a_vel = list1[4]
 b_vel = list1[5]
 #a_vel = 0.426
 #b_vel = 0.428
 #if len(list1)==7:
 c_vel = list1[6]
 #c_vel = 0.3

 if len(list_a)==1 and len(list_b)==1:
  obs_diff_AB = obs_diff_ab
 if len(list_b)==1 and len(list_c)==1:
  obs_diff_BC = obs_diff_bc                    ## observed time difference
 if len(list_a)==1 and len(list_c)==1:
  obs_diff_AC = obs_diff_ac

 #if a_range < b_range:
 #    alfa = b_range/2
 #else:
 #    alfa = a_range/2

 #a_distance = math.sqrt((a_x - x_cross)**2 + (a_y - y_cross)**2)
     ## distance between array A and crossing point
 #b_distance = math.sqrt((b_x - x_cross)**2 + (b_y - y_cross)**2)
     ## distance between array B and crossing point
 #c_distance = math.tan(math.radians(alfa)) * a_distance
     ## the other side of the triangle
 #resolution = 3 * c_distance
     ## made resolution three times bigger than wedge
 ab_distance = math.sqrt((a_x - b_x)**2 + (a_y - b_y)**2)
     ## distances between geophones
 bc_distance = math.sqrt((b_x - c_x)**2 + (b_y - c_y)**2)
 ac_distance = math.sqrt((a_x - c_x)**2 + (a_y - c_y)**2)

 y_grid_array = np.arange(-3,3,0.05)
 y_grid_list = y_grid_array.tolist()
 x_grid_array = np.arange(-2.5,2.6,0.05)
 x_grid_list = x_grid_array.tolist()
 g_list = []
 x_list = []
 y = []
 z = []
```

```
for a in range(0, len(y_grid_list)):     ### grid search
  y1 = y_grid_list[a]

  for b in range(0, len(x_grid_list)):
    x1 = x_grid_list[b]

    a_g_distance = math.sqrt((a_x - x1)**2 + (a_y - y1)**2)
        ## distance between array A and grid point
    b_g_distance = math.sqrt((b_x - x1)**2 + (b_y - y1)**2)
        ## distance between array B and grid point
    c_g_distance1 = math.sqrt((c_x - x1)**2 + (c_y - y1)**2)
        ## distance between array C and grid point
    c_g_distance = c_g_distance1 + 0.5
        ## elevation correction
    #g_distance = math.sqrt((x_cross - x1)**2 + (y_cross - y1)**2)
        ## distance between crossing point and grid point
    g_list.append(c_g_distance)
    #c_g_extra = c_g_distance + 0.4
    #print 'number', c_g_distance

    time_a = a_g_distance/a_vel
    time_b = b_g_distance/b_vel
    #if len(list1)==7:
    time_c = c_g_distance/c_vel

    comp_diff_AB = time_a - time_b        ## time difference computed
    #if len(list1)==7:
    comp_diff_BC = time_b - time_c
    comp_diff_AC = time_a - time_c


    ### difference between observed and calculated time shift


    if len(list_a)==1 and len(list_b)==1:
      AB = math.sqrt((comp_diff_AB - obs_diff_AB)**2)
    if len(list_b)==1 and len(list_c)==1:
      BC = math.sqrt((comp_diff_BC - obs_diff_BC)**2)
    if len(list_a)==1 and len(list_c)==1:
      AC = math.sqrt((comp_diff_AC - obs_diff_AC)**2)


    if len(list_a)==1 and len(list_b)==1 and len(list_c)==0:
      t_diff = AB
      #print 't_diff = AB', t_diff
    if len(list_a)==0 and len(list_b)==1 and len(list_c)==1:
      t_diff = BC
      #print 't_diff = BC', t_diff
    if len(list_a)==1 and len(list_b)==0 and len(list_c)==1:
      t_diff = AC
      #print 't_diff = AC', t_diff
```

```
    if len(list_a)==1 and len(list_b)==1 and len(list_c)==1:
      t_diff = AB + BC + AC
      t_diff_list.append(t_diff)
      #print 't_diff = ABC', t_diff
    x_list.append(x1)
    y.append(y1)
    z.append(t_diff)      ### color gradient

lowest = min(t_diff_list)
position = t_diff_list.index(lowest)
print lowest, position
lon, lat = utlLonLat(orig_lon, orig_lat, x_list[position], y[position])
numbers = '%.4f %.4f\t' % (lon, lat)
final_text = time + ' ' + numbers + '\n'
pick_locations.write(final_text)



fig=plt.figure()
ax=fig.add_subplot(111)
plt.scatter(x_list, y, c=z, marker = 's', edgecolor='none',
     cmap=cm.gist_yarg)
x2 = [a_x, b_x, c_x]
y2 = [a_y, b_y, c_y]
plt.plot(x2, y2, 'rD', markersize=7)
plt.plot(x_list[position], y[position], 'ro', markersize = 10)
circle=Circle((x_cross, y_cross), radius=c_distance, color='b',
    alpha=0.2)
ax.add_artist(circle)
plt.colorbar()
plt.show()
text2 = 'vel_comp_' + text1 + 'const_vel.png'
fig.savefig(text2)
plt.close('all')
```